BACHELOR THESIS – ME234804

CFD Analysis of HVAC Airflow, Thermal, and Humidity Distribution in a 1MW Floating Data Center Server Room

GEMILANG FRIYAN FINN PAKPAHAN

NRP 5019221062

Advisor

Sutopo Purwono Fitri, S.T., M.Eng., Ph.D.

NIP. 197510062002121003

Dr. Eng. Ede Mehta Wardhana, S.T., M.T.

NIP. 1992201711048

Double Degree Program

Department of Marine Engineering

Faculty of Marine Technology

Institut Teknologi Sepuluh Nopember

Surabaya

2026

TUGAS AKHIR – ME234804

Analisis CFD Distribusi Aliran Udara, Temperatur, dan Kelembapan pada Ruang Server Floating Data Center (FDC) Kapasitas 1 MW

GEMILANG FRIYAN FINN PAKPAHAN

NRP 5019221062

Dosen Pembimbing

Sutopo Purwono Fitri, S.T., M.Eng., Ph.D.

NIP. 197510062002121003

Dr. Eng. Ede Mehta Wardhana, S.T., M.T.

NIP. 1992201711048

Program Gelar Ganda

Departemen Teknik Sistem Perkapalan

Fakultas Teknologi Kelautan

Institut Teknologi Sepuluh Nopember

Surabaya

2026

BACHELOR THESIS – ME234804

CFD Analysis of HVAC Airflow, Thermal, and Humidity Distribution in a 1MW Floating Data Center Server Room

GEMILANG FRIYAN FINN PAKPAHAN

NRP 5019221062

Advisor

Sutopo Purwono Fitri, S.T., M.Eng., Ph.D.

NIP. 197510062002121003

Dr. Eng. Ede Mehta Wardhana, S.T., M.T.

NIP. 1992201711048

Double Degree Program

Department of Marine Engineering

Faculty of Marine Technology

Institut Teknologi Sepuluh Nopember

Surabaya

2026

APPROVAL SHEET

CFD ANALYSIS OF HVAC AIRFLOW, THERMAL, AND HUMIDITY DISTRIBUTION IN A 1MW FLOATING DATA CENTER SERVER ROOM

BACHELOR THESIS

Submitted to fulfill one of the requirements
for obtaining a double bachelor's degree in Engineering at
Undergraduate Study Program of Marine Engineering
Department of Marine Engineering
Faculty of Marine Technology
Institut Teknologi Sepuluh Nopember

By: **GEMILANG FRIYAN FINN PAKPAHAN**
NRP. 5019221062

Approved by Representative of Hochschule Wismar Germany:

Signature : ....
Representative : Sunarsih, S.T., M.Eng., Ph.D.
NIP. : 1980202012010
Date : 31 July 2026

Approved by Head of Marine Engineering Department:

Signature : ....
Head of Department : Dr. Indra Ranu Kusuma, S.T., M.Sc.
NIP. : 197903272003121001
Date : 3 Agustus 2026

SURABAYA
JULY, 2026

This page is intentionally left blank

APPROVAL SHEET

CFD ANALYSIS OF HVAC AIRFLOW, THERMAL, AND HUMIDITY DISTRIBUTION IN A 1MW FLOATING DATA CENTER SERVER ROOM

BACHELOR THESIS

Submitted to fulfil one of the requirements

For obtaining a double bachelor's degree in engineering at

Undergraduate Study Program of Marine Engineering

Department of Marine Engineering

Faculty of Marine Technology

Sepuluh Nopember Institute of Technology

Prepared by:

GEMILANG FRIYAN FINN PAKPAHAN

NRP. 5019221062

Approved by Final Examiner Team:

1.	Sutopo Purwono Fitri, S.T., M.Eng., Ph.D.	Supervisor	( )
2.	Dr. Eng. Ir., Ede Mehta Wardhana, S.T., M.T.	Co-Supervisor	( )
3.	Prof. Dr. Ir. Agoes Santoso, MSc., Mphil.	Examiner	( )
4.	Danang Jawara Ditya, S.T., M.T.	Examiner	( )
5.	Handi Rahmannuri, S.T., M.T.	Examiner	( )

SURABAYA

July, 2026

This page is intentionally left blank

STATEMENT OF ORIGINALITY

The undersign below:

Name of student / NRP	:	Gemilang Friyan Finn Pakpahan / 5019221062
Department	:	Marine Engineering
Supervisor / NIP	:	1. Sutopo Purwono Fitri, S.T., M.Eng., Ph.D. 197510062002121003
		2. Dr. Eng. Ir., Ede Mehta Wardhana, S.T., M.T 1992201711048

Hereby declare that the Final Project with the title of "CFD ANALYSIS OF HVAC AIRFLOW, THERMAL, AND HUMIDITY DISTRIBUTION IN A 1 MW FLOATING DATA CENTER SERVER ROOM" is the result of my own work, is original, and is written by following the rules of scientific writing.

If in the future there is a discrepancy with this statement, then I am willing to accept sanctions in accordance with the provisions that apply at Sepuluh Nopember Institute of Technology.

Surabaya, 30 July 2026

Student

(Gemilang Friyan Finn Pakpahan)
NRP. 5019221062

Acknowledge,

Supervisor 1	Supervisor 2
(Sutopo Purwono Fitri, S.T., M.Eng., Ph.D.)	(Dr. Eng. Ir., Ede Mehta Wardhana, S.T., M.T.)
NIP. 197510062002121003	NIP. 1992201711048

This page is intentionally left blank

ABSTRAK

Analisis CFD Distribusi Aliran Udara, Temperatur, dan Kelembapan pada Ruang Server Floating Data Center (FDC) Kapasitas 1 MW

Nama Mahasiswa / NRP : Gemilang Friyan Finn Pakpahan / 5019221062

Departemen : Teknik Sistem Perkapalan FTK – ITS

Nama Pembimbing : 1. Sutopo Purwono Fitri, S.T., M.Eng., Ph.D.

2. Dr. Eng. Ede Mehta Wardhana, S.T., M.T.

Abstrak

Floating Data Center muncul sebagai solusi menjanjikan untuk mengatasi keterbatasan lahan dan meningkatnya kebutuhan pendinginan pada pengembangan pusat data konvensional, dengan keunggulan modularitas, skalabilitas, dan kedekatan dengan air laut sebagai potensi sumber daya termal. Namun, menjaga kestabilan aliran udara, suhu, dan kelembapan di ruang server yang terbatas pada platform terapung tetap menjadi tantangan desain yang krusial. Penelitian ini menyajikan analisis *Computational Fluid Dynamics (CFD)* terhadap distribusi aliran udara *HVAC*, termal, dan kelembapan relatif di ruang server *Floating Data Center* berkapasitas 1 MW dengan konfigurasi hot aisle–cold aisle. Rak server dimodelkan menggunakan pendekatan media berpori dengan resistansi viskos anisotropik dan sumber momentum terarah untuk merepresentasikan karakteristik aliran udara internal peralatan. Dua simulasi steady-state dilakukan pada beban IT 50% dan 70%, dilengkapi simulasi perpindahan panas dinding dan simulasi transient tambahan untuk mengevaluasi respons ruang server terhadap infiltrasi udara luar sementara. Pada beban 50%, udara suplai bersuhu 20°C meninggalkan domain dengan suhu rata-rata 25,72°C, dengan suhu rak server berkisar 20,04–28,79°C; pada beban 70%, suhu maksimum mencapai 31,79°C, tetap dalam rentang ASHRAE TC 9.9 *Allowable Class A2* sebesar 10–35°C. Peningkatan suhu lokal terjadi di sekitar rak yang berada di tengah ruangan, disebabkan oleh udara buang dari rak-rak di sekitarnya yang sebagian bersirkulasi kembali alih-alih mengalir langsung ke outlet. Kelembapan relatif menurun dari 30% pada suplai menjadi rata-rata 18,95–21,04% pada outlet, tetap dalam rentang yang diizinkan yaitu 8–80%. Pada skenario infiltrasi transient, suhu dan kelembapan relatif rata-rata ruangan hanya meningkat masing-masing sebesar 0,14°C dan 4,76 poin persentase, kembali mendekati kondisi awal dalam 60 detik setelah pintu ditutup. Temuan ini menunjukkan bahwa konfigurasi yang diusulkan mampu menjaga kondisi ASHRAE *Class A2* dan kenaikan maksimal untuk temperature dan kelembapan relatif SNI di seluruh skenario, sekaligus menyoroti resirkulasi lokal sebagai faktor untuk optimasi aliran udara di masa mendatang.

Kata kunci: *Computational Fluid Dynamics, Floating Data Center, HVAC, hot aisle–cold aisle*, hotspot termal, kelembapan relatif, ASHRAE, SNI

This page is intentionally left blank

ABSTRACT

CFD Analysis of HVAC Airflow, Thermal, and Humidity Distribution in a 1MW Floating Data Center Server Room

Student name / NRP : **Gemilang Friyan Finn Pakpahan / 5019221062**

Department : **Department of Marine Engineering FTK – ITS**

Supervisor names : **1. Sutopo Purwono Fitri, S.T., M.Eng., Ph.D.**

2. Dr. Eng. Ede Mehta Wardhana, S.T., M.T.

Abstract

Floating Data Centers have emerged as a promising solution to land constraints and rising cooling demands in conventional data center development, offering modularity, scalability, and proximity to seawater as a potential thermal resource. However, maintaining stable airflow, temperature, and humidity within the confined server room of a floating platform remains a critical design challenge. This study presents a Computational Fluid Dynamics (CFD) analysis of HVAC airflow, thermal, and relative humidity distribution in the server room of a 1 MW Floating Data Center employing a hot aisle–cold aisle configuration. Server racks were modeled using a porous-media approach with anisotropic viscous resistance and a directional momentum source to represent internal equipment airflow. Two steady-state simulations were performed at 50% and 70% IT workload, complemented by a wall heat transfer simulation and a supplementary transient simulation evaluating server room response to temporary outdoor air infiltration. At 50% load, supply air at 20°C exited the domain at an average of 25.72°C, with server row temperatures between 20.04–28.79°C; at 70% load, the maximum reached 31.79°C, remaining within the ASHRAE TC 9.9 Allowable Class A2 range of 10–35°C. A localized temperature increase occurred around the racks near the middle of the room, attributed to exhaust air from neighboring racks partially recirculating instead of flowing directly to the outlet. Relative humidity decreased from 30% supply to an average of 18.95–21.04% at the outlet, within the 8–80% allowable range. Under transient infiltration, room-average temperature and relative humidity increased by only 0.14°C and 4.76 percentage points, returning close to baseline within 60 seconds after the door closed. These findings demonstrate that the proposed configuration maintains ASHRAE Class A2 conditions and SNI maximum rise of Temperature and Relative Humidity across all scenarios, while highlighting localized recirculation as a factor for further airflow optimization.

Keywords: Computational Fluid Dynamics, Floating Data Center, HVAC, hot aisle–cold aisle, thermal hotspot, relative humidity, ASHRAE, SNI

This page is intentionally left blank

PREFACE

First and foremost, I offer my highest praise and deepest gratitude to my Lord and Savior, Jesus Christ, for His boundless grace, unconditional love, and continuous guidance that have empowered me to complete this bachelor thesis. This milestone is not merely a personal achievement but a collective one, made possible by the unwavering support, wisdom, and prayers of those who have walked this path with me. Therefore, I wish to extend my sincerest appreciation to:

1. My beloved parents, Mr. Mangatur Disneyland and Mrs. Agatha Kristina. Thank you for your unconditional love, endless sacrifices, and for always being my greatest source of strength. Everything I have achieved is dedicated to you.
2. My two brothers, for the constant support, laughter, and for always cheering me on through every step of my life.
3. My beloved grandparents, whose sincere and unceasing prayers have provided me with spiritual strength, protection, and blessings from afar.
4. Sutopo Purwono Fitri, S.T., M.Eng., Ph.D., as my supervisor, and Dr. Eng. Ede Mehta Wardhana, S.T., M.T., as my co-supervisor. I am profoundly grateful for your invaluable mentorship, constructive feedback, and the immense patience you demonstrated in shaping this research.
5. Prof. Ir. Aguk Zuhdi M. Fathallah, M.Eng., Ph.D., my academic advisor, for the continuous guidance and encouragement provided throughout my entire undergraduate journey.
6. My esteemed examiners, Prof. Dr. Ir. Agoes Santoso, MSc., Mphil., Danang Jawara Ditya, S.T., M.T., and Handi Rahmannuri, S.T., M.T., for their insightful evaluations, constructive criticisms, and valuable inputs during my thesis defense.
7. The members of the Marine Fluid Machinery (MMS) laboratory and my thesis partner, for the shared knowledge, collaborative spirit, and discussions that greatly enriched my research process.
8. My Double Degree classmates, for the shared struggles, late-night study sessions, and mutual support that made this academic journey truly remarkable.
9. Kolega Jangkar P62, my amazing batchmates, for the strong camaraderie, unforgettable memories, and for making my university years so vibrant and full of joy.
10. My friends outside of campus, who provided a much-needed escape, endless laughter, and a fresh perspective whenever I needed a break from academic routines.
11. Finally, I want to thank myself. Thank you for persevering through self-doubt, for putting in the long hours, and for refusing to quit. This thesis marks not a finish line, but the promising start of a new chapter.

The author is fully aware that this bachelor thesis is far from perfect and remains open to improvement. Therefore, constructive criticism and suggestions are greatly appreciated. It is hoped that this research will provide valuable contributions to future studies.

Surabaya, July 2026

This page is intentionally left blank

TABLE OF CONTENTS

LIST OF FIGURES

LIST OF TABLES

LIST OF SYMBOLS

ρ	Fluid Density
u,v,w	Velocity Components
T	Temperature
P	Pressure
k	Turbulent Kinetic Energy
ϵ	Turbulent Dissipation Rate
μ	Dynamic Viscosity
Cp	Specific Heat Capacity
Q	Heat Load / Heat Source
RH	Relative Humidity
g	Gravitational Acceleration
h	Convective Heat Transfer Coefficient
λ	Thermal Conductivity
ν	Kinematic Viscosity

This page is intentionally left blank

CHAPTER I

INTRODUCTION

1.1 Background

The rapid growth of cloud computing, artificial intelligence, big data analytics, and digital services has significantly increased the global demand for data processing and storage capacity. As a result, modern data centers are required to operate at increasingly high-power densities, where large amounts of electrical energy are consumed by information technology (IT) equipment (Herlin, 2008). Almost all of this electrical energy is ultimately converted into heat, making thermal management a critical factor in ensuring reliable and continuous data center operation (Hassan et al., 2013; Herlin, 2008).

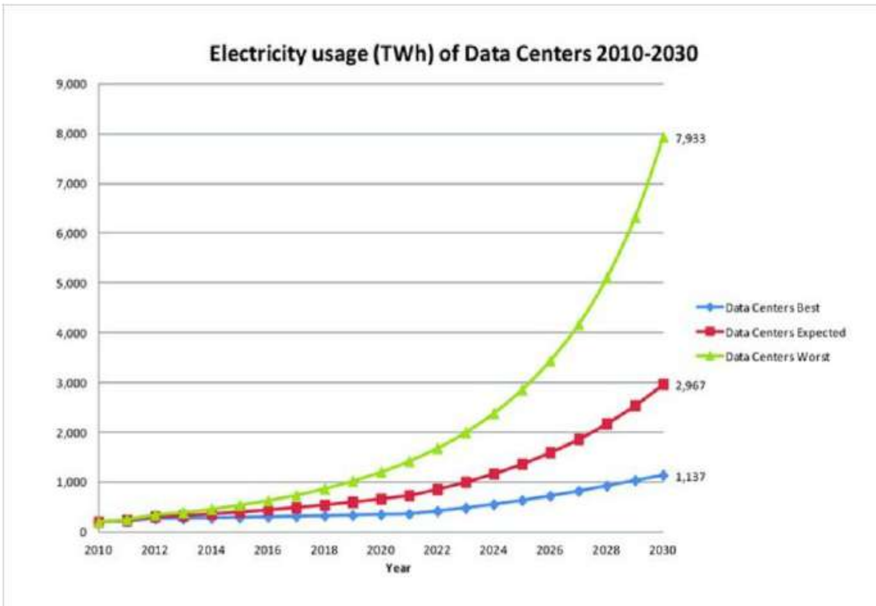

Figure 1. 1 Electricity usage of Data Centers (Andrae & Edler, 2015)

Inadequate thermal control can lead to overheating, reduced equipment lifespan, performance degradation, and unexpected system failures, which may cause significant financial losses and service disruptions. Therefore, effective heat removal and thermal management strategies are essential in maintaining stable operating conditions within data center environments.

One of the primary factors influencing thermal performance in data centers is airflow management within the server room. Improper airflow distribution can result in non-uniform temperature fields, recirculation of hot exhaust air, and insufficient cooling air reaching server inlets (Hassan et al., 2013; Macedo et al., 2019). These conditions often lead to the formation of localized hotspots, where server inlet temperatures exceed recommended operating limits. Hotspots are a major concern in data center operation, as they can accelerate component degradation, increase failure rates, and compromise overall system reliability. Therefore, effective airflow organization within the server room is essential to ensure that cooling air is delivered efficiently and heat is removed uniformly from IT equipment.

In addition to airflow, heat transfer through physical boundaries such as walls may also influence the overall thermal behavior of the server room. Although its contribution is generally smaller compared to IT heat loads, heat transfer through walls can still affect temperature distribution, particularly when there is a temperature difference between indoor and ambient conditions. Therefore, considering wall heat transfer can improve the accuracy of thermal analysis in CFD simulations. In recent years, Floating Data Centers (FDCs) have emerged as an alternative approach to conventional land-based data centers. The FDC concept aims to address challenges such as land scarcity, high construction costs, and cooling efficiency limitations in densely populated coastal regions. By placing data center facilities on floating platforms, FDCs offer potential advantages including modular construction, scalability, proximity to coastal load centers, and access to seawater as a relatively stable thermal environment. These advantages make Floating Data Centers an attractive option for future large-scale data center deployment.

In addition to temperature control, humidity management plays a vital role in maintaining reliable data center operation. Excessively high humidity levels may cause condensation and corrosion on electronic components, while excessively low humidity increases the risk of electrostatic discharge (ESD). To mitigate these risks, ASHRAE Technical Committee 9.9 recommends maintaining server inlet air temperatures within 18–27 °C and relative humidity within approximately 40–60% (ASHRAE TC 9.9, 2021; Seong et al., 2017).

In recent years, Floating Data Centers (FDCs) have emerged as an alternative approach to conventional land-based data centers. The FDC concept aims to address challenges such as land scarcity, high construction costs, and cooling efficiency limitations in densely populated coastal regions. By utilizing floating platforms, FDCs offer advantages such as modularity, scalability, and access to seawater as a potential heat sink.

Despite these advantages, the internal environmental requirements of server rooms in Floating Data Centers remain fundamentally similar to those of conventional data centers. Proper airflow distribution, temperature control, and humidity management are still required to ensure reliable server operation. In addition, compact layouts and space limitations in floating installations may further influence airflow behavior and thermal performance.

A typical Floating Data Center may operate at high IT loads, such as 1 MW, consisting of multiple server racks arranged in hot aisle–cold aisle configurations. Due to the large scale of such systems, CFD analysis is commonly performed on a representative modular server room to evaluate airflow behavior and thermal performance while maintaining manageable computational cost.

Computational Fluid Dynamics (CFD) has been widely applied as an effective tool for analyzing airflow patterns, temperature distribution, and humidity characteristics within data center environments. Previous studies have shown that CFD can identify airflow recirculation, thermal gradients, and potential hotspot formation (Hassan et al., 2013; Macedo et al., 2019). However, studies that simultaneously consider airflow, thermal behavior, and humidity distribution in Floating Data Center server rooms remain limited

Therefore, this study focuses on the CFD analysis of airflow, temperature, and relative humidity distribution within a modular server room of a 1 MW Floating Data Center. The analysis considers variations in server load conditions to evaluate their impact on thermal performance and airflow effectiveness. The results are expected to provide insight into

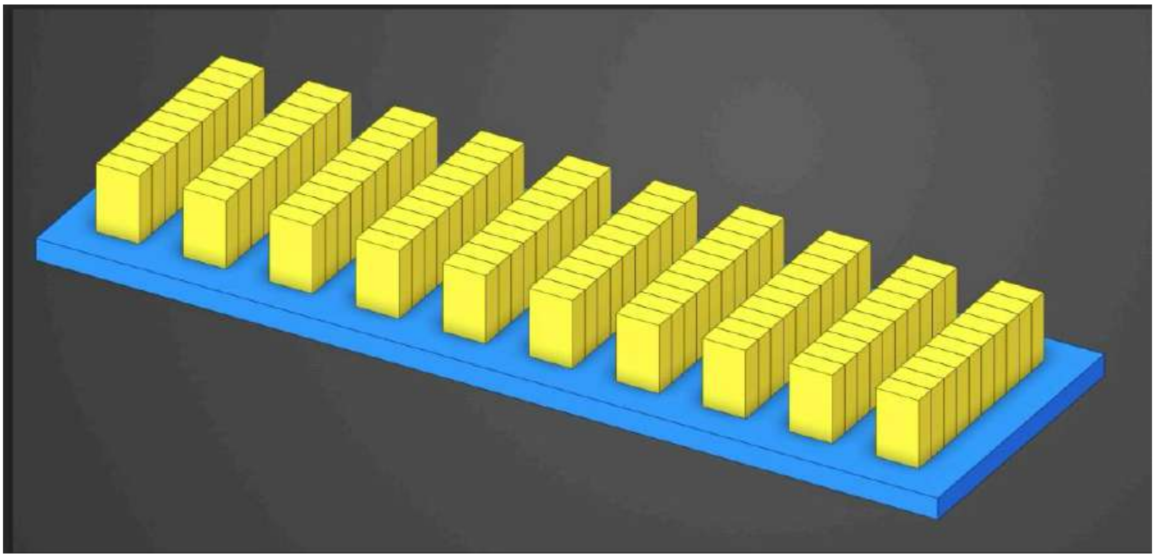

Figure 1. 2 Server Room Configuration

the behavior of airflow and thermal distribution under different operating conditions and support the evaluation of cooling performance in Floating Data Center applications.

1.2 Problem Formulation

From the background that has been explained above, the problem formulations of this research are:

1. How do airflow patterns within a fixed hot aisle–cold aisle server room configuration of a 1 MW Floating Data Center influence temperature distribution and contribute to the formation of thermal hotspots around server Racks?
2. How does the airflow configuration affect the distribution of relative humidity within the server room, and does the resulting humidity remain within commonly accepted operational standards for data center environments?

1.3 Research Limitations

In this research, the limitations are:

1. The analysis is limited to airflow, temperature, and relative humidity distribution inside a representative modular server room corresponding to a 1 MW Floating Data Center.
2. The server room geometry represents a typical hot aisle–cold aisle configuration and does not model the entire Floating Data Center facility.
3. Server racks are modeled as simplified volumetric heat sources with uniform heat generation, without explicitly modelling internal server components such as fans, heat sinks, and circuit boards.

4. The cooling system is not modeled in detail and is represented through prescribed airflow boundary conditions at the supply and return locations.
5. The CFD simulation for normal conditions is performed under steady-state operating conditions, and transient effects are used for infiltration simulation only.
6. The analysis considers two server load conditions (70% and 50%), without performing a full parametric variation of IT load.
7. Heat transfer through the server room walls is considered using simplified assumptions, and detailed multi-layer wall structures or radiation simulated explicitly
8. External environmental effects specific to floating platforms, such as wave motion, platform vibration, and seawater dynamics, are not considered in this study.
9. The study focuses on environmental condition assessment and does not aim to redesign or optimize the HVAC system.
10. Grid/mesh independence analysis was not performed due to limitations in available computational resources. Mesh quality was instead evaluated using orthogonal quality and skewness metrics to ensure adequate discretization of the computational domain.

1.4 Research Objectives

From the problem formulation that has been state, the Objective of this research are:

1. To analyze airflow patterns and temperature distribution within a fixed hot aisle–cold aisle server room configuration of a 1 MW Floating Data Center and to identify thermal hotspot formation around server racks using Computational Fluid Dynamics (CFD).
2. To evaluate the distribution of relative humidity within the server room and assess whether acceptable operating conditions can be maintained based on commonly accepted operational standards for data center environments.

1.5 Research Benefits

The benefits of this research are:

1. To improve understanding of airflow behavior and its influence on temperature distribution and thermal hotspot formation within a modular Floating Data Center server room under different server load conditions.
2. To provide insight into the overall thermal environment of the server room, including the effect of wall heat transfer, and to evaluate whether the resulting temperature and relative humidity conditions remain within acceptable operating limits.

CHAPTER II

LITERATURE REVIEW

2.1 Basic Theory

2.1.1 Floating Data Center

A Floating Data Center (FDC) is a data center facility deployed on a floating platform, such as a barge or offshore structure, typically located in coastal or marine environments. This concept has been introduced as an alternative to conventional land-based data centers to address challenges related to land scarcity, high construction costs, and cooling efficiency. By utilizing the surrounding seawater as a thermal sink, Floating Data Centers offer potential advantages in terms of energy efficiency and modular deployment.

Despite differences in external location and infrastructure, the internal environmental requirements of server rooms in Floating Data Centers remain fundamentally similar to those of conventional data centers. Server equipment still requires controlled airflow, temperature, and humidity conditions to ensure reliable and continuous operation. Therefore, the thermal and airflow performance of the server room is a critical aspect that must be evaluated regardless of the data center deployment concept.

Large-capacity Floating Data Centers are commonly designed using a modular approach, in which the overall facility consists of multiple server room modules with similar layouts and operating conditions. This modular concept allows room-level analysis to be used as a representative model for evaluating the environmental performance of the entire facility.(Charara, 2023)

2.1.2 HVAC Concept in Data Centers

HVAC systems play a critical role in maintaining acceptable environmental conditions within data center server rooms. In data center applications, HVAC systems are primarily responsible for supplying conditioned air at controlled temperature and humidity levels, as well as removing heat generated by IT equipment through return air pathways.

Rather than being analyzed as a complete mechanical system, HVAC operation in this study is represented through airflow boundary conditions. The supply air provided by the HVAC system determines inlet air temperature, humidity, and airflow rate entering the server room, while return outlets represent the removal of heated air. This simplified representation is commonly adopted in CFD-based data center studies to focus on room-level airflow and thermal behavior. Airflow management strategies such as hot aisle–cold aisle configurations have been recognized as effective approaches to improve cooling performance and reduce thermal recirculation in data centers.

Therefore, HVAC systems in this research are not evaluated in terms of equipment performance or energy efficiency, but are treated as supporting systems that define the operating conditions for airflow, temperature, and humidity analysis within the server room. (Hassan et al., 2013; Herlin,

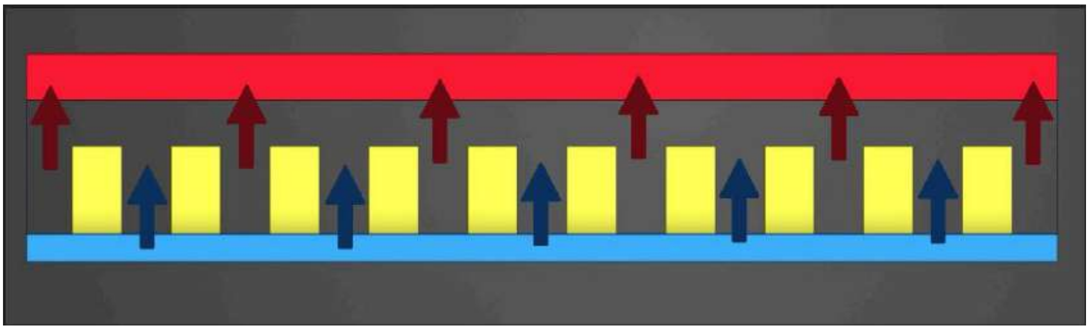

Figure 2. 1 Cold aisle – Hot Aisle Illustration

2.1.3 Server Room and Airflow Management

The server room is the primary space within a data center where server racks, air distribution systems, and heat removal pathways are located. Almost all electrical energy consumed by server equipment is converted into heat, making effective airflow management essential for maintaining acceptable operating conditions.

One of the most widely adopted airflow management strategies in data centers is the hot aisle–cold aisle configuration. In this arrangement, cold air is supplied to the front of server racks through cold aisles, while hot exhaust air is discharged into hot aisles and removed from the server room. This configuration is intended to minimize mixing between cold supply air and hot exhaust air, thereby improving cooling efficiency and reducing inlet temperature variations.

In practice, however, airflow distribution within server rooms is often non-uniform. Air recirculation and bypass airflow may occur due to layout constraints or insufficient airflow control, allowing hot air to re-enter server inlets. Such conditions can degrade cooling performance and increase the risk of elevated inlet temperatures, highlighting the need for detailed airflow analysis at the room level.(Herlin, 2008; Macedo et al., 2019)

In addition, variations in server load can significantly affect heat generation and consequently influence airflow behavior and temperature distribution within the server room.

2.1.4 Raised Floor System in Data Center Server Room

Raised floor systems are commonly applied in data center server rooms to distribute conditioned air from the cooling system to server inlets. In this configuration, a raised platform forms an underfloor plenum that functions as a supply air chamber. Conditioned air is delivered through perforated floor tiles located in the cold aisle, allowing cold air to enter the front of server racks.

The raised floor approach supports improved airflow distribution by separating supply air from hot exhaust air, thereby reducing the potential for hot air recirculation. When combined with a hot aisle–cold aisle configuration, raised floor systems have been shown to enhance cooling effectiveness and maintain stable thermal conditions within data center server rooms(ASHRAE Technical Committee 9.9, 2021; Herlin, 2008).

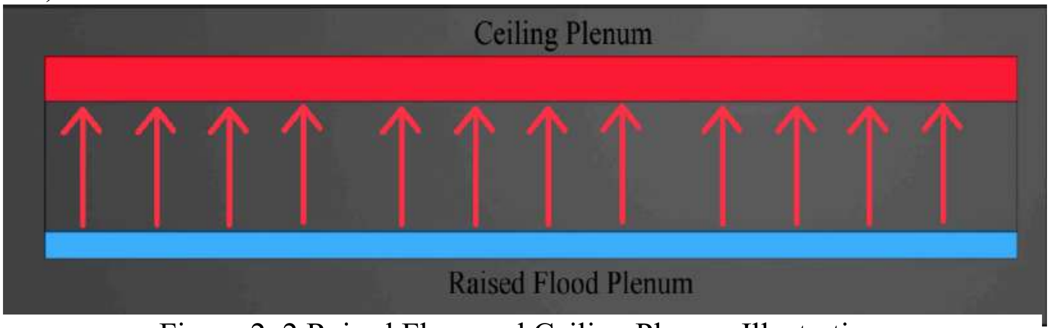

Figure 2. 2 Raised Floor and Ceiling Plenum Illustration

2.1.5 Thermal Hotspots in Server Room

Thermal hotspots refer to localized regions within a server room where air temperature, particularly at server inlets, exceeds acceptable operating limits. Hotspots are commonly caused by uneven airflow distribution, hot air recirculation, or imbalances between server heat generation and supplied cooling air.

The presence of thermal hotspots can have adverse effects on server reliability and performance. Elevated inlet temperatures may lead to reduced computational performance, accelerated aging of electronic components, and an increased likelihood of hardware failure. In addition, hotspots often force cooling systems to operate at higher capacities, resulting in increased energy consumption and operational costs.

Consequently, identifying and evaluating thermal hotspots is a key objective in server room thermal analysis. Understanding the relationship between airflow patterns and temperature distribution provides valuable insight into the effectiveness of airflow configurations and the potential risks associated with non-uniform cooling.(Hassan et al., 2013; Macedo et al., 2019)

2.1.6 Thermal Performance Indicators in Data Center Server Room

Thermal performance in data center server rooms is commonly evaluated using several key indicators that reflect the effectiveness of airflow management and cooling strategies. One of the most important indicators is the server inlet air temperature, as it directly affects the operating conditions and reliability of IT equipment. Elevated inlet temperatures may lead to performance degradation, accelerated component aging, and increased failure rates.

In addition to absolute temperature levels, temperature uniformity within the server room is also a critical indicator of thermal performance. Non-uniform temperature distribution often indicates ineffective airflow delivery, hot air recirculation, or bypass airflow, which may result in localized thermal hotspots. The presence of hotspots is particularly undesirable, as localized overheating can occur even when average room temperatures appear acceptable.

Therefore, thermal performance assessment in data center server rooms typically focuses on inlet temperature distribution, temperature gradients, and hotspot formation. These indicators are commonly used in CFD-based studies to evaluate whether airflow configurations are capable of maintaining acceptable and reliable thermal conditions throughout the server room(Herlin, 2008).

2.1.7 Humidity Conditions in Server Room

Although temperature is the prim ary parameter in most data center studies, relative humidity is also considered an important environmental factor that affects equipment reliability and compliance with ASHRAE guideline.

Excessively high relative humidity may cause condensation on electronic components, leading to corrosion and electrical failures. Conversely, excessively low humidity increases the risk of electrostatic discharge, which can damage sensitive electronic devices.

Humidity distribution within a server room is influenced by supply air conditions, airflow patterns, and heat transfer processes. Non-uniform airflow may result in localized variations in relative humidity, creating areas that are more susceptible to moisture-related or electrostatic risks.

Therefore, humidity analysis should be conducted alongside temperature and airflow analysis. Evaluating relative humidity distribution helps ensure that environmental conditions within the server room support safe and reliable server operation under steady-state conditions.(Seong et al., 2017; Zhang & Ryu, 2021)

2.1.8 Humidity Modelling in CFD Studies

Relative humidity is an important environmental parameter that influences the reliability of electronic equipment in data center server rooms. In CFD studies, humidity can be analyzed by modeling the transport of water vapor within the airflow field. One commonly adopted approach is the species transport method, where water vapor is treated as a passive scalar transported by airflow and diffusion processes.

In this approach, CFD simulations solve an additional transport equation for the mass fraction of water vapor, which is coupled with the airflow and temperature fields. The local relative humidity is then calculated based on the local water vapor concentration and temperature. This method allows the spatial distribution of relative humidity to be evaluated consistently with airflow patterns and thermal behavior.

Previous CFD studies have demonstrated that this approach is effective for predicting humidity distribution and identifying regions prone to condensation or low-humidity risks in indoor environments. However, the application of CFD-based humidity modeling to data center server rooms, particularly under high heat-density conditions, remains limited. As a result, humidity analysis is often conducted separately from airflow and thermal studies, highlighting the need for integrated CFD analysis that considers airflow, temperature, and relative humidity simultaneously(Seong et al., 2017; Zhang & Ryu, 2021).

2.1.9 Environmental Guidelines for Data Centers

Environmental operating guidelines are commonly used as references to evaluate thermal and humidity conditions within data center server rooms. One of the most widely adopted guidelines is published by the American Society of Heating, Refrigerating and Air-Conditioning Engineers (ASHRAE), which provides recommended and allowable ranges for temperature and relative humidity at server inlets.

According to ASHRAE Thermal Guidelines for Data Processing Environments, maintaining appropriate inlet air temperature is essential to ensure reliable operation and prevent thermal stress on server equipment. Inlet temperatures exceeding recommended limits may increase the risk of performance degradation and hardware failure. Therefore, inlet temperature is often used as a key indicator in assessing the effectiveness of airflow distribution within server rooms.

In addition to temperature, ASHRAE also emphasizes the importance of controlling relative humidity within acceptable limits. Excessively high humidity may lead to condensation and corrosion, while excessively low humidity increases the risk of electrostatic discharge. As a result, relative humidity is considered an important parameter in evaluating environmental suitability for data center operation.

In this study, ASHRAE guidelines are used as a reference framework to assess the simulated temperature and relative humidity distributions obtained from CFD analysis. The guidelines are not treated as design targets, but rather as comparative criteria to evaluate whether the environmental conditions within the server room remain within generally accepted operational ranges.(ASHRAE Technical Committee 9.9, 2021)

2.1.10 Data Center Classification Based on Standar Nasional Indonesia (SNI)

In addition to international standards such as ASHRAE TC 9.9, Indonesia has established SNI 8799-1:2023 as the national standard for data center facilities. This standard specifies the technical requirements for the design and operation of data centers, covering building facilities, electrical systems, cooling systems, data network infrastructure, fire protection systems, monitoring systems, and physical security. The objective of the standard is to ensure that data center facilities are designed and operated with adequate levels of reliability, availability, and operational continuity.

SNI 8799-1:2023 also establishes the recommended environmental operating conditions for server rooms, including allowable room temperature, relative humidity, dew point, and the maximum permissible rates of temperature and humidity variation. These environmental requirements are intended to maintain stable operating conditions for information technology equipment while minimizing the risk of equipment failure caused by excessive thermal or moisture fluctuations.

In this study, SNI 8799-1:2023 is used as one of the reference standards to evaluate the environmental performance of the proposed floating data center server room. The simulated temperature and relative humidity obtained from the CFD analysis are compared with the recommended operating limits specified by the standard to assess the suitability of the proposed cooling system under the investigated operating conditions.

2.1.11 Heat Transfer Through Walls

Heat transfer through walls is an important factor in enclosed thermal systems, including data center server rooms. Although the dominant heat source originates from IT equipment, heat exchange between the indoor environment and the surrounding ambient through walls can influence temperature distribution.

Heat transfer through walls generally occurs by conduction within the wall material and convection at the inner and outer surfaces. The rate of heat transfer depends on the thermal properties of the wall material, its thickness, and the temperature difference between indoor and outdoor environments.

In CFD simulations, wall heat transfer is commonly modeled using simplified approaches such as conductive walls with external convective boundary conditions. This approach allows the interaction between the server room and the surrounding environment to be considered without introducing excessive computational complexity.

2.1.12 Sandwich Wall

Sandwich wall panels are widely used in modular structures, refrigerated containers, and cold storage facilities because they provide high thermal insulation while maintaining a lightweight and rigid structural configuration. A sandwich panel generally consists of two thin metal face sheets bonded to a low thermal conductivity core material, such as polyurethane foam. The metal layers provide structural strength and mechanical protection, whereas the insulation core minimizes heat transfer between the external and internal environments. This construction is particularly suitable for conditioned spaces where stable indoor temperatures must be maintained.

The thermal performance of a sandwich wall is commonly evaluated using the overall heat transfer coefficient (U-value), which represents the rate of heat transfer through the entire wall assembly. The overall thermal resistance consists of the external convective resistance, conductive resistance of each material layer, and internal convective resistance. Consequently, the overall heat transfer coefficient can be expressed as. (Budiyanto et al., 2023)

$$U = \frac{1}{\frac{1}{h_o} + \sum_{i=1}^{n} \frac{x_i}{k_i} + \frac{1}{h_i}} \quad \text{..(2.1)}$$

where h_o and h_i are the external and internal convective heat transfer coefficients, x_i is the thickness of each layer, and k_i is the thermal conductivity of each material. A lower U-value indicates better thermal insulation and lower heat gain into the conditioned space. (Budiyanto et al., 2023)

In modular cold storage applications, sandwich wall panels commonly consist of an outer aluminium layer, a polyurethane insulation core, and an inner stainless-steel layer. This multilayer configuration provides low thermal transmittance while maintaining sufficient structural integrity for modular systems. The same insulation concept is applicable to enclosed spaces requiring controlled environmental conditions, including modular server rooms and floating data center containers. Therefore, the sandwich wall construction is adopted in this study to represent heat transfer through the server room enclosure.

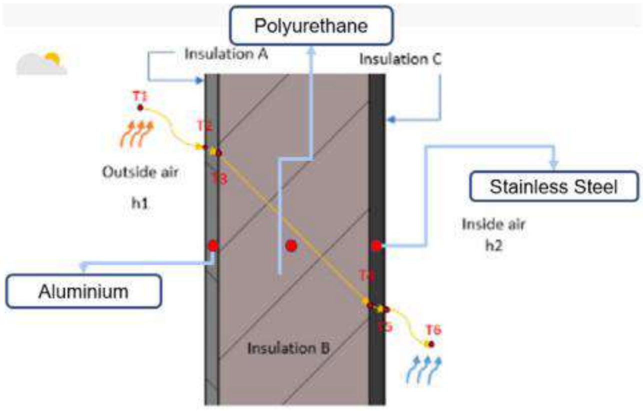

Figure 2. 3 Sandwich Wall (Budiyanto et al., 2023)

2.1.13 Common CFD Assumption in Data Center Studies

CFD analysis of data center server rooms typically relies on several simplifying assumptions to balance computational accuracy and efficiency. Depending on the objective of the analysis, simulations may be conducted under either steady-state or transient conditions. Steady-state operation is where transient effects such as time-dependent IT load variations and short-term environmental fluctuations are neglected. This assumption allows the simulation to represent average operating conditions that are relevant for thermal and airflow performance assessment. In the present study, steady-state simulations are employed to evaluate normal operating conditions, whereas transient simulations are additionally performed to investigate temporary air infiltration during door opening.

Airflow inside server rooms is generally modeled as an incompressible flow, as air velocities are relatively low and density variations due to temperature differences are small. In addition, turbulence effects are commonly represented using Reynolds-averaged turbulence models, which provide a practical balance between computational cost and predictive capability for indoor airflow applications.

To reduce modeling complexity, server racks are often represented as simplified volumetric heat sources with uniform heat generation, rather than explicitly modeling internal server components such as fans and heat sinks. Consequently, the CFD model focuses on predicting room-scale airflow and thermal behavior rather than the detailed thermal characteristics of individual electronic components. This simplification is widely accepted for evaluating environmental conditions in data center server rooms. These assumptions have been widely adopted in previous CFD-based data center studies and have been shown to provide sufficiently accurate predictions of airflow patterns and thermal behavior at the room level(Hassan et al., 2013)

2.2 Computational Fluid Dynamics

Computational Fluid Dynamics (CFD) is a numerical simulation technique used to analyze fluid flow, heat transfer, and the distribution of environmental parameters within a defined computational domain. CFD solves the governing equations of fluid motion and energy transport in a discretized form, allowing detailed three-dimensional visualization of airflow patterns, temperature fields, and humidity distribution. Due to its ability to capture complex flow behavior and thermal interactions, CFD has been widely applied in the analysis of data center server rooms to evaluate airflow effectiveness, identify recirculation zones, and predict the formation of thermal hotspots.

In this study, CFD is employed to analyze airflow, temperature, and relative humidity distribution inside a modular Floating Data Center server room under steady-state operating conditions. The CFD approach enables a detailed assessment of whether the applied airflow configuration is capable of maintaining acceptable environmental conditions at server inlet locations in accordance with ASHRAE guidelines.(Versteeg & Malalasekera, n.d.)

2.2.1 Governing Equations

The airflow inside the server room is modeled as an incompressible Newtonian fluid. Since the flow velocities are relatively low and density variations are negligible, the incompressible flow assumption is commonly adopted in data center CFD studies. The governing equations consist of the conservation of mass, momentum, and energy, which are solved simultaneously to obtain the airflow and thermal fields.

- Continuity Equation

The conservation of mass for incompressible flow is expressed as:

$$\nabla \cdot \vec{V} = 0 \qquad (2.2)$$

where $\vec{V}$ is the velocity vector of the airflow.

- Momentum Equation

The conservation of momentum is governed by the Navier–Stokes equations, which describe the balance between inertial forces, pressure forces, and viscous forces acting on the fluid:

$$\rho(\vec{V} \cdot \nabla)\vec{V} = -\nabla p + \mu \nabla^2 \vec{V} \qquad (2.3)$$

where ρ is the air density, p is the static pressure, and μ is the dynamic viscosity of air.

- Energy Equation

To evaluate temperature distribution and thermal hotspot formation, the energy equation is solved together with the airflow equations:

$$\rho c_p(\vec{V} \cdot \nabla T) = k\nabla^2 T + S_T \quad (2.4)$$

where c_p is the specific heat of air at constant pressure, k is the thermal conductivity, T is the temperature, and S_T represents the volumetric heat source term.

2.2.2 Turbulence Modelling

Airflow inside data center server rooms is generally turbulent due to the presence of multiple obstructions, such as server racks, aisles, and supply diffusers. To account for turbulence effects, a turbulence model is required. In this study, the standard k–ε turbulence model is employed due to its robustness, computational efficiency, and widespread application in indoor airflow and data center CFD studies.

The transport equations for turbulent kinetic energy (k) and its dissipation rate (ε) are expressed as:

$$\frac{\partial(\rho k)}{\partial t} + \nabla \cdot (\rho k\vec{V}) = \nabla \cdot \left[\left(\mu + \frac{\mu_t}{\sigma_k}\right)\nabla k\right] + G_k - \rho\varepsilon \quad (2.5)$$

$$\frac{\partial(\rho \varepsilon)}{\partial t} + \nabla \cdot (\rho \varepsilon\vec{V}) = \nabla \cdot \left[\left(\mu + \frac{\mu_t}{\sigma_\varepsilon}\right)\nabla \varepsilon\right] + C_{1\varepsilon}\frac{\varepsilon}{k}G_k - C_{2\varepsilon}\rho\frac{\varepsilon^2}{k} \quad (2.6)$$

where μ_t is the turbulent viscosity and G_k represents the production of turbulent kinetic energy. The standard model constants are adopted as recommended in the literature.

In this study, turbulence was modeled using the Realizable k-ε model coupled with Enhanced Wall Treatment (EWT). The Realizable k-ε model was selected because it provides improved predictions for flows involving recirculation, separation, and rotational effects compared with the Standard k-ε model. Enhanced Wall Treatment enables accurate near-wall flow prediction by combining a two-layer approach with enhanced wall functions, making it suitable for indoor airflow simulations where heat transfer between air and solid surfaces plays an important role.

2.2.3 Server Rack Heat Source Modelling

In order to reduce computational complexity while maintaining thermal accuracy, server racks are modeled as simplified solid volumes with uniform volumetric heat generation. This approach represents the total heat dissipation from IT equipment without explicitly modeling internal server components such as fans and heat sinks.

The volumetric heat source term S_T applied in the energy equation is defined as:

$$S_T = \frac{P}{V} \quad (2.7)$$

where P is the total heat dissipation of a server rack and V is the volume of the rack. This modeling approach has been widely adopted in CFD-based data center studies and provides a practical representation of IT heat loads at the room level (Hassan et al., 2013; Zhang et al., 2016).

2.2.4 Species Transport and Humidity Modelling

In addition to airflow and temperature, relative humidity distribution is analyzed in this study to assess environmental suitability for reliable server operation. Humidity transport is modeled using the species transport approach, where water vapor is treated as a passive scalar transported by airflow.

The transport equation for the mass fraction of water vapor (Y_v) is expressed as:

$$\frac{\partial(\rho Y_v)}{\partial t} + \nabla \cdot (\rho \vec{V} Y_v) = \nabla \cdot (\rho D \nabla Y_v) \quad (2.8)$$

where $D$is the mass diffusion coefficient of water vapor in air.

The relative humidity is then calculated based on the ratio between the partial pressure of water vapor and the saturation vapor pressure at the local temperature:

$$RH = \frac{p_v}{p_{vs}} \times 100\% \quad (2.9)$$

This approach allows humidity distribution to be evaluated consistently with the airflow and thermal fields obtained from the CFD simulation.

2.2.5 Steady State and Transient Assumption

The CFD simulation in this study is performed under steady-state conditions. Transient effects are considered only during infiltration simulation. This assumption is commonly adopted in data center CFD studies to evaluate average airflow behavior, temperature distribution, and humidity conditions under normal operating scenarios.

2.3 Bibliography Analysis

Figure 2.3 shows the bibliometric analysis of research publications related to CFD-based airflow and thermal studies in data center applications. The analysis indicates a general increasing trend in research activity over recent years, reflecting growing interest in data center thermal management and CFD methodologies. This trend highlights the

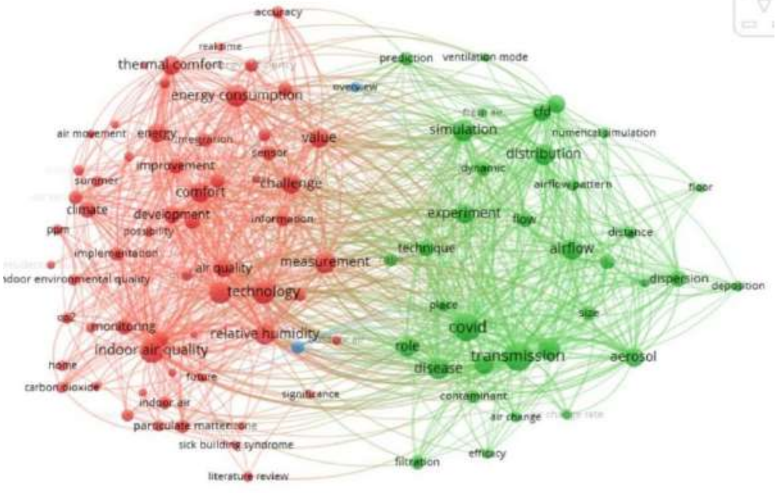

Figure 2. 4 Bibliometric Analysis

relevance of CFD as a tool for analyzing airflow and environmental conditions in data center server rooms, including emerging applications such as Floating Data Centers.

2.4 Related Studies

Table 2. 1 Related Studies

No	Title	Author(s);(Year)	Key Findings	Limitations
1	Temperature monitoring and CFD analysis of data center	Hassan et al. (2013)	CFD effectively identifies airflow patterns and thermal hotspots in server rooms	Humidity effects not considered.
2	CFD analysis of airflow and thermal management in data centers	Charara (2023)	CFD simulation confirmed that hot aisle–cold aisle configuration plays a critical role in controlling airflow patterns and inlet temperatures in server rooms.	Humidity effects were not considered and the study was conducted on a conventional land-based data center.
3	Environmental analysis of temperature and relative humidity in high heat-density indoor spaces	Seong et al. (2017)	The study highlighted that inappropriate relative humidity levels may lead to condensation and electrostatic discharge risks, even when temperature is controlled.	The study did not apply CFD simulation and did not analyze airflow distribution.
4	Simulation study on indoor air distribution and indoor humidity distribution using CFD	Zhang & Ryu (2021)	CFD with species transport successfully predicted coupled airflow, temperature, and humidity distribution and identified condensation behavior under different ventilation patterns.	The study was limited to small indoor spaces and was not applied to high heat-density data center or floating data center environments.

5	A Parametric Numerical Study of the Airflow and Thermal Performance in a Real Data Center for Improving Sustainability	Macedo et al. (2019)	CFD simulations showed that airflow distribution and rack thermal load variations strongly influence temperature distribution and hotspot formation in a real large-scale data center.	The study focused on airflow and thermal performance without considering relative humidity distribution.

Based on the reviewed related studies, CFD has been widely applied to analyze airflow and thermal behavior in data center server rooms, particularly in hot aisle–cold aisle configurations. Several studies also highlight the importance of airflow management and HVAC configuration in maintaining acceptable thermal conditions. However, most existing studies focus on land-based data centers and primarily evaluate airflow and temperature distribution, while studies that include relative humidity analysis remain limited. Therefore, this study aims to address this gap by investigating airflow, temperature, and relative humidity distribution in a modular server room of a Floating Data Center.

CHAPTER III

METHODOLOGY

3.1 Research Flowchart

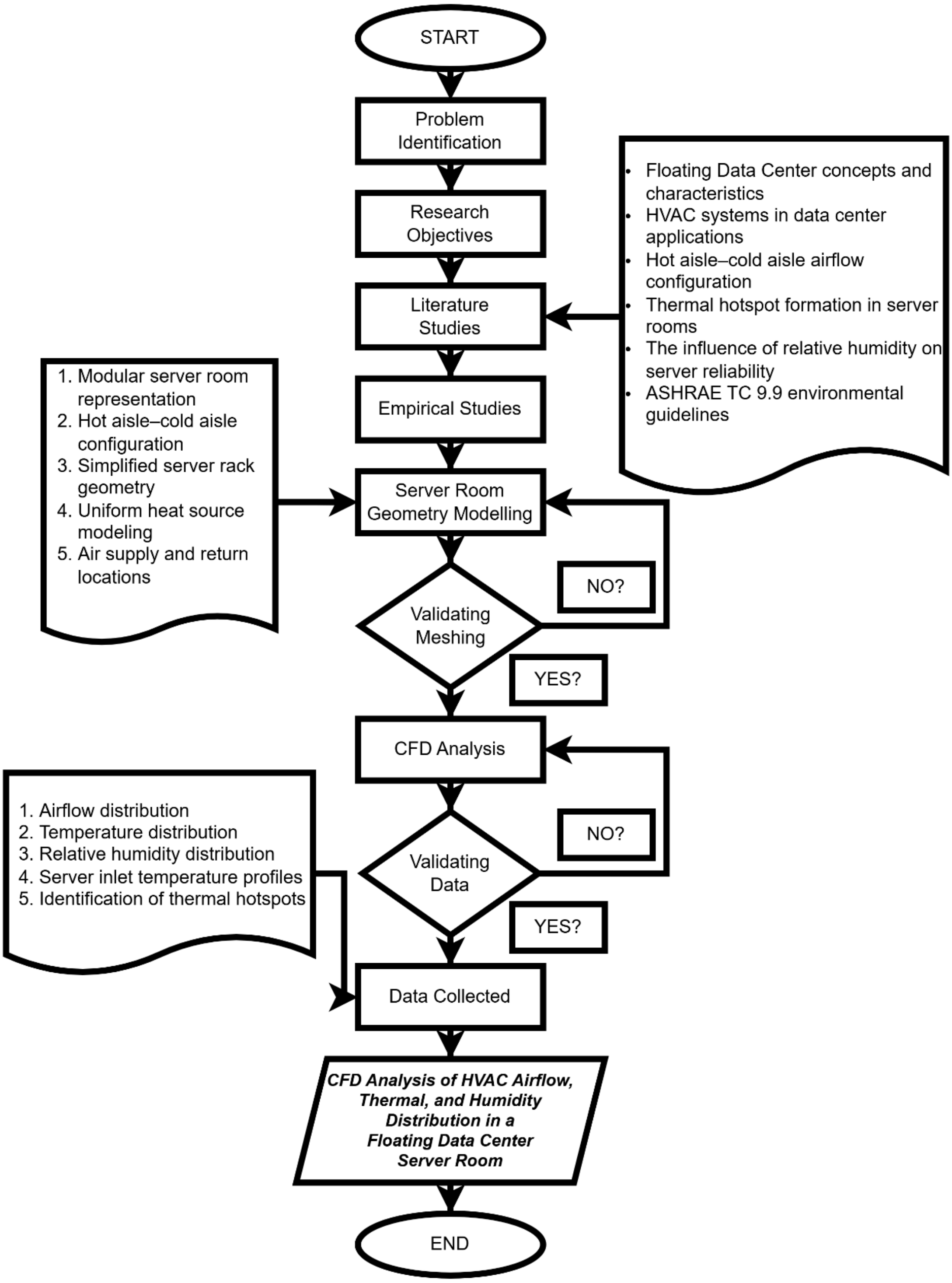

Figure 3. 1 Research Flowchart

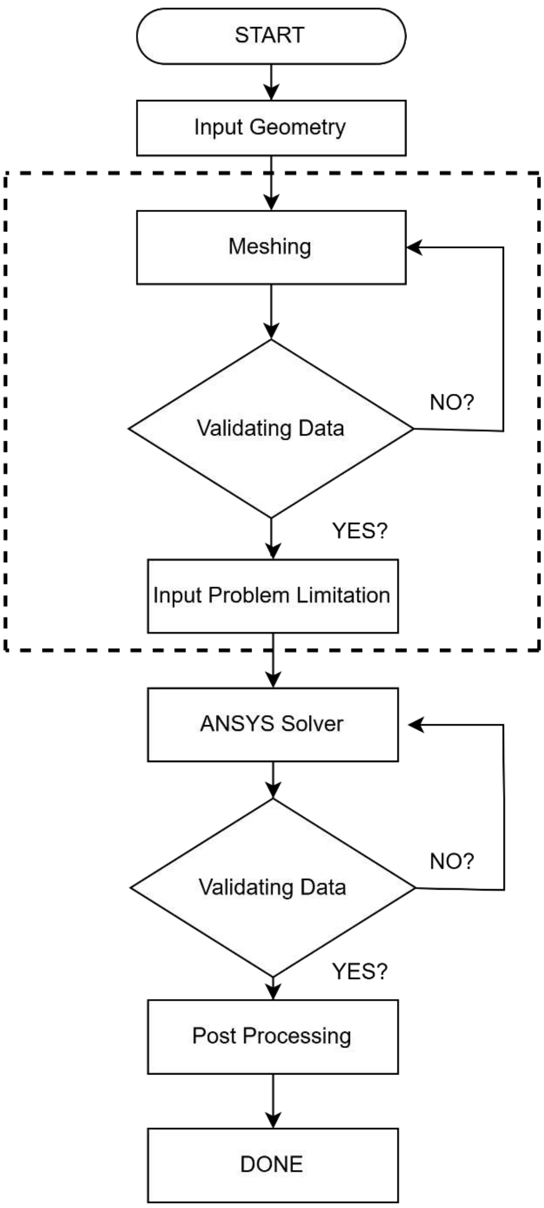

Figure 3. 2 Software Flowchart

3.2 Research Methodology

This research employs a numerical simulation approach using Computational Fluid Dynamics (CFD) to analyze airflow, temperature, and relative humidity distribution inside a modular Floating Data Center server room. CFD is selected as the primary research method due to its capability to provide detailed three-dimensional visualization of airflow behavior, thermal distribution, and moisture characteristics within enclosed spaces. The analysis is conducted under steady-state operating conditions using ANSYS Fluent as the simulation software. The methodology focuses on evaluating airflow patterns, identifying potential thermal hotspots at server inlets, and assessing whether the simulated temperature and humidity conditions remain within the recommended operational ranges of ASHRAE TC 9.9

3.3 Problem Identification

The problem addressed in this research arises from the challenge of maintaining uniform airflow distribution and stable thermal conditions within a floating data center server room. High server heat loads combined with limited space and compact layouts increase the risk of airflow recirculation and thermal hotspot formation. In addition, improper airflow patterns may lead to non-uniform humidity distribution, which can negatively affect server reliability. Therefore, it is necessary to evaluate whether the HVAC airflow configuration can provide adequate cooling performance and maintain acceptable temperature and humidity levels throughout the server room under steady-state conditions.

3.4 Literature Study

The literature study was conducted to establish the numerical modelling approach adopted in this research. Previous studies, international standards, equipment datasheets, and engineering references were systematically reviewed to determine the appropriate computational domain, modelling assumptions, physical models, boundary conditions, and evaluation criteria. Parameters that could not be measured directly were selected based on engineering judgement supported by validated literature and standardized guidelines.

Table 3. 1 Literature Study

Aspect	Basis	Reference
Server room layout	Representative modular server room	(Macedo et al., 2019)
Hot aisle–cold aisle configuration	Standard airflow arrangement	(ASHRAE Technical Committee 9.9, 2021)
Raised floor cooling	Previous CFD studies	(Herlin, 2008)
Turbulence model	Realizable k-ε	(Hassan et al., 2013; Macedo et al., 2019)
Heat source modelling	Volumetric heat source	(Hassan et al., 2013)
Humidity modelling	Species Transport	(Seong et al., 2017)
Wall construction	Sandwich wall	(Budiyanto et al., 2023)
Thermal assessment	Temperature & RH criteria	(ASHRAE Technical Committee 9.9, 2021)
Porous zone momentum source	Anisotropic porous resistance with fan momentum source	(Chethana & Sadashivegowda, 2024)

3.5 Geometry Modelling

The geometry model represents a modular server room of a 1 MW Floating Data Center configured using a hot aisle–cold aisle arrangement. Server racks are arranged in parallel rows, forming alternating cold aisles at the front and hot aisles at the rear to support efficient airflow management. Each server rack is modeled as a simplified solid volume without detailed internal components to reduce computational complexity while maintaining overall thermal behavior. The server room is equipped with a raised floor system, where conditioned air is supplied through perforated tiles located along the cold aisle. These tiles act as air supply outlets that distribute airflow into the server racks. The geometry is simplified to focus on airflow distribution and temperature characteristics while preserving key features required for CFD simulation.

Table 3. 2 Server Room Domain

Server Room Domain	
Area	25m x 8m
Height	2,9m
	Rack Clearance (1m); Racks (1,9m)
Cold Aisle width	1,2m
Hot Aisle width	1,2m
Room Configuration	10 Rows of Racks

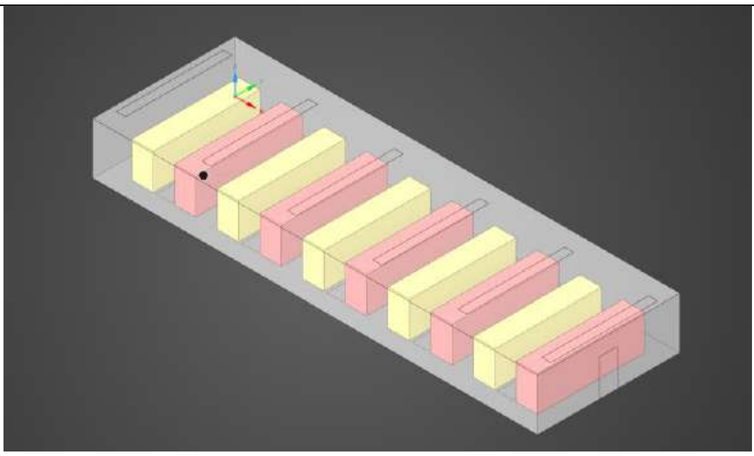

Figure 3. 3 Server Room Domain

Figure 3.3 illustrates the computational geometry used in this study, while the detailed dimensions and configuration of the server room are summarized in Table 3.1. The computational domain represents a modular server room arranged using a conventional hot aisle–cold aisle configuration with a raised-floor air distribution system. The model consists of multiple server racks positioned symmetrically to create alternating cold and hot aisles, enabling the simulation to capture the airflow circulation, heat transfer, and humidity distribution under representative operating conditions. The geometric dimensions and layout presented in Table 3.1 were defined based on common data center design practices and were used consistently throughout all CFD simulations.

Table 3. 3 Room Inlet Outlet

Room Inlet Outlet	
Inlet Length	6 m
Inlet Width	0,86 m
Inlet Area	5,16 m^2
Number of Inlets	5
Outlet Length	6 m
Outlet Width	0,5 m
Outlet Area	3 m^2
Number of Outlets	6

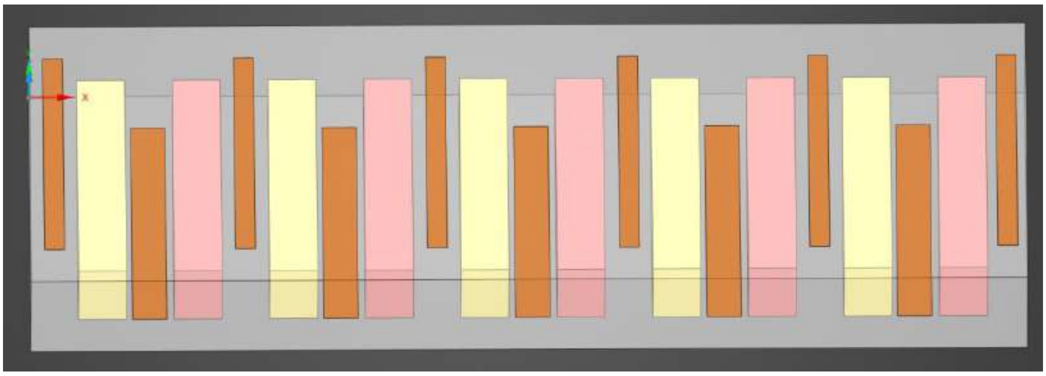

Figure 3. 4 Room Inlet and Outlet

Figure 3.4 illustrates the locations of the supply air inlet and return air outlet adopted in the computational domain, while the corresponding specifications are summarized in Table 3.2. The supply air inlet was positioned beneath the perforated floor tiles to represent the conditioned air delivered from the cooling system into the cold aisles. After passing through the porous server rows and absorbing the heat generated by the IT equipment, the heated air rises naturally toward the ceiling and is discharged through the return air outlet. This inlet–outlet arrangement represents the typical airflow pattern employed in raised-floor data centers and provides the basis for evaluating the thermal and airflow performance of the server room.

Table 3. 4 Room Door Specification

Room Door	
Type	Latham's Custom-Made Steel Thermally Rated Door
Width	1 m
Height	2,13 m
Area	2,13 m^2
Location	Width Side of the Room; Facing Aft of the Barge

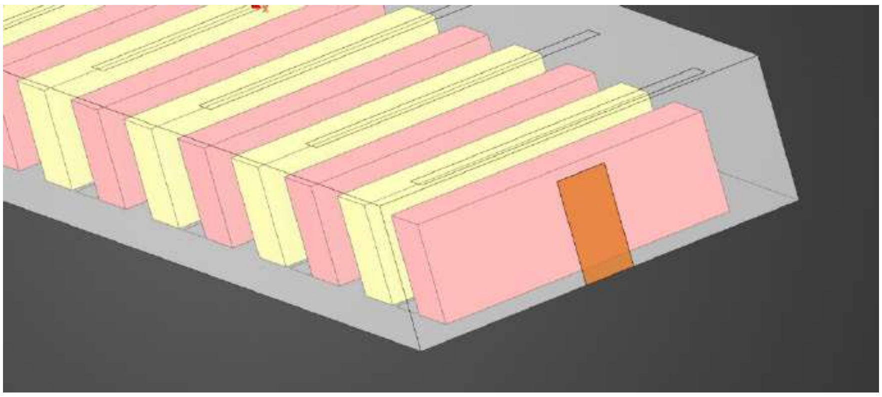

Figure 3. 5 Room Door

Figure 3.5 illustrates the location and dimensions of the server room access door, while the corresponding geometric specifications are summarized in Table 3.3. The access door was incorporated into the computational domain to represent the physical configuration of the server room and to facilitate the transient air infiltration analysis. Under normal operating conditions, the door remains closed and does not influence the steady-state simulations. However, during the transient simulation, the door opening is modeled as an additional airflow boundary to represent the ingress of ambient air into the server room. Therefore, the door geometry is included in the computational model to support both the steady-state and transient simulation scenarios.

Table 3. 5 Server Racks Specification

Server Racks	
Type	42U
Height	1,991m
Dimension	0,6m x 1,2m
Volume	1,443 m^3
Load	10 kW
Configuration	10 Racks per Row

Server Used	
Parameter	**Specification**
Server Model	Dell PowerEdge R760
ASHRAE Environmental Class	A2
Allowable Operating Temperature	10–35°C
Allowable Relative Humidity	8–80% RH, non-condensing

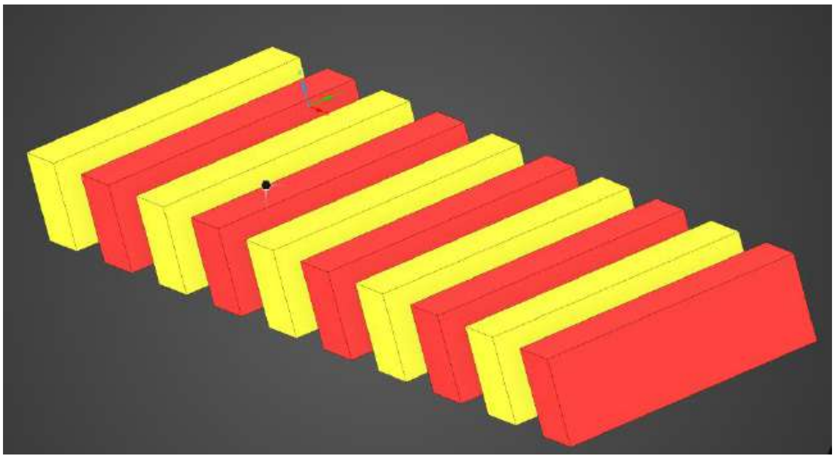

Figure 3. 6 Server Rows of Racks

Figure 3.6 presents the server row geometry incorporated into the computational domain, while the corresponding dimensions are summarized in Table 3.4. Each server row represents a group of IT racks arranged in a hot aisle–cold aisle configuration. To improve computational efficiency while preserving the overall airflow characteristics, the server rows were modeled as porous media instead of explicitly representing the internal server components. This approach enables the simulation to reproduce the pressure drop, airflow resistance, and heat generation associated with the server equipment while maintaining a reasonable computational cost.

Table 3. 6 Sandwich Wall Geometry and Layers

Wall Geometry		
Wall Length	2 m	
Wall Width	1 m	
Wall Area	2 m^2	
Wall Thickness	0.0811 m	
Sandwich Wall Layer Specification		
Polyurethane Coating	0,00005	Excluded
Epoxy Coating	0,00005	Excluded
Steel Sheet	0,0005	Included
Polyurethane Foam	0,08	Included
Aluminum Ceiling	0,0005	Included

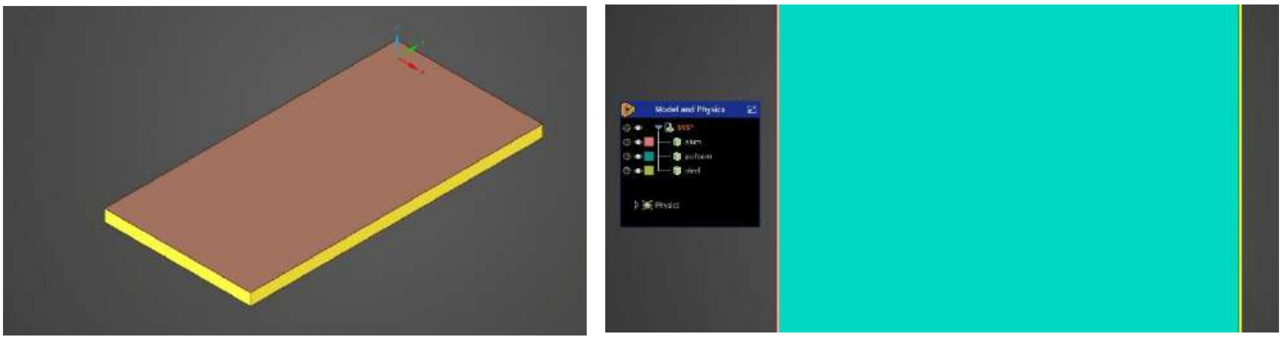

Figure 3. 7 Wall Geometry

Figure 3.7 illustrates the wall geometry incorporated into the computational domain, while the wall specifications are summarized in Table 3.5. The server room walls were modeled to represent the thermal boundary separating the conditioned indoor environment from the surrounding ambient conditions. The wall geometry and material properties were subsequently used in a separate wall heat transfer simulation to determine the inner wall surface temperature. The resulting wall temperature was then applied as the thermal boundary condition for the server room CFD simulations to account for heat transfer through the building envelope.

3.6 Mesh Generation

Mesh generation is performed using ANSYS Meshing to discretize the computational domain into finite control volumes. A three-dimensional unstructured mesh is applied to accommodate the complex geometry of the server room and server racks. Mesh refinement is applied in regions with expected high velocity and temperature gradients, such as near server racks and air supply outlets. The mesh is designed to balance computational accuracy and simulation efficiency while ensuring stable numerical convergence.

3.7 Governing Equations and Physical Model

The CFD simulation solves the governing equations of fluid flow and heat transfer, including the continuity equation, momentum equations, and energy equation. Air is modeled as an incompressible fluid with constant physical properties. Turbulence effects are accounted for using an appropriate turbulence model to capture airflow behavior within the enclosed server room. Relative humidity distribution is modeled through species transport, allowing moisture concentration to be calculated based on airflow and thermal conditions.

3.8 Boundary Conditions

Boundary conditions are defined to represent the operating conditions of the server room HVAC system. Conditioned air is supplied through perforated floor tiles located along the cold aisle and is modeled as a velocity inlet with specified airflow rate, temperature, and relative humidity. The airflow is assumed to be uniformly distributed across all perforated tiles. Heated air exits the domain through return outlets modeled as pressure outlets. The inlet temperature and relative humidity are defined based on ASHRAE recommended operating conditions and are used as baseline values for the simulation.

Server racks are modeled as volumetric heat sources with uniform heat generation to represent the total IT load, which is adjusted according to different operating conditions. Humidity is treated as a constant inlet condition and is included in the simulation to evaluate its distribution within the server room. In this study, the effect of wall heat transfer is not directly coupled with the main CFD simulation. Instead, a simplified or separate analysis is conducted to evaluate its contribution. This approach is adopted because the dominant heat source in the server room is the IT load, and including detailed wall conduction in the main simulation would increase computational cost without significantly affecting airflow and temperature distribution. Main boundary conditions are shown in Table 3.6.

Table 3. 7 Main Boundary Conditions

Category	Parameter	Value	Unit
Inlet	Velocity	2	m/s
Inlet	Temperature	20	C
Inlet	Humidity	30	%
Outlet	Pressure	0	Pa

3.9 Simulation

The CFD simulation is performed under steady-state conditions to evaluate the airflow and thermal behavior within the server room. The governing equations are solved using an appropriate turbulence model to capture the characteristics of indoor airflow. Two simulation scenarios are considered to represent different operating conditions of the server room. The first scenario corresponds to full load operation (70% IT load), while the second scenario represents partial load operation (50% IT load). These variations are applied by adjusting the heat generation of the server racks. The simulation results are analyzed in terms of temperature distribution, airflow pattern, and relative humidity distribution to assess the overall thermal performance of the server room.

In addition to the two steady-state scenarios developed to address the primary research questions, a supplementary transient simulation scenario was included in this study at the recommendation of the thesis advisor. This scenario evaluates the response of the server room environment to a temporary outdoor air infiltration event and is presented as an extension to the core research scope, providing additional insight into the operational resilience of the proposed airflow configuration. Heat source applied on each workload variation is described in Table 3.7.

Table 3. 8 Volumetric Heat Source

Load	Heat Source (W/m3)
70%	3418
50%	2441

3.10 Post Processing and Analysis

Post-processing is performed to analyze airflow patterns, temperature distribution, and relative humidity throughout the server room. Velocity vectors and streamlines are used to identify airflow paths and potential recirculation zones. Temperature contours are evaluated to detect thermal hotspots, particularly at server inlet regions. Relative humidity distribution is analyzed to assess environmental uniformity and compliance with ASHRAE guidelines. The results are used to evaluate the effectiveness of the airflow configuration in maintaining acceptable operating conditions.

3.11 Research Output and Conclusions

The expected outputs of this research include three-dimensional airflow visualization, temperature and humidity distribution maps, and identification of potential thermal hotspots within the server room. These outputs are used to assess whether the simulated environmental conditions meet recommended operational ranges and to provide insight into the effectiveness of airflow management strategies for Floating Data Center applications.

This page is intentionally left blank

CHAPTER IV

RESULTS AND DISCUSSIONS

4.1 Determination of CFD Simulation Input Parameters

This section presents the calculations performed to determine the input values applied to the boundary and cell zone conditions in the CFD simulation. The calculations were conducted to ensure that the simulation parameters represent the specified operating conditions of the server room. The calculated parameters were subsequently used as input values in the CFD model.

4.1.1 IT Load Distribution

The IT load represents the heat generated by the server equipment during operation. In this study, the floating data center is designed with a total IT capacity of 1 MW, distributed across 100 server racks arranged into 10 rows, with 10 racks in each row. The IT load was determined based on the design load factor and the selected server workload variations. The resulting heat load was subsequently used to determine the volumetric heat source applied to the server rack cell zones in the CFD simulation.

Table 4.1 IT Load Distribution

IT Load Distribution	
IT Load	1 MW
	1000000 W
Load Factor	0,7
Heat Load	700000 W
Server Volume	1,433 m^3
Total Volume	143,352 m^3

From the Data above we can calculate,

$$Q_{\mathrm{IT,design}} = 700\ \mathrm{kW}$$

Calculate for 70% Workload

$$Q_{\mathrm{IT,70\%}} = 700\ \mathrm{kW} \times 0{,}7$$

$$Q_{\mathrm{IT,70\%}} = 490\ \mathrm{kW}$$

Calculate the Volumetric Heat Source

$$q'''_{70\%} = \frac{490.000\ \mathrm{W}}{143{,}352\ \mathrm{m}^3}$$

$$q'''_{70\%} = 3.418{,}16\ \mathrm{W/m}^3$$

Table 4. 2 Volumetric Heat Source Applied

Load	Heat Source (W/m3)
70%	3418
50%	2441

4.1.2 Room Humidity

Humidity is an important environmental parameter in data center server rooms, as inappropriate moisture conditions may affect the reliability and operation of IT equipment. Therefore, the humidity input used in the CFD simulation was determined based on the specified server room environmental condition. The resulting humidity parameter was subsequently applied to the CFD model to evaluate the humidity distribution within the server room.

Table 4. 3 Humidity Data

Input Humidity	
Target	30%
Atmospheric Pressure	101325 Pa
Temperature	20 C
Saturation Vapor Pressure (20°C)	2338 Pa
Molecular Weight H_2O	18,015 g/mol
Molecular Weight Air	28,97 g/mol

From the data above we can calculate,

$$\omega = 0.622\left(\frac{0.30 \times 2{,}339}{101{,}325 - (0{,}30 \times 2{,}339)}\right)$$

$$\omega = 0{,}00433\ \text{kg}_{\text{water}}/\text{kg}_{\text{dry air}}$$

Then Calculate the Water Vapor Mass

$$Y_{H_2O} = \frac{0{,}00433}{1 + 0{,}00433}$$

$$Y_{H_2O} = 0{,}00431$$

Table 4. 4 Air Composition RH 30%

Air Composition RH 30%	
Water Vapor	0,00431
Oxygen	0,232
Nitrogen	0,7636

4.1.3 Outside Conditions

The outside air condition was determined to define the environmental boundary condition surrounding the server room. The specified outdoor temperature and relative humidity were used to calculate the corresponding water vapor mass fraction. The calculated value was subsequently applied as the outside air condition in the CFD simulation.

a. Outside Temperature

The outside air temperature was specified to represent the environmental condition surrounding the proposed floating data center during the CFD simulation. In accordance with SNI 6390:2020, the default outdoor design condition for cooling load calculation is 33°C dry-bulb (DB) and 27°C wet-bulb (WB). However, the standard also permits the use of more representative outdoor design conditions when justified by specific local climatic considerations. Since the proposed floating data center is intended to operate in Indonesian coastal waters, an outside air temperature of 32°C was selected based on representative coastal temperature data. This value is close to the default outdoor design temperature specified in SNI 6390:2020 and therefore provides a realistic environmental boundary condition for the CFD simulation while remaining consistent with the Indonesian design standard.

Table 4. 5 Outside Temperature

Outside Temperature	
Design Temperature	32 C

b. Outside Airflow

The outside airflow was determined to represent the external airflow condition surrounding the floating data center. The airflow parameter was calculated based on the specified outside air velocity and subsequently applied as an external boundary condition in the CFD simulation.

Table 4. 6 Outside Air Data

Outside Air	
Door Area	2,13 m^2
Wind Velocity	3 m/s
Opening Duration	15 s

From the data above we can calculate,

$$Q = 3 \times 2{,}13$$

$$Q = 6{,}39\ \mathrm{m}^3/\mathrm{s}$$

Convert to m^3/h,

$$Q_{m^3/h} = Q \times 3600$$

$$Q_{m^3/h} = 6{,}39 \times 3600$$

$$Q_{m^3/h} = 23{,}004 \text{ m}^3/\text{h}$$

Convert to CFM,

$$Q_{CFM} = Q \times 2118{,}88$$

$$Q_{CFM} = 6.39 \times 2118{,}88$$

$$Q_{CFM} = 13{,}539{,}64 \text{ CFM}$$

Table 4. 7 Outside Air

Outside Air	
Q (m^3/s)	6,39
Q (m^3/h)	23004
Q (CFM)	13539,64

c. Outside Humidity

The outside humidity was specified to represent the ambient moisture condition surrounding the floating data center. In this study, an outside relative humidity of **85%** was assumed as the representative ambient humidity condition and subsequently used to determine the water vapor mass fraction applied to the external airflow boundary in the CFD simulation.

Table 4. 8 Outside Humidity 85% Parameters

Outside Humidity 85% Parameters	
Atmospheric Pressure	101325
Temperature	32
Wind Speed	3
Saturation Vapor Pressure (32°C)	4758
Molecular Weight H_2O	18,015
Molecular Weight Air	28,97

From the data above we can calculate

$$Y_{H_2O} = \frac{(4044{,}30)(18{,}015)}{(4044{,}30)(18{,}015) + (101{,}325 - 4044{,}30)(28{,}97)}$$

$$Y_{H_2O} = 0{,}025200986$$

Table 4. 9 Air Composition RH 85%

Air Composition RH 85%	
Water Vapor	0,0252

Oxygen	0,232
Nitrogen	0,7428

4.2 Wall Heat Transfer Simulation

The wall heat transfer simulation was conducted to evaluate the thermal behavior of the server room wall under the specified outside environmental conditions. The simulation was performed separately from the server room airflow simulation to determine the temperature distribution across the wall structure. The resulting wall thermal condition was subsequently used to represent the effect of the outside environment on the server room CFD simulation.

4.2.1 Simulation Setup

The wall structure consists of multiple material layers with different thermophysical properties. The material properties were defined in the CFD model to represent the heat transfer characteristics of each wall layer. The density, specific heat, and thermal conductivity of the materials used in the wall simulation are presented in Table 4.10.

Table 4. 10 Material Properties

Material	Density (kg/m^3)	Specific Heat (J/kg.K)	Thermal Conductivity (W/m.K)
Steel	2719	871	247
PU Foam	30	1400	0,03
Aluminum	7850	500	50

The material properties were obtained from the ANSYS Fluent material database where available, while properties not provided in the database were manually defined based on the specified material data. These properties were subsequently assigned to the corresponding wall layers in the CFD model.

4.2.2 Mesh Generation and Mesh Quality

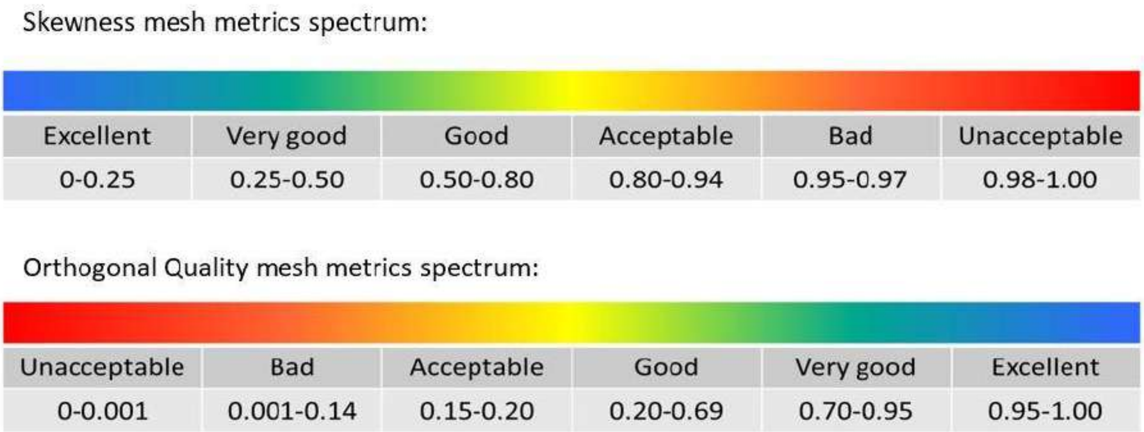

Figure 4. 1 Mesh Quality Recommendation

The mesh quality was evaluated to ensure that the computational domain was adequately discretized for the wall heat transfer simulation. The assessment was performed based on the orthogonal quality and skewness of the generated mesh. These mesh quality parameters were examined prior to the simulation to identify the overall quality of the computational cells and their suitability for the CFD analysis. The mesh quality assessment was conducted with reference to the mesh quality criteria provided by ANSYS, as presented in Figure 4.1.

Table 4. 11 Orthogonal Quality Results

Orthogonal Quality	
Max	1
Min	0,99947
Average	1
Category	Excellent

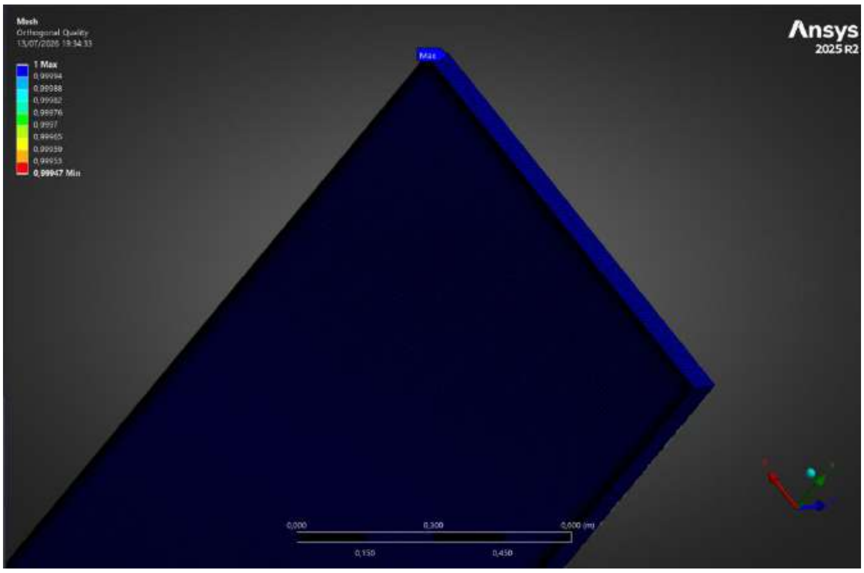

Figure 4. 2 Orthogonal Quality Contour

According to the orthogonal quality contour presented in Figure 4.2 and the statistical results summarized in Table 4.11, the generated mesh achieved a maximum orthogonal quality of 1, a minimum value of 0,99947, and an average value of 1. Based on the ANSYS mesh quality criteria presented in Figure 4.2, these values are classified as Excellent, indicating that the generated mesh possesses excellent geometric quality with minimal numerical distortion. Therefore, the mesh is considered suitable for the wall heat transfer simulation and is expected to produce reliable numerical results.

Table 4. 12 Mesh Skewness Results

Skewness	
Max	0,00000000013057
Min	0,0017537
Average	0,00010688
Category	Excellent

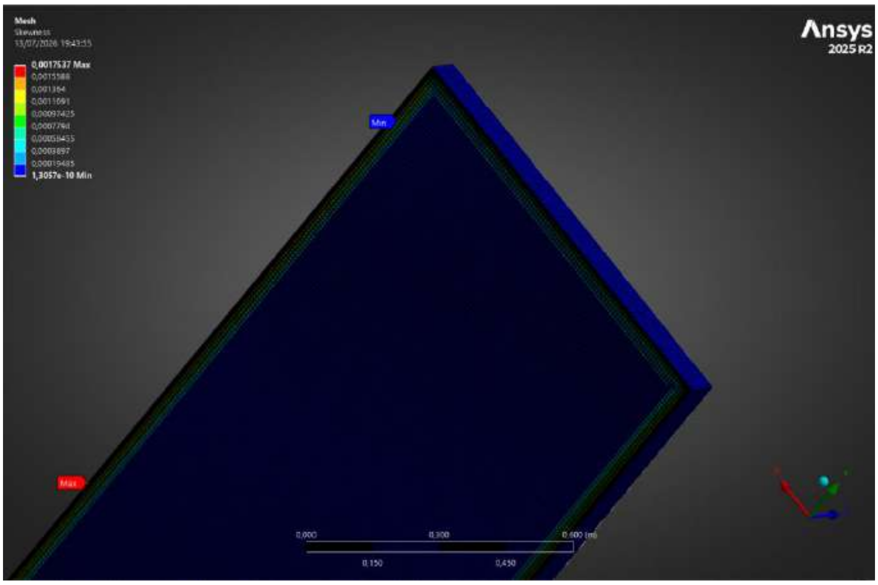

Figure 4. 3 Skewness Contour

According to the skewness contour presented in Figure 4.3 and the statistical results summarized in Table 4.12, the generated mesh achieved a minimum skewness of 1,3057 × 10^{-10}, a maximum value of 1,7537 × 10^{-3}, and an average value of 1,0688 × 10^{-4}. Based on the ANSYS mesh quality criteria presented in Figure 4.3, the obtained skewness values fall within the Excellent category, indicating that the computational cells exhibit extremely low geometric distortion. Therefore, the generated mesh is considered suitable for the wall heat transfer simulation and is expected to provide accurate and reliable numerical results.

Table 4. 13 Mesh Statistics

Mesh Statistics	
Nodes	381388
Elements	317030

As summarized in Table 4.13, the computational domain consists of 381388 nodes and 317030 elements. The generated mesh provides adequate spatial resolution to represent the wall geometry and capture the heat transfer behavior within the computational domain. Together with the excellent mesh quality obtained from the orthogonal quality and skewness evaluations, the mesh is considered suitable for the numerical simulation conducted in this study.

4.2.3 Boundary Conditions

The physical models and boundary conditions were defined to represent the thermal and environmental conditions applied to the wall heat transfer simulation. The selected physical models, together with the prescribed boundary conditions, were established to simulate the heat transfer process through the multilayer wall under the specified outdoor and indoor environmental conditions. The simulation settings applied in this study are presented in the following sections.

Table 4. 14 Model Setup

Model Setup	
Energy	On
Viscous	Laminar
Radiation	Discrete Ordinates (DO)

As presented in Table 4.14, the Energy equation was activated to account for heat transfer within the computational domain. In addition, the laminar viscous model and the Discrete Ordinates (DO) radiation model were employed to simulate conductive and radiative heat transfer through the wall.

Table 4. 15 Outer Wall Boundary

Outer Wall	
Thermal Condition	Convection
Heat Transfer Coefficient	15
Free Stream Temperature	32
BC Type	Opaque
Emissivity	0,8

As shown in Table 4.15, the outer wall boundary was assigned a convective thermal condition representing the ambient environment surrounding the floating data center. The applied heat transfer coefficient, free-stream temperature, wall type, and surface emissivity were specified to simulate heat transfer from the outdoor environment to the wall.

Table 4. 16 Inner Wall Boundary

Inner Wall	
Thermal Condition	Convection
Heat Transfer Coefficient	7
Free Stream Temperature	22
BC Type	Opaque
Emissivity	0,2

As shown in Table 4.16, the inner wall boundary was also defined using a convective thermal condition to represent the indoor server room environment. The specified heat transfer coefficient, free-stream temperature, wall type, and emissivity were applied to simulate heat transfer between the wall surface and the conditioned air inside the server room. These physical models and boundary conditions were subsequently used throughout the wall heat transfer simulation.

4.2.4 Simulation Convergence

The convergence of the wall heat transfer simulation was evaluated using the scaled residuals of the governing equations. The residual histories were monitored throughout the iterative process to verify the numerical stability of the solution. The convergence history obtained from the simulation is presented in Figure 4.4.

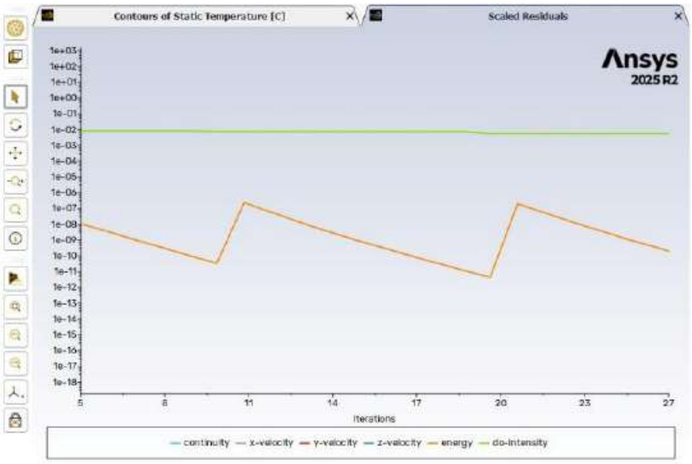

Figure 4. 4 Scaled Residual Graphic

As shown in Figure 4.4, the residual values exhibit a decreasing trend and remain stable throughout the iterative process. The continuity residual converged to approximately 10^{-3}, while the energy residual decreased to approximately 10^{-10}. Since the wall heat transfer simulation primarily involves conductive and radiative heat transfer, the energy equation is the most important convergence indicator. The very low energy residual indicates that the thermal solution has converged satisfactorily. Therefore, the simulation is considered numerically stable, and the resulting temperature distribution is suitable for further analysis.

4.2.5 Results and Discussions

This section presents and discusses the results of the wall heat transfer simulation. The analysis focuses on the temperature distribution across the multilayer wall and the thermal response of each wall layer under the specified indoor and outdoor boundary conditions. The simulation results are evaluated to assess the effectiveness of the wall structure in reducing heat transfer from the outdoor environment into the server room.

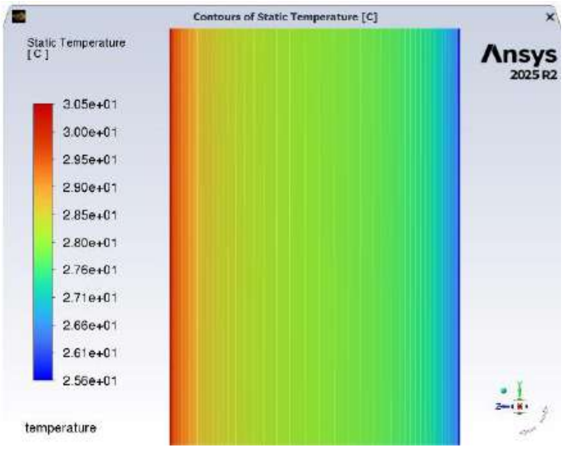

Figure 4. 5 Temperature Contour

Figure 4.5 illustrates the static temperature distribution across the multilayer wall obtained from the CFD simulation. The contour shows a continuous temperature gradient from the outer wall surface toward the inner wall surface, indicating heat transfer from the warmer outdoor environment to the conditioned server room. The highest temperature is observed at the outer wall surface, while the temperature gradually decreases through the wall thickness and reaches the lowest value at the inner wall surface. This gradual temperature reduction indicates that heat is transferred primarily by conduction through the wall layers. Furthermore, the absence of abrupt temperature discontinuities demonstrates that the thermal contact between adjacent wall layers is properly represented in the numerical model. Overall, the contour confirms that the multilayer wall effectively reduces heat transfer from the outdoor environment, thereby limiting the amount of heat entering the server room.

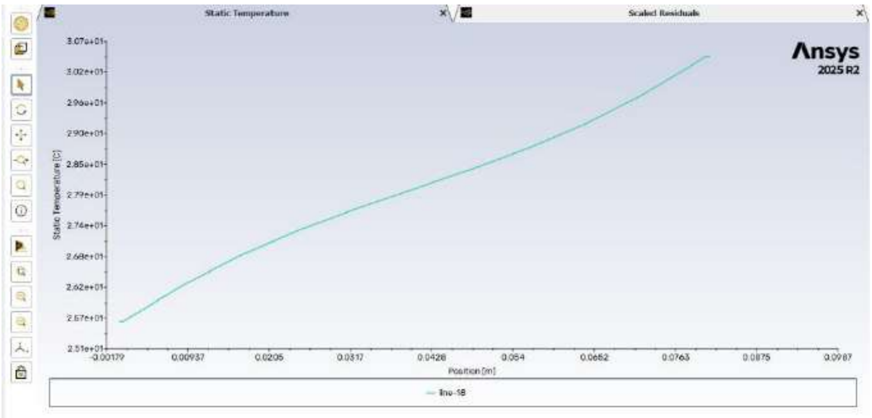

Figure 4. 6 Temperature Graphic

Figure 4.6 presents the temperature profile extracted along the wall thickness. The profile shows a continuous increase in temperature from the inner wall surface toward the outer wall surface. This trend is consistent with the applied boundary conditions, where the outdoor temperature (32 °C) is higher than the conditioned indoor temperature (22 °C). The smooth temperature gradient indicates that heat is transferred continuously through the multilayer wall by conduction without any abrupt temperature discontinuities between adjacent material layers. Furthermore, the change in the slope of the temperature profile reflects the difference in thermal conductivity of each wall material, indicating that each layer contributes differently to the overall thermal resistance of the wall.

Table 4. 17 Average Temperature on each Layer

Average Temperature	
Steel	30,20 C
PU Foam	28,05 C
Aluminum	25,86 C

As summarized in Table 4.17, the highest average temperature was observed in the steel layer at 30.20 °C, followed by the PU foam layer at 28.05 °C, while the aluminum layer exhibited the lowest average temperature of 25.86 °C. The progressive reduction in temperature across the wall layers confirms that heat is transferred from the outdoor environment toward the conditioned server room. The largest temperature drop occurs across the PU foam layer, indicating its dominant contribution to the overall thermal resistance due to its low thermal conductivity. Consequently, the multilayer wall configuration effectively reduces heat transfer through the wall, resulting in a lower temperature at the inner wall surface before heat enters the server room.

It should be noted that the inner wall boundary condition used in the wall heat transfer simulation assumed a free-stream indoor temperature of 22°C, representing a nominal conditioned-space target. This value was intentionally decoupled from the server room CFD results, which were solved separately to reduce computational cost. The subsequent server room simulations indicated a higher average room temperature (25.3–26.95°C), which differs from this initial 22°C assumption. However, since wall heat transfer contributes only a minor fraction of the total thermal load compared to the dominant IT heat generation, the resulting wall surface temperature is expected to be relatively insensitive to this discrepancy. This assumption is considered acceptable within the scope of this study but represents a simplification that could be refined through iterative coupling between the wall and room simulations in future work.

4.3 Server Room CFD Steady-State Simulation Setup

Following the determination of the CFD simulation input parameters presented in Section 4.1 and the wall heat transfer simulation described in Section 4.2, the server room CFD model was established to evaluate the thermal performance and airflow distribution within the floating data center. The same computational domain and general numerical model were employed for both the steady-state and transient simulations to maintain consistency across the investigated cases. This section describes the numerical model configuration, mesh quality, boundary conditions, and convergence criteria applied to the server room CFD simulations. Case-specific settings and modifications associated with the transient air infiltration scenario are further described in Section 4.6.

4.3.1 Simulation Setup

Prior to performing the CFD simulations, the numerical model was configured to represent the airflow and heat transfer phenomena within the server room. The simulation setup included the solver configuration, physical models, and cell zone settings applied to the computational domain. Each server row was modeled as a porous fluid zone with volumetric heat generation corresponding to the IT workload. An anisotropic viscous resistance was applied to the porous server rack zone to represent the directional airflow path through the server equipment. A relatively low resistance value was assigned in the streamwise direction (X) to allow cooling air to pass through the rack with minimal obstruction, consistent with the front-to-back airflow pattern of typical IT equipment. In contrast, significantly higher resistance values were applied in the transverse directions (Y, Z) to prevent unphysical lateral and vertical flow through the solid rack structure. The exact magnitude of the transverse resistance was not derived from a specific empirical measurement; rather, a sufficiently large value was selected to effectively suppress cross-flow relative to the streamwise direction, consistent with common directional porous-zone modeling practices adopted in CFD-based data center studies. In addition, a distributed momentum source of ±25 N/m³ was applied within the porous zone to represent the airflow induced by the internal server cooling fans, adopted from Chethana and Sadashivegowda (2024), who applied an equivalent fan momentum source in a porous-media rack model for data center airflow analysis. The general simulation setup adopted for the server room CFD model is summarized in Table 4.18.

Table 4. 18 Simulation Setup

Parameter	50% IT Workload	70% IT Workload	Unit
Solver Type	Pressure-Based		–
Time	Steady		–
Velocity Formulation	Absolute		–
Gravity (Z)	-9,81		m/s^2
Energy Equation	Enabled		–
Turbulence Model	Realizable k-ε		–
Wall Treatment	Enhanced Wall Treatment		–
Air Domain	Fluid		–
Server Row	Porous Fluid Zone		–
Porosity	0,70		–
Viscous Resistance (X)	1000		m^{-2}
Viscous Resistance (Y, Z)	$2{,}111 \times 10^8$		m^{-2}
Inertial Resistance (X, Y, Z)	0		m^{-1}
Momentum Source	±25		N/m^3
Energy Source	2441	3418	W/m^3

4.3.2 Mesh Generation and Mesh Quality

This section describes the mesh generation and quality assessment of the server room computational domain. Since the same computational domain was employed for both the steady-state and transient simulations, a consistent mesh configuration was maintained across all simulation cases. The mesh quality validation was performed using the same quality criteria illustrated in Figure 4.1. The resulting mesh quality statistics and spatial quality distributions are presented and discussed in this section.

Table 4. 19 Server Room Orthogonal Quality

Orthogonal Quality	
Max	1
Min	0,20216
Average	0,80409
Category	Very Good

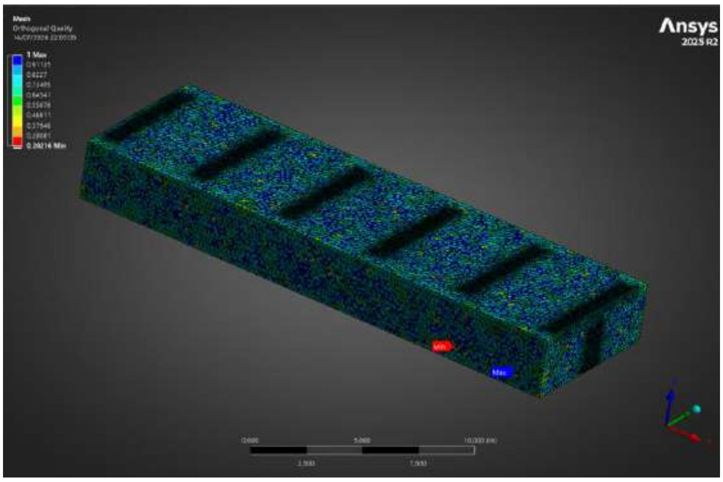

Figure 4. 7 Contour of Server Room Orthogonal Quality

The orthogonal quality results of the server room mesh are summarized in Table 4.19. The mesh achieved an average orthogonal quality of 0.80409, with a minimum value of 0.20216, resulting in a Very Good mesh quality category. The spatial distribution of the orthogonal quality throughout the computational domain is illustrated in Figure 4.7. As shown in the contour, the mesh quality is generally well distributed across the server room domain, with only limited regions exhibiting lower orthogonal quality. Therefore, the generated mesh is considered suitable for the subsequent CFD simulations.

Table 4. 20 Server Room Meshing Skewness

Skewness	
Max	0,79784
Min	1,3057e-010
Average	0,18974
Category	Excellent

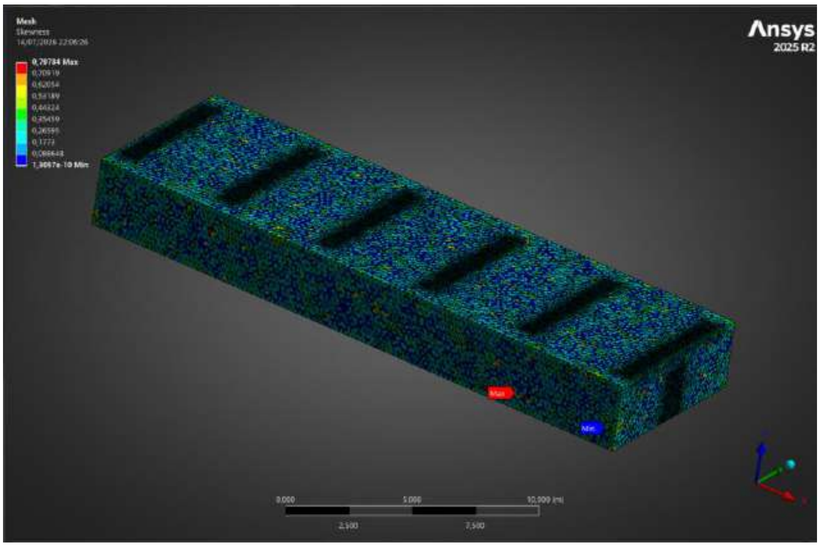

Figure 4. 8 Contour of Server Room Meshing Skewness

The skewness results of the server room mesh are summarized in Table 4.20. The mesh achieved an average skewness value of 0.18974, with a maximum value of 0.79784, resulting in an Excellent mesh quality category. The spatial distribution of mesh skewness throughout the computational domain is presented in Figure 4.8. The contour indicates that the majority of the computational domain consists of low-skewness elements, while higher skewness values are limited to localized regions. Based on these results, the mesh demonstrates acceptable element quality and is considered suitable for the subsequent CFD simulations.

Table 4. 21 Server Room Mesh Statistics

Mesh Statistics	
Nodes	610056
Elements	2101894

The overall mesh statistics of the server room computational domain are presented in Table 4.21. The generated mesh consists of 610056 nodes and 2101894 elements. The number of mesh elements provides sufficient spatial discretization to represent the server room geometry and the porous server rows. Combined with the orthogonal quality and skewness results previously discussed, the generated mesh is considered suitable for the subsequent CFD simulations.

4.3.3 Boundary Conditions

This section describes the boundary conditions applied to the server room CFD model. The boundary conditions were defined to represent the airflow and thermal operating conditions within the computational domain. The same baseline boundary configuration was employed for the steady-state and transient simulations, while an additional infiltration boundary was introduced for the transient case to represent outdoor air entering through the access door. The applied boundary conditions are summarized in the following table.

Table 4. 22 Boundary Conditions in Server Room

Boundary	Parameter	50% IT Workload	70% IT Workload	Unit
Supply Air Inlet	Boundary Type	Velocity Inlet	Velocity Inlet	–
	Velocity Magnitude	2	2	m/s
	Supply Air Temperature	20	20	°C
	H_2O Mass Fraction	0.0043	0.0043	–
	Turbulence Intensity	5	5	%
Return Air Outlet	Boundary Type	Pressure Outlet	Pressure Outlet	–
	Gauge Pressure	0	0	Pa
Server Room Wall	Thermal Condition	Temperature	Temperature	–
	Wall Temperature	25,86	25,86	°C

As summarized in Table 4.22, the server room was supplied with conditioned air through a velocity inlet boundary with an inlet velocity of 2 m/s and a supply air temperature of 20°C, representing the airflow delivered by the cooling system. The inlet moisture content was defined using an H_2O mass fraction of 0.0043 to account for the indoor humidity condition, while a turbulence intensity of 5% was specified to represent the incoming airflow characteristics. Air was discharged through a pressure outlet with a gauge pressure of 0 Pa, allowing the airflow to leave the computational domain under atmospheric conditions. In addition, a constant wall temperature of 25,86°C, obtained from the wall heat transfer simulation presented in Section 4.2, was applied to all server room walls to represent the heat transfer between the room enclosure and the surrounding environment.

4.3.4 Simulation Convergence

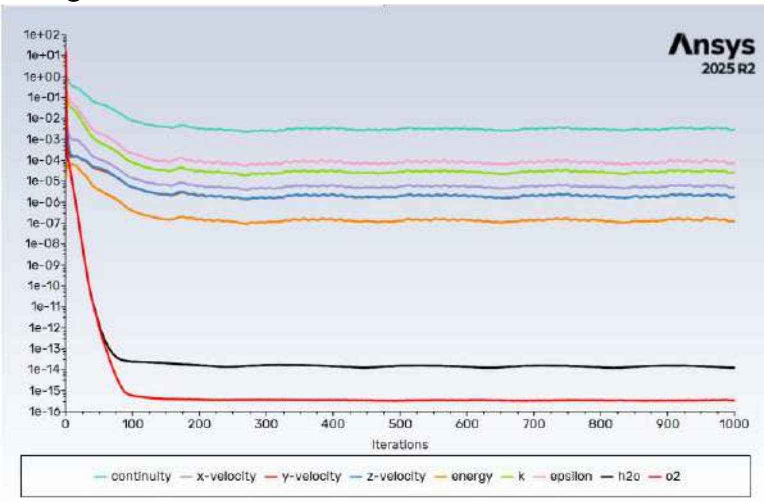

Figure 4. 9 Scaled Residuals of Server Room CFD Simulation

Figure 4.9 presents the convergence history of the residuals during the steady-state CFD simulation. The residuals for all governing equations decreased rapidly during the initial iterations and gradually approached stable values as the simulation progressed. At approximately 200 iterations, all residuals had reached a nearly constant level with only minor oscillations, indicating that the numerical solution had converged. The continuity residual stabilized at approximately 10^{-3}, while the momentum, turbulence, species, and energy residuals decreased to values ranging from 10^{-4} to 10^{-16}. These residual levels satisfy the convergence criteria adopted in this study, indicating that the simulation results are numerically stable and suitable for post-processing and further analysis.

4.4 Single Rack Simulation

Prior to the full server room simulations, a single rack CFD simulation was conducted as a preliminary assessment of the numerical model. The simulation was used to evaluate the airflow, temperature, and relative humidity distribution around a single server rack before applying the same modeling approach to the complete server room configuration.

4.4.1 Geometry

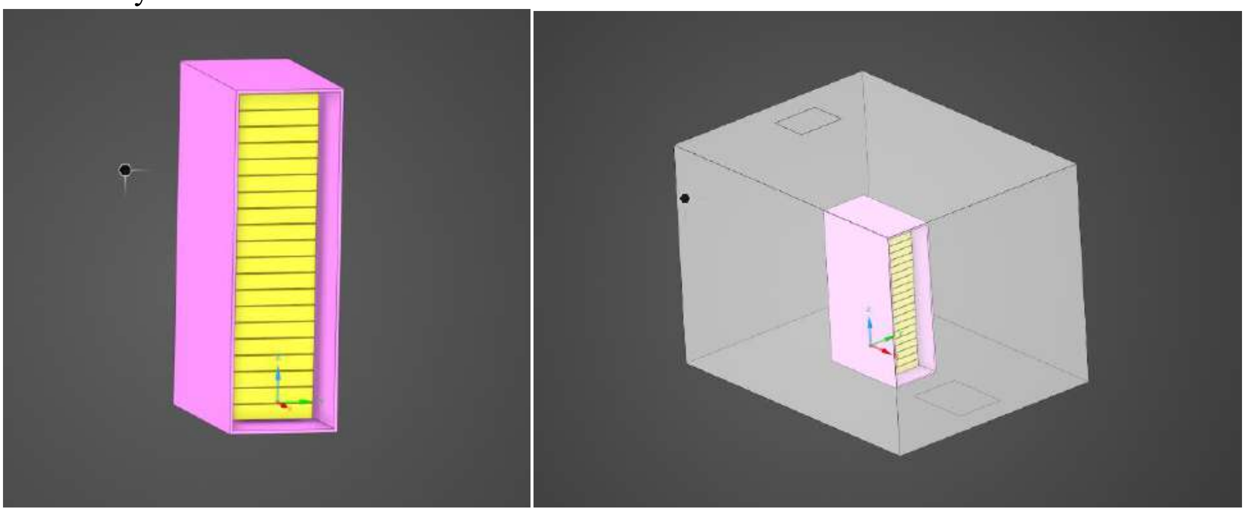

Figure 4. 10 Single Rack Geometry

Figure 4.10 presents the geometry of the single rack model developed for the preliminary CFD simulation. The model consists of a single 42U server rack positioned at the center of a computational domain with dimensions of 4.0 m × 3.0 m × 2.9 m. The overall rack dimensions were adopted from the manufacturer's datasheet to accurately represent the physical characteristics of a standard server rack, while the internal IT equipment was simplified into twenty server modules to represent the distributed heat sources within the rack. This simplification was implemented to preserve the overall thermal characteristics of the rack while reducing the computational complexity of the CFD model. In addition, the computational domain was designed with sufficient clearance surrounding the rack to allow the airflow to develop naturally before entering and after leaving the rack, thereby minimizing the influence of boundary effects on the simulation results. The detailed dimensions of the server rack and the computational domain used in this study are summarized in Table 4.23.

Table 4. 23 Single Rack Geometry Dimensions

Single Rack Geometry Dimensions		
Parameter	Value	Unit
Rack Height	1,991	m
Rack Width	0,6	m
Rack Depth	1,2	m
Rack Type	42U	
Number of Server Modules	20	units
Computational Domain Length	4.0	m
Computational Domain Width	3.0	m
Computational Domain Height	2.9	m

4.4.2 Mesh Generation and Quality

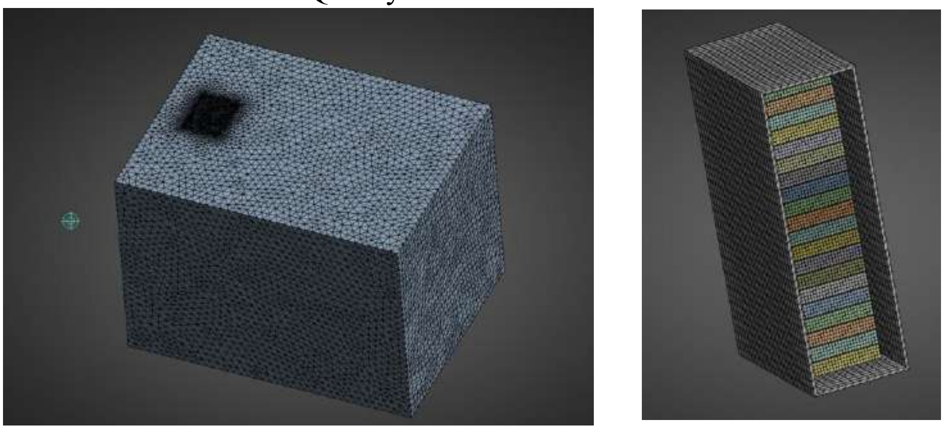

Figure 4. 11 Mesh Generation

The computational mesh generated for the single rack model is illustrated in Figure 4.11. An unstructured tetrahedral mesh was employed for the computational domain, while a structured hexahedral mesh was applied to the server rack and the twenty server modules to accurately capture the airflow and heat transfer around the heat-generating components. A finer mesh was applied in the vicinity of the server rack to improve the resolution of the flow field, whereas a relatively coarser mesh was used in regions farther from the rack to reduce the computational cost. As summarized in Table 4.24, the generated mesh consists of 848,494 elements and 218,014 nodes. The mesh quality was evaluated using the skewness and orthogonal quality metrics, yielding an average skewness of 0.29158 and an average orthogonal quality of 0.70272. According to the ANSYS Meshing quality criteria, these values fall within the very good mesh quality range, indicating that the generated mesh is suitable for obtaining stable and reliable CFD simulation results.

Table 4. 24 Mesh Statistics

Mesh Statistics	
Parameter	**Value**
Number of Elements	848,494
Number of Nodes	218,014
Average Skewness	0.29158
Average Orthogonal Quality	0.70272

4.4.3 Boundary conditions

The boundary conditions applied in the single rack simulation were defined to represent the operating conditions of an individual server within the data center environment. The simulation employed a uniform inlet air velocity and supply air temperature, while each server module was assigned a specified heat generation based on the assumed peak power, heat dissipation factor, and operating workload. The complete boundary conditions used in the simulation are summarized in Table 4.25.

Table 4. 25 Single Rack Boundary Conditions

Single Rack Geometry Dimensions		
Parameter	**Value**	**Unit**
Inlet Air Velocity	2.0	m/s
Supply Air Temperature	20	°C
Peak Power per Server	500	W
Heat Dissipation Factor	0,7	
Server Workload	70	%
Heat Generation per Server	245	W
Volumetric Heat Generation	7,950	W/m^3

Table 4.25 presents the boundary conditions applied in the single rack CFD simulation. The conditioned air entered the server rack with an inlet velocity of 2.0 m/s and a supply air temperature of 20°C, representing the cooling air delivered by the HVAC system. Each server was assumed to have a peak power consumption of 500 W, while a heat dissipation factor of 0.7 was adopted to represent the actual operating condition, corresponding to a 70% server workload. This assumption reflects that the servers operate below their maximum capacity under normal conditions.

Based on these operating parameters, the heat generated by each server was calculated to be 245 W, which represents the thermal load released into the surrounding airflow. To simplify the CFD model, this heat load was converted into a uniform volumetric heat generation of 7,950 W/m^3 and applied within the porous server rack region. These boundary conditions provide the thermal and airflow inputs required to evaluate the airflow characteristics, temperature distribution, and relative humidity within the

4.4.4 Airflow Distribution

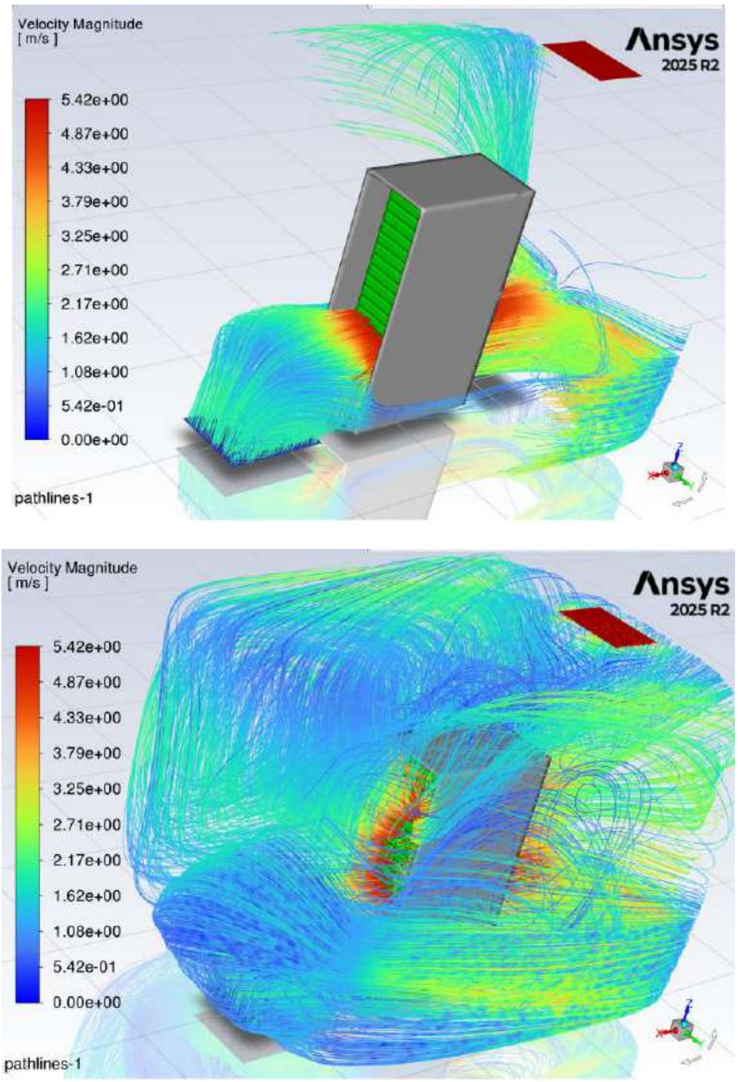

Figure 4. 12 Single Rack Airflow Pathlines

Figure 4.12 presents the airflow pathlines around the single server rack. Figure 4.12(1) illustrates the initial airflow entering the rack, while Figure 4.12(2) shows the complete airflow distribution within the computational domain. As shown in Figure 4.12(1), the supplied air is initially directed toward the lower front section of the rack before passing through the server modules. At this stage, the upper region of the rack appears to receive limited airflow because the incoming airflow has not yet fully developed. This behavior is expected since the simulation represents a single-rack configuration with only one air supply inlet and no additional airflow sources. As the airflow continues to develop, it spreads throughout the computational domain and reaches the upper section of the rack, as illustrated in Figure 4.12(2). The complete pathline distribution indicates that the cooling air is able to circulate around the entire rack and pass through the server modules without significant stagnant regions, demonstrating an effective airflow distribution within the computational domain.

4.4.5 Temperature Distribution

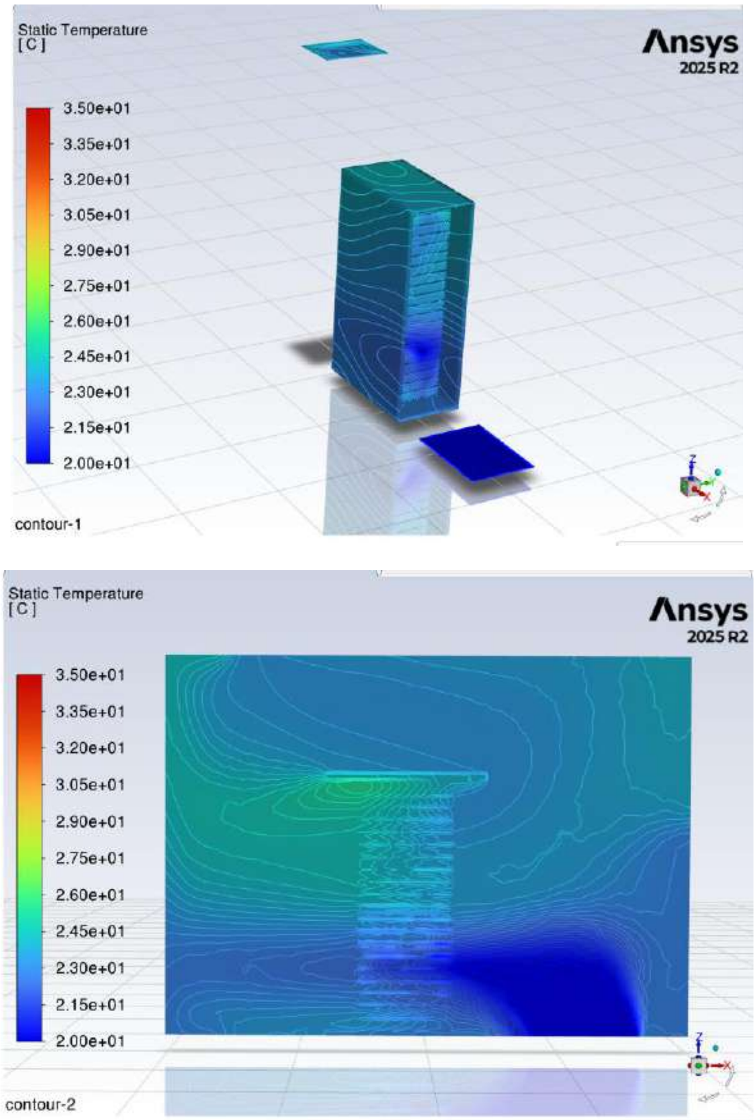

Figure 4. 13 Single Rack Temperature Contour Full View and Plane view

Figure 4.13 presents the temperature distribution obtained from the single rack simulation. Figure 4.13(1) shows the overall temperature distribution around the server rack, while Figure 4.13(2) presents the vertical cross-sectional temperature contour through the rack. The cooling air enters the computational domain at a supply temperature of 20°C and gradually absorbs heat generated by the server modules as it flows through the rack. Consequently, the air temperature increases from the lower section toward the upper section of the rack, producing a gradual temperature gradient without abrupt localized hot spots.

The sampled server temperatures at different rack elevations are summarized in Table 4.26. The bottom of the rack recorded a temperature of 23.53°C, which increased to 23.97°C at the middle section and reached 24.97°C at the top of the rack. This gradual increase indicates that the cooling air continuously absorbs heat while flowing upward through the rack. Nevertheless, the maximum server temperature remains below 25°C, indicating that the supplied cooling air effectively removes the generated heat and maintains a relatively uniform temperature distribution throughout the rack.

Table 4. 26 Server Temperature Sample

Server Temperature Sample	
Location	**Temperature (°C)**
Bottom of Rack	23,53
Middle of Rack	23.97
Top of Rack	24,97

4.4.6 Relative Humidity Distribution

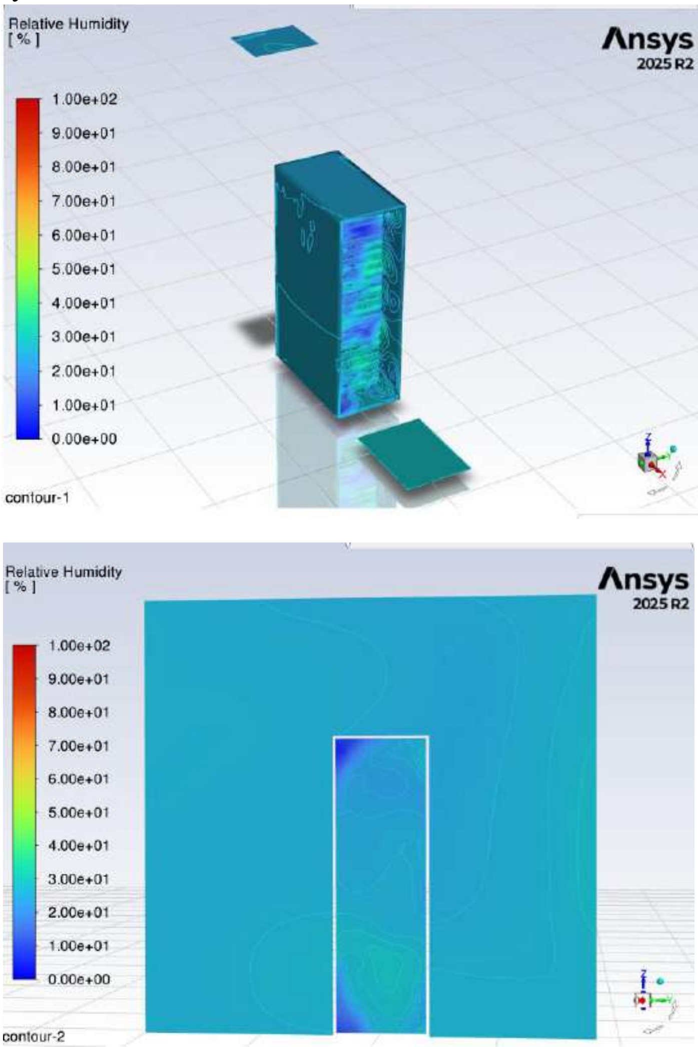

Figure 4. 14 Single Rack Relative Humidity Contour Full View and Plane view

Figure 4.14 presents the relative humidity distribution obtained from the single rack simulation. Figure 4.14(1) illustrates the overall relative humidity distribution within the computational domain, while Figure 4.14(2) presents the vertical cross-sectional view through the server rack. The results indicate that the relative humidity remains generally uniform throughout the computational domain, with only minor local variations observed around the server modules due to heat generation and the associated temperature increase. Despite these localized changes, no regions with excessive or insufficient relative humidity are identified. The supplied cooling air is therefore able to maintain stable humidity conditions around the server rack, indicating that the environmental conditions remain suitable for data center operation.

4.5 Case 1: Steady-State Simulation with 50% Workload

This section presents the CFD simulation results for the server room operating at a 50% IT workload under steady-state conditions. The simulation was performed using the common numerical model and boundary conditions described in Section 4.3, with the corresponding heat generation representing 50% of the total IT load. The airflow, temperature, and relative humidity distributions are evaluated to assess the thermal performance of the server room under partial-load operation.

4.5.1 Airflow Distribution

This section discusses the airflow characteristics inside the server room under the steady-state operating condition at a 50% IT workload. The airflow distribution is evaluated to determine whether the supplied cooling air is evenly distributed throughout the cold aisles, passes effectively through the server rows, and is subsequently transported toward the return outlet. The analysis is presented through airflow pathlines, velocity contours, velocity vectors, and quantitative airflow parameters to provide a comprehensive understanding of the cooling air circulation within the server room.

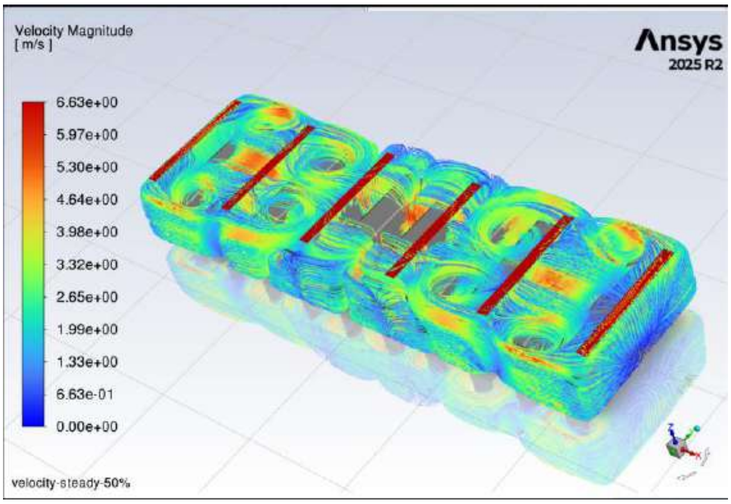

Figure 4.15 Pathline of Airflow Distribution Steady-State Load 50%

Figure 4.15 illustrates the airflow pathlines within the server room under the steady-state 50% IT workload. The supplied air enters the room through the floor inlets and is distributed into the cold aisles before passing through the porous server rows. The airflow is then directed toward the hot aisles and finally rises toward the ceiling return outlet. Several recirculation regions are observed above the server rows, which are expected due to the interaction between the supply airflow and the upward movement of heated air. In summary, the airflow pattern indicates that cooling air is able to circulate throughout the entire server room without significant stagnant regions.

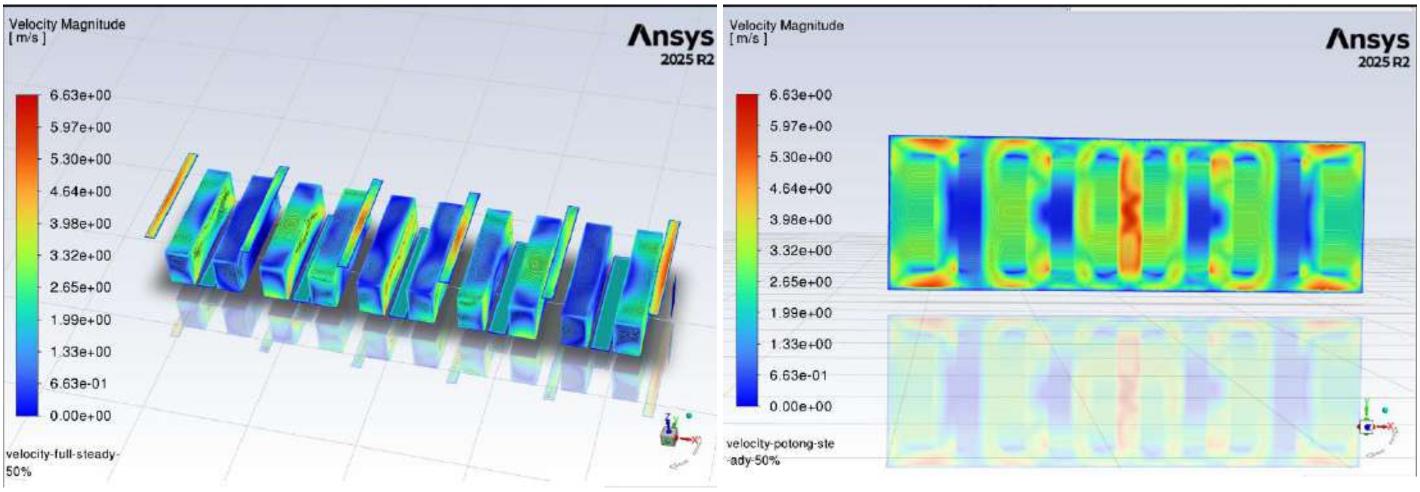

Figure 4. 16 Contour of Velocity Around Steady-State Load 50%

Figure 4.16 presents the velocity magnitude contour within the computational domain. The airflow velocity ranges from approximately 0 to 6.63 m/s, with the highest velocities observed near the supply openings and the cold aisle entrances. Lower velocities are observed after the airflow passes through the porous server rows, indicating a reduction in airflow momentum caused by the flow resistance of the server racks.

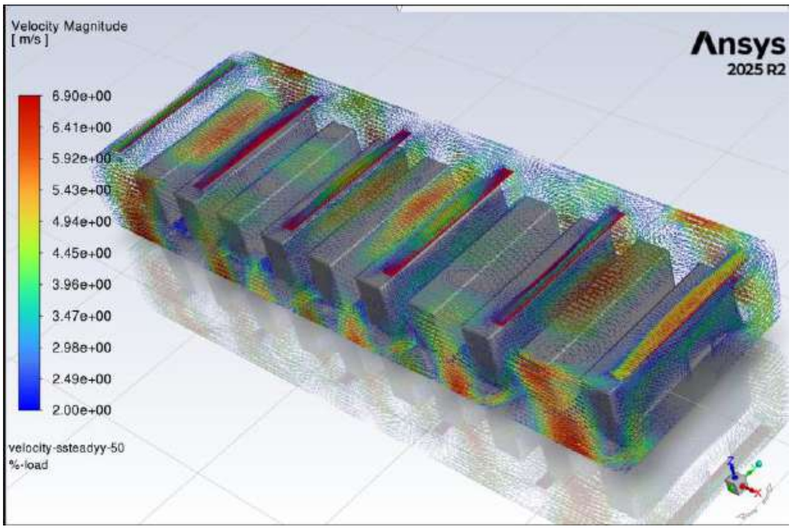

Figure 4. 17 Velocity Vector Along the Domain Steady-State Load 50%

Figure 4.17 illustrates the airflow vectors throughout the server room. The vectors indicate that the primary airflow direction remains from the floor supply toward the server rows before moving upward to the ceiling return outlet. The airflow velocity shown in the vector field ranges approximately from 2,0 to 6,9 m/s, while localized recirculation zones are observed above several server rows due to flow interaction

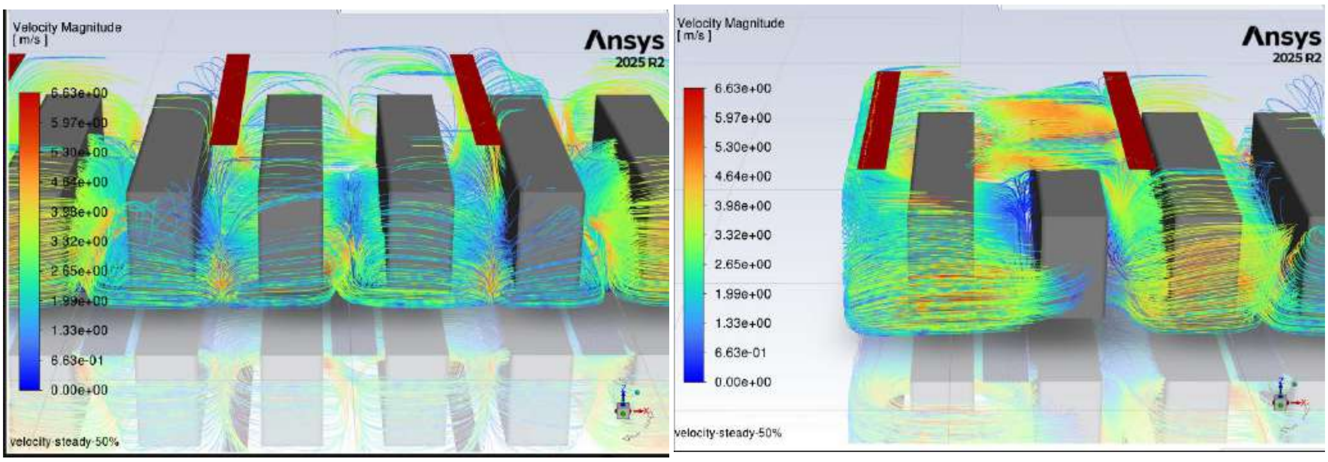

Figure 4. 18 Pathline Through The Racks Steady-State Load 50%

Figure 4.18 provides a closer view of the airflow passing through the server rows. The airflow enters the front side of each porous server row, penetrates the rack region, and exits toward the hot aisle. The streamline pattern indicates that airflow is continuously distributed across the server rows without significant blockage or stagnant regions.

Table 4. 27 Airflow Characteristics

Airflow Characteristics	
Surface	Area-Weighted Average Velocity (m/s)
Inlet	2
Outlet	3,467
Left Server Rows	1,756
Right Server Rows	1,7385

Table 4.27 presents the area-weighted average airflow velocities at several key locations within the server room. The prescribed inlet velocity is maintained at 2 m/s, while the average outlet velocity increases to 3,467 m/s due to the reduction of the effective flow area at the return outlet. The average airflow velocities through the left and right server row groups are 1,756 m/s and 1,739 m/s, respectively. The difference between both groups is only 0,017 m/s, corresponding to less than 1%, indicating that the supplied cooling air is distributed almost uniformly across both sides of the server room. This balanced airflow distribution suggests that each server row receives a comparable amount of cooling air under the steady-state operating condition.

Based on the airflow visualization and quantitative results, the steady-state simulation at a 50% IT workload demonstrates that the proposed cooling configuration is capable of distributing cooling air effectively throughout the server room. The airflow follows the intended cold aisle–hot aisle arrangement, passes continuously through the porous server rows, and is subsequently discharged through the ceiling return outlet. In addition, the small mass imbalance and the nearly identical average airflow velocities between the left and right server row groups indicate that the airflow remains well balanced within the computational domain. These results provide a reliable basis for evaluating the thermal performance of the server room, which is further discussed in the following section through the temperature distribution analysis.

4.5.2 Temperature Distribution

The temperature distribution analysis was conducted to evaluate the thermal condition of the server room under steady-state operation at 50% server load. The analysis focuses on the temperature distribution across the server room, server rows, and cold and hot aisle regions to identify the thermal response of the airflow after passing through the server racks. The temperature contours and pathlines are presented to illustrate the spatial temperature variation and the heat transfer characteristics within the server room.

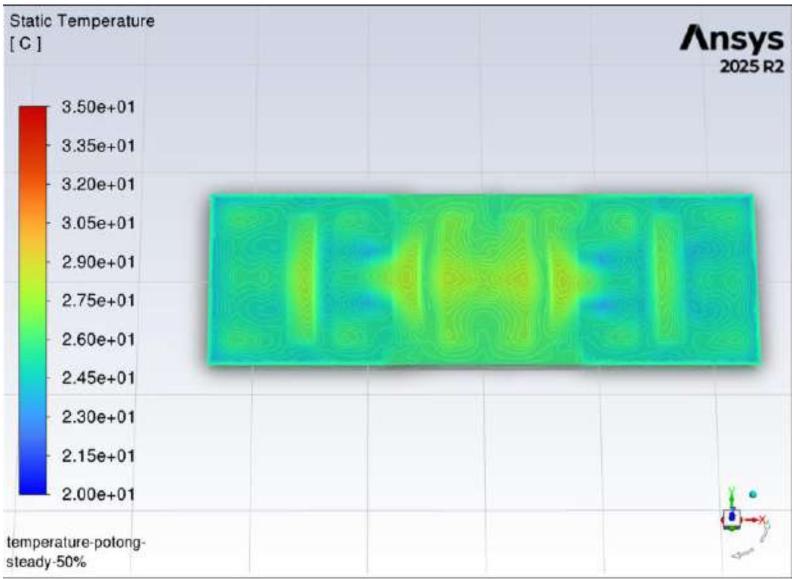

Figure 4. 19 Temperature Contour Plane on Server Room Steady-State 50%

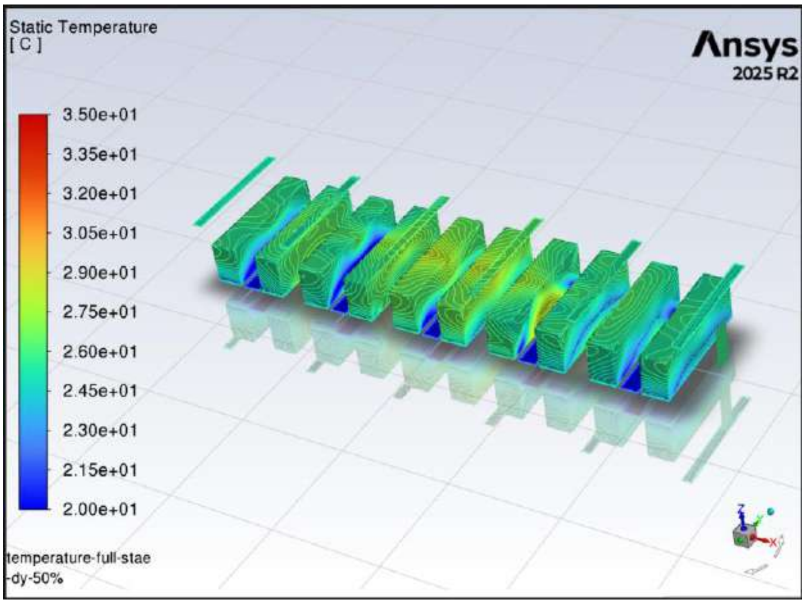

Figure 4. 20 Temperature Contour on Server Room Steady-State 50%

Figures 4.19 and 4.20 present the temperature distribution within the server room under steady-state operation at 50% server load. Figure 4.14 illustrates the overall temperature variation across the server room domain, while Figure 4.15 provides a more detailed visualization of the temperature distribution around the server rows. The results indicate that the supplied air at approximately 20°C enters the server room and subsequently experiences a temperature increase as it circulates through the server rows and absorbs the heat generated by the server equipment. The temperature distribution is predominantly observed within the range of approximately 24,5°C to 29°C, with localized higher-temperature regions occurring around several server rows. This temperature variation demonstrates the thermal interaction between the supplied cooling air and the heat generated by the server racks under the 50% load condition.

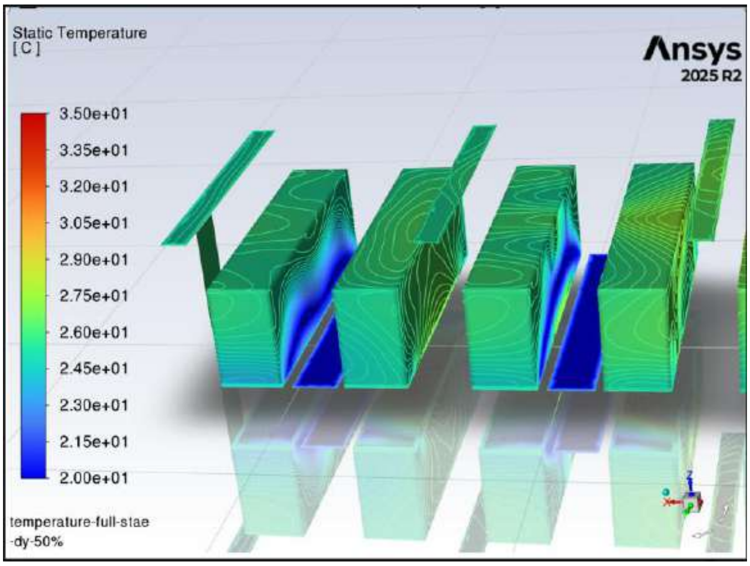

Figure 4. 21 Temperature Contour around The Racks Steady-State 50%

Figure 4.21 provides a closer view of the temperature distribution around the server rows under the 50% load condition. The contour indicates a gradual temperature increase from the lower section of the server racks toward the upper region as the cooling air passes through and absorbs the heat generated by the servers. Localized temperature variations are also observed between adjacent server rows, indicating the influence of airflow circulation and mixing within the aisle regions on the resulting thermal distribution.

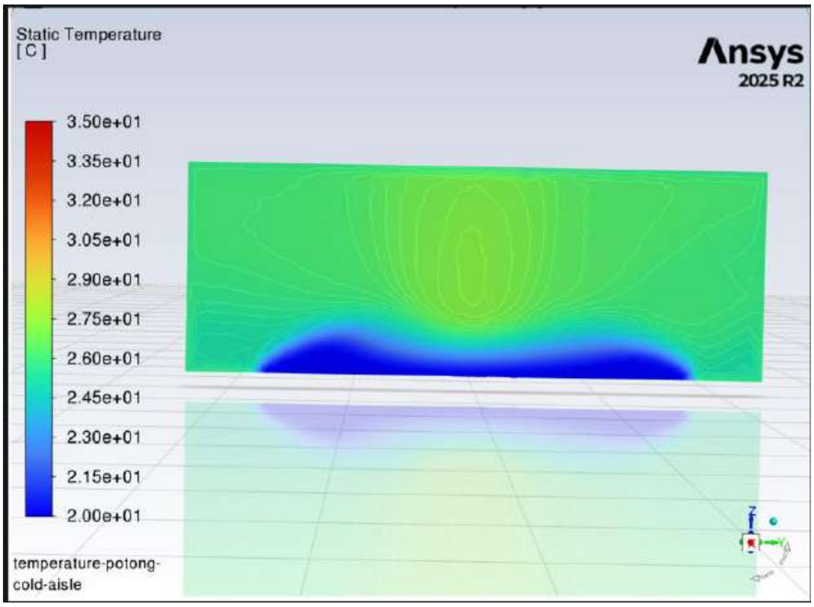

Figure 4. 22 Temperature Contour Plane on Cold Aisle Steady-State 50%

Figure 4.22 presents the temperature distribution within the cold aisle region under steady-state operation at 50% server load. Lower-temperature air is concentrated near the lower section of the cold aisle, corresponding to the cooling air supplied into the server room. As the air moves upward within the aisle, the temperature gradually increases due to airflow mixing and thermal interaction with the surrounding server rows. The contour shows that the cold aisle temperature is predominantly distributed within approximately 24,5°C to 29°C, with the higher-temperature region occurring in the upper section of the aisle.

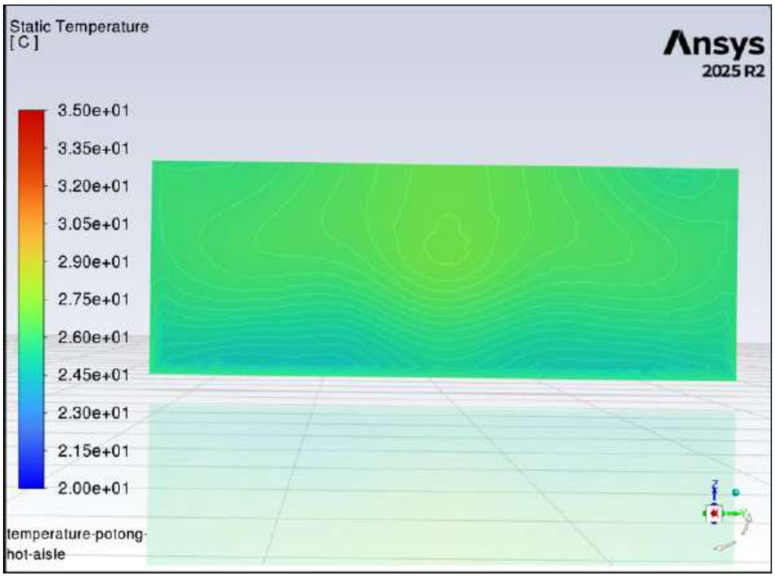

Figure 4. 23 Temperature Contour Plane on Hot Aisle Steady-State 50%

Figure 4.23 presents the temperature distribution within the hot aisle region under steady-state operation at 50% server load. Compared with the cold aisle, a higher temperature distribution is observed throughout the hot aisle as the air has absorbed heat while passing through the server racks. The temperature gradually increases toward the upper and central regions of the aisle, with the contour predominantly distributed within approximately 26°C to 30°C. This distribution indicates the accumulation of heated air discharged from the server rows and its subsequent movement within the hot aisle region.

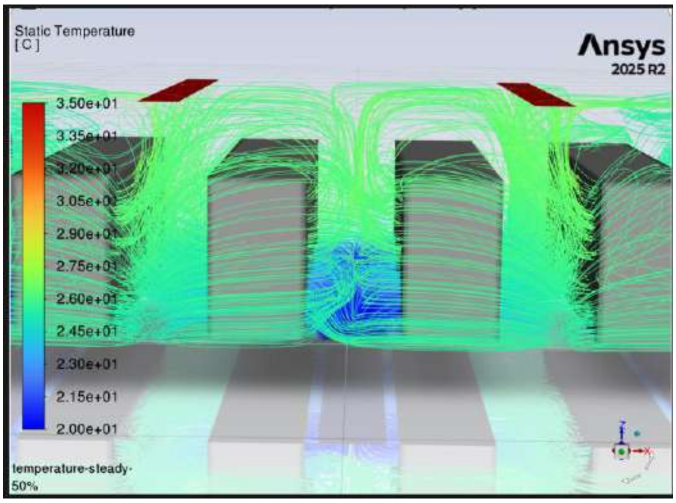

Figure 4. 24 Temperature Pathline Along the Room Steady-State 50%

Figure 4.24 illustrates the temperature variation along the airflow pathlines within the server room under steady-state operation at 50% server load. The pathlines show that the cooling air is initially supplied at a lower temperature and subsequently experiences a gradual temperature increase as it flows through the porous server rows. After absorbing the heat generated by the server equipment, the warmer airflow is discharged into the hot aisle and moves upward toward the return outlet. The variation in pathline temperature demonstrates the heat absorption process of the supplied cooling air and confirms the relationship between the airflow pattern and the resulting thermal distribution within the server room.

Table 4. 28 Case 1 Temperature

Temperature	
Parameter	**Temperature (°C)**
Inlet Average Temperature	20
Outlet Average Temperature	25,72
Left Server Rows Average Temperature	25,43
Right Server Rows Average Temperature	25,47
Cold Aisle Average Temperature	25,57
Hot Aisle Average Temperature	25,95
Minimum Server Row Temperature	20,04
Maximum Server Row Temperature	28,79

Table 4.28 summarizes the thermal characteristics of the server room under steady-state operation at 50% server load. The results show that the supplied cooling air enters the server room at 20°C and leaves the domain with an average temperature of 25,72°C after absorbing heat from the server rows. The average temperatures of the left and right server rows are 25,43°C and 25,47°C, respectively, indicating a nearly uniform thermal distribution between both server-row arrangements. Similarly, the average temperatures within the cold aisle and hot aisle are 25,57°C and 25,95°C, respectively, confirming that the hot aisle maintains a higher temperature due to the accumulation of heat rejected from the server racks. Furthermore, the minimum and maximum temperatures observed on the server rows are 20,04°C and 28,79°C, respectively, demonstrating that the server-room temperature remains well below the upper limit of the temperature scale applied in this study. These results indicate that the cooling airflow effectively absorbs and transports the generated heat while maintaining a relatively uniform thermal distribution throughout the server room under the 50% load condition.

The temperature distribution under the 50% server load condition demonstrates a consistent thermal response throughout the server room. The supplied cooling air undergoes a gradual temperature increase as it passes through the server rows and absorbs the generated heat, resulting in a distinguishable temperature variation between the cold and hot aisle regions. Although the overall thermal distribution remained relatively balanced, a slightly higher localized temperature was observed at Left Rack 3 and Right Rack 3, corresponding to the third rack position from the inlet on each side of the room. This was attributed to exhaust air discharged from neighboring racks that partially recirculated toward this row position instead of flowing directly to the designated outlet, indicating that localized airflow recirculation rather than the heat load itself contributed to this minor temperature increase, which nonetheless remained within the acceptable operating range. The relatively similar average temperatures between the left and right server rows also indicate a balanced thermal distribution across the server arrangement. These results demonstrate the heat removal characteristics of the proposed cooling configuration under partial-load operation and provide the basis for the subsequent analysis of relative humidity distribution within the server room.

4.5.3 Relative Humidity Distribution

The relative humidity distribution analysis was conducted to evaluate the moisture condition within the server room under steady-state operation at 50% server load. The analysis focuses on the spatial variation of relative humidity across the server room, particularly around the server rows and aisle regions, as influenced by the airflow and temperature distribution. The relative humidity contours and pathlines are presented to illustrate the moisture distribution characteristics and the interaction between thermal conditions and air humidity within the server room.

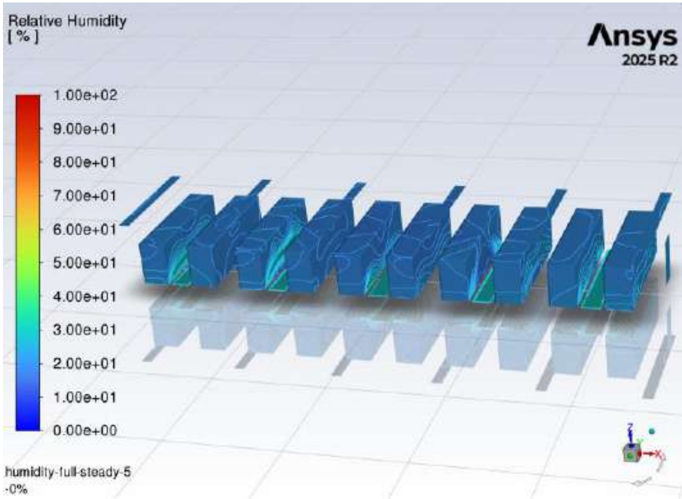

Figure 4. 25 Relative Humidity Countour Steady-State 50%

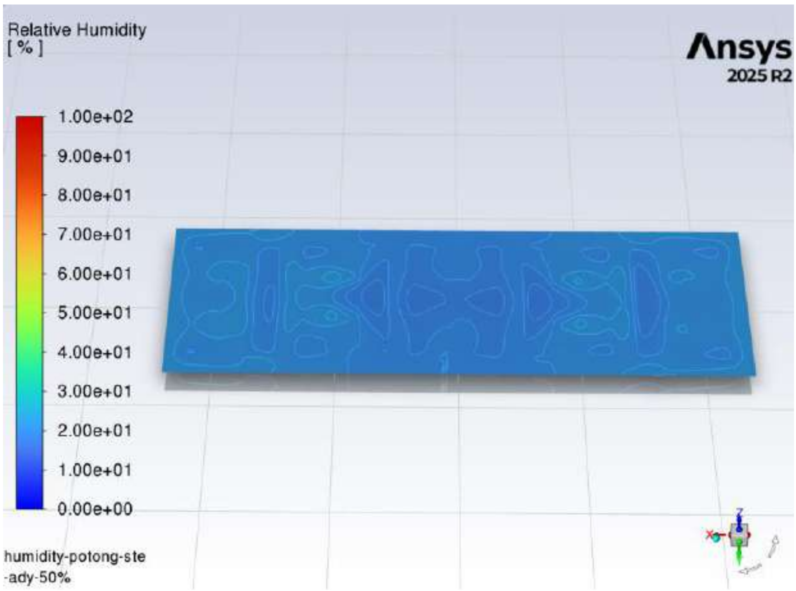

Figure 4. 26 Relative Humidity Contour along The Room Steady-State 50%

Figures 4.25 and 4.26 present the relative humidity distribution within the server room under steady-state operation at 50% server load. The contours illustrate the spatial variation of relative humidity across the room domain and around the server-row arrangement. The relative humidity is predominantly distributed within the lower range of the applied scale, with localized variations observed between the aisle and server-row regions. These variations are associated with the temperature and airflow distribution within the server room, as the increase in air temperature after passing through the server rows affects the resulting relative humidity. The contour patterns indicate a relatively uniform moisture distribution throughout the server room, with no significant localized region of high relative humidity observed.

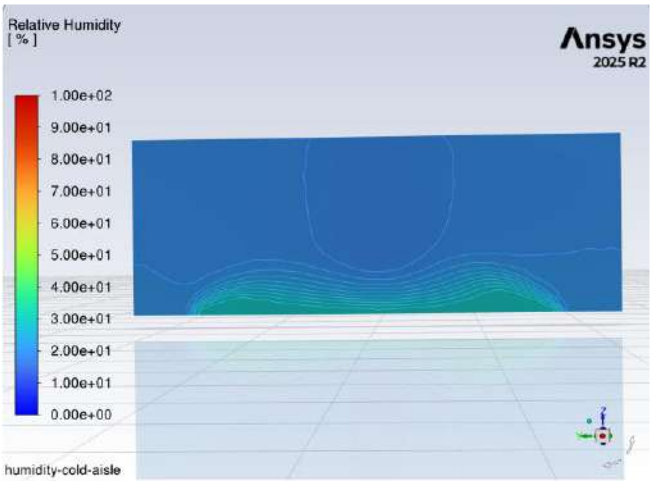

Figure 4. 27 Relative Humidity Contour in Cold Aisle Steady-State 50%

Figure 4.27 presents the relative humidity distribution within the cold aisle under steady-state operation at 50% server load. The contour shows a higher relative humidity concentration near the lower section of the aisle, corresponding to the region directly influenced by the supplied cooling air. As the air moves upward and interacts with the surrounding thermal environment, the relative humidity gradually decreases due to the increase in air temperature. This distribution demonstrates the relationship between the supplied cooling air condition and the resulting moisture variation within the cold aisle region.

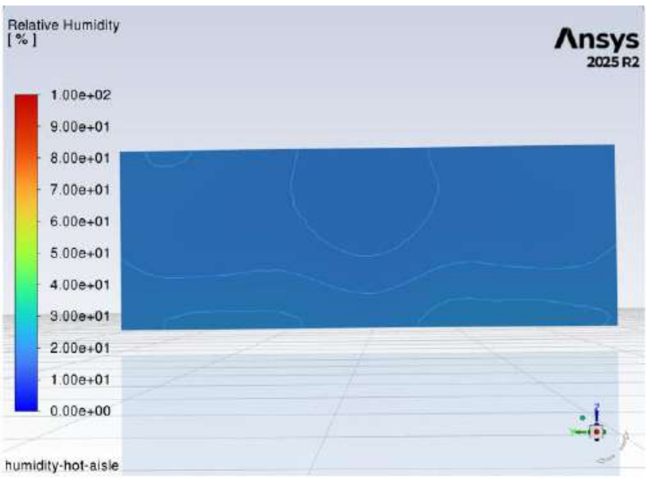

Figure 4. 28 Relative Humidity Contour in Hot Aisle Steady-State 50%

Figure 4.28 presents the relative humidity distribution within the hot aisle under steady-state operation at 50% server load. Compared with the cold aisle, the relative humidity is generally distributed at a lower level due to the increase in air temperature after the airflow passes through the server rows and absorbs the generated heat. The contour indicates a relatively uniform humidity distribution across the hot aisle, with only minor spatial variations observed within the region. This condition reflects the influence of the thermal load on the relative humidity of the heated airflow discharged from the server rows.

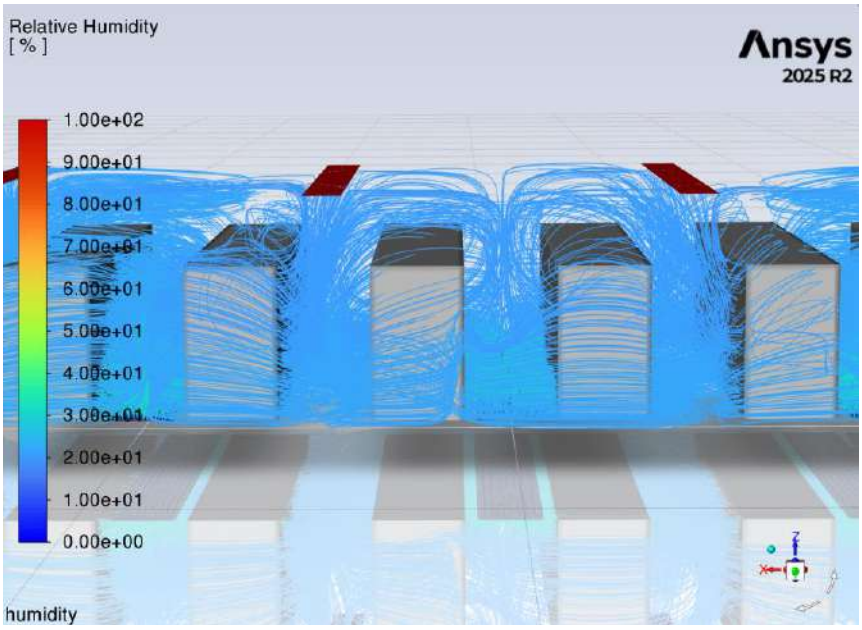

Figure 4. 29 Humidity Pathline Steady-State 50%

Figure 4.29 illustrates the relative humidity variation along the airflow pathlines within the server room under steady-state operation at 50% server load. The pathlines indicate that the relative humidity changes as the supplied cooling air circulates through the aisle regions and passes across the server rows. As the airflow absorbs heat from the servers, the increase in air temperature results in a reduction in relative humidity along the airflow path. The distribution observed along the pathlines further demonstrates the interaction between airflow circulation, thermal conditions, and moisture distribution within the server room.

Table 4. 29 Case 1 Relative Humidity

Relative Humidity	
Parameter	Relative Humidity (%)
Inlet Average Relative Humidity	30
Outlet Average Relative Humidity	21,04
Left Server Rows Average Relative Humidity	21,49
Right Server Rows Average Relative Humidity	21,44
Cold Aisle Average Relative Humidity	21,36
Hot Aisle Average Relative Humidity	20,76
Minimum Server Row Relative Humidity	17,57
Maximum Server Row Relative Humidity	29,67

Table 4.29 summarizes the relative humidity characteristics of the server room under steady-state operation at 50% server load. The supplied air enters the server room at a relative humidity of 30%, while the average relative humidity at the outlet decreases to 21,04%. A similar distribution is observed across the left and right server rows, with average relative humidity values of 21,49% and 21,44%, respectively, indicating a nearly uniform moisture condition between both server-row arrangements. The cold aisle maintains an average relative humidity of 21,36%, while the hot aisle shows a slightly lower value of 20,76%, corresponding to the higher air temperature after heat absorption from the server racks. The relative humidity across the server rows ranges from 17,57% to 29,67%, demonstrating the spatial variation of moisture conditions resulting from the interaction between airflow and temperature distribution.

Overall, the relative humidity distribution under the 50% server load condition demonstrates a consistent response to the thermal and airflow characteristics within the server room. The decrease in relative humidity from the supplied air condition is associated with the increase in air temperature as the airflow circulates through the server rows and absorbs the generated heat. The relatively similar humidity levels between the left and right server rows indicate a balanced moisture distribution across the server arrangement. These results characterize the humidity condition of the proposed cooling configuration under partial-load operation and provide a basis for the subsequent evaluation of server-room environmental compliance.

4.6 Case 2: Steady-State Simulation with 70% Workload

This section presents the steady-state simulation results of the server room under the 70% server load condition. The analysis evaluates the airflow, temperature, and relative humidity distributions using the same computational domain, numerical models, and boundary configuration applied in the 50% load case. The increased server load represents a higher heat generation condition within the server room and is used to assess the response of the proposed cooling configuration under the design operating load. The simulation results are discussed based on the airflow distribution, thermal characteristics, and relative humidity distribution throughout the server room.

4.6.1 Airflow Distribution

The airflow distribution under the 70% server load condition was evaluated to examine the air circulation characteristics within the server room at an increased thermal load. The analysis focuses on the velocity magnitude distribution, airflow direction, and flow paths around the server rows. Velocity contours, pathlines, and vector representations are presented to provide a visual assessment of the airflow behavior and to identify local flow variations and recirculation patterns within the computational domain.

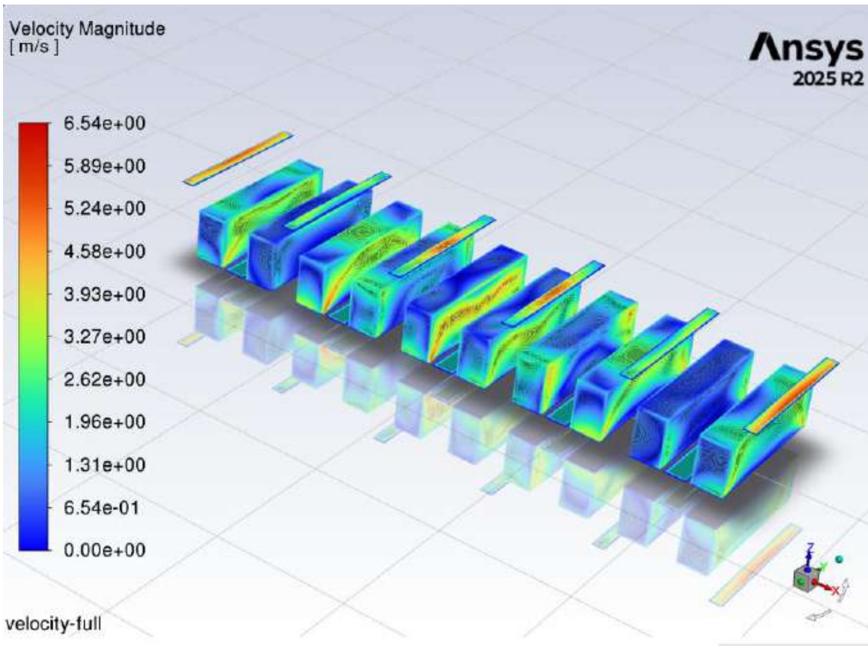

Figure 4. 30 Velocity Contour around the Room Steady-State 70%

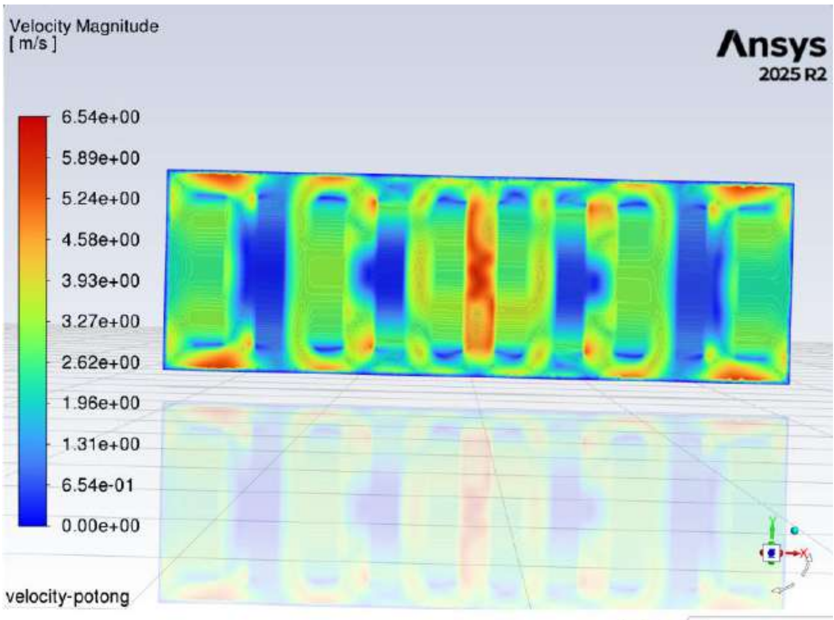

Figure 4. 31 Velocity Contour Plane Around the Room Steady-State 70%

Figures 4.30 and 4.31 present the velocity magnitude distribution within the server room under the 70% server load condition. A similar airflow distribution pattern to the previous operating condition is observed, as the same air supply configuration and server room geometry are maintained. Higher velocity regions remain concentrated near the air supply openings and along the primary airflow passages between the server rows, while lower velocity regions are observed around several rack surfaces and recirculation zones. The longitudinal contour further indicates that the airflow is distributed across the server room, although local variations in velocity magnitude occur between individual server rows.

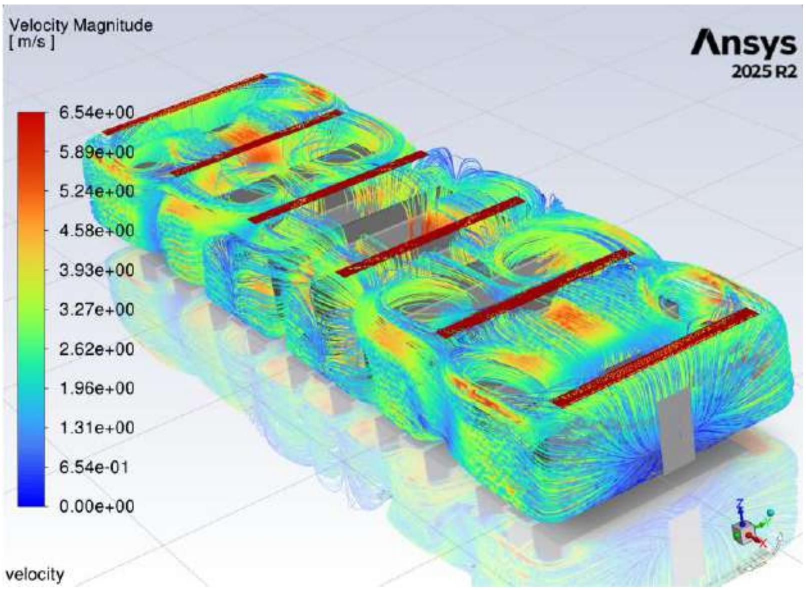

Figure 4. 32 Airflow Pathline Distribution Steady-State 70%

Figure 4.32 illustrates the airflow pathline distribution within the server room under the 70% server load condition. The airflow forms continuous circulation paths around the server rows, with several local recirculation regions observed along the room and between adjacent rack arrangements. The supplied air is distributed through the server rows before circulating toward the upper region of the domain and the outlet locations. Overall, the pathline distribution indicates that airflow circulation is maintained throughout the server room despite the increased thermal load.

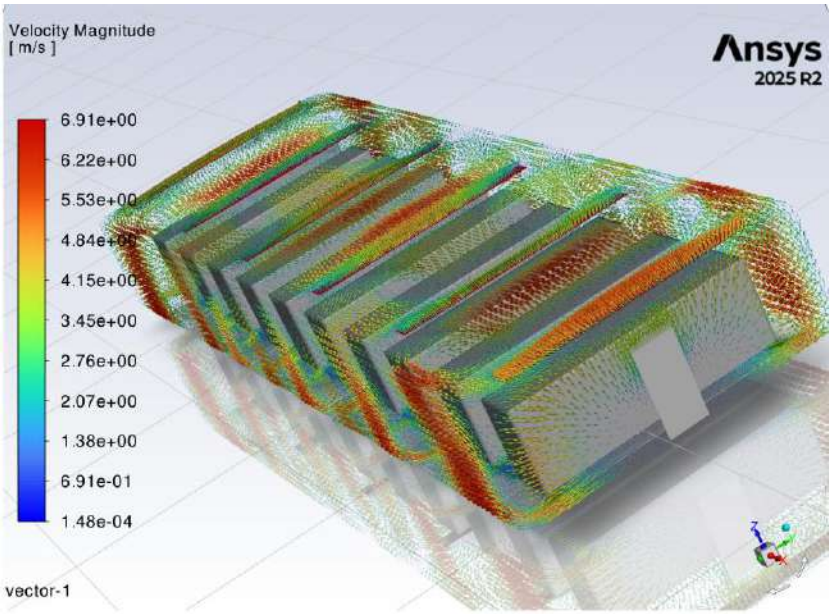

Figure 4. 33 Velocity Vector Steady-State 70%

Figure 4.33 presents the velocity vector distribution within the server room under the 70% server load condition. The vectors indicate the direction of airflow movement around the server rows and demonstrate the development of circulating flow regions within the domain. Higher velocity vectors are mainly observed along the primary airflow paths and near the upper circulation region, while changes in vector direction indicate local recirculation around the server rows. The vector distribution confirms the airflow behavior observed from the velocity contours and pathline visualization.

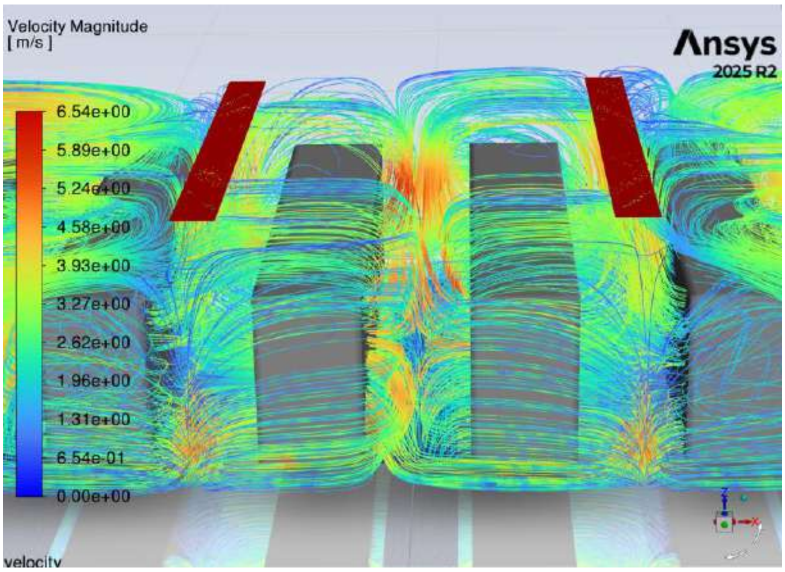

Figure 4. 34 Airflow Pathline through the Racks Steady-State 70%

Figure 4.34 shows the airflow pathlines through and around the server rows under the 70% server load condition. The supplied air is directed toward the server rows and passes through the rack regions before being discharged into the surrounding room domain. The airflow subsequently moves upward and circulates toward the outlet region. Local flow recirculation is observed between adjacent server rows; however, airflow remains distributed across the rack arrangement, indicating continuous air circulation through the server region.

Table 4. 30 Case Airflow Characteristics

Airflow Characteristics	
Surface	Area-Weighted Average Velocity (m/s)
Inlet	2
Outlet	3,481
Left Server Rows	1,7598
Right Server Rows	1,7429

Table 4.30 summarizes the airflow characteristics obtained under the 70% server load condition. The inlet area-weighted average velocity remains at 2 m/s, while the outlet average velocity reaches 3,481 m/s. The average velocities across the left and right server rows are 1,7598 m/s and 1,7429 m/s, respectively. The relatively small difference between the two server row groups indicates a generally balanced airflow distribution across the rack arrangement, although local variations and recirculation regions remain visible in the airflow contours and pathline results.

The airflow analysis under the 70% server load condition demonstrates that the established air supply configuration maintains continuous circulation throughout the server room. The velocity contours, pathlines, and vector distributions show similar general airflow characteristics across the server rows, while the quantitative results indicate comparable average velocities between the left and right server row groups. Furthermore, the small net mass flow imbalance confirms a consistent mass balance within the computational domain. These results provide the airflow characteristics required for the subsequent evaluation of temperature and relative humidity distributions under the 70% server load condition.

4.6.2 Temperature Distribution

The temperature distribution under the 70% server load condition was evaluated to assess the thermal behavior of the server room at an increased heat load. The analysis focuses on the temperature distribution throughout the computational domain, across the server rows, and within the cold and hot aisle regions. Temperature contours and airflow pathlines colored by static temperature are presented to identify local temperature variations, heat accumulation regions, and the thermal interaction between the supplied air and the server racks.

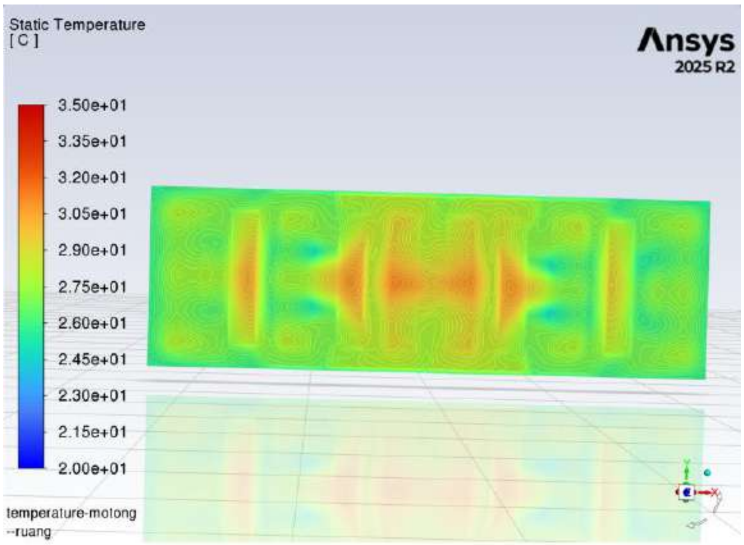

Figure 4. 35 Temperature Contour Plane Steady-State 70%

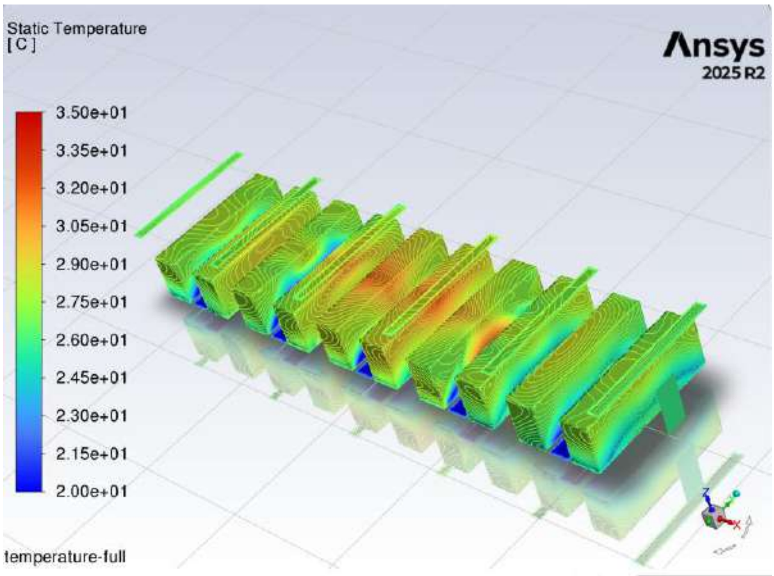

Figure 4. 36 Temperature Contour Room Steady-State 70%

Figures 4.35 and 4.36 present the static temperature distribution within the server room under the 70% server load condition. The temperature contours show variations across the computational domain and server row arrangement, with relatively higher temperature regions concentrated around the central server rows and several downstream rack regions. Lower temperature regions are mainly observed near the air supply openings, indicating the direct influence of the supplied cooling air. Compared with the lower-load condition, the thermal distribution visually indicates greater heat accumulation across the server rows as the server heat load increases.

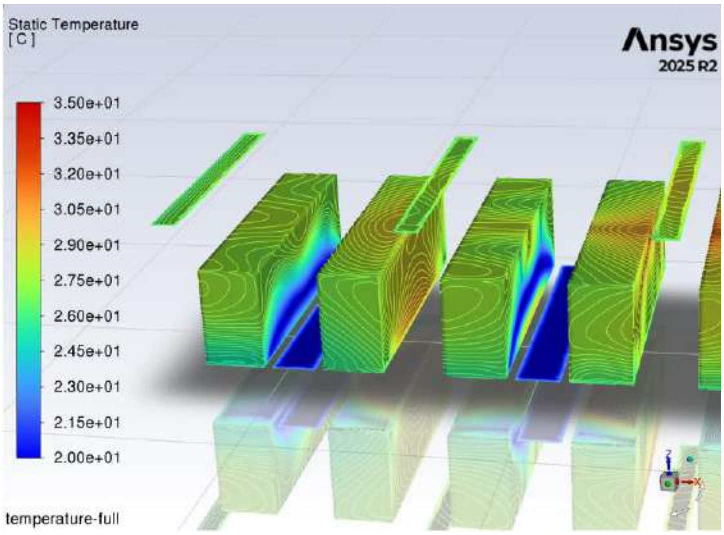

Figure 4. 37 Temperature Contour Between Racks Steady-State 70%

Figure 4.37 illustrates the temperature distribution around the server rows under the 70% server load condition. The supplied air enters the server region at a lower temperature and interacts with the rack surfaces, resulting in a gradual temperature increase across the server row arrangement. Local temperature variations are observed between adjacent server rows, particularly in regions influenced by airflow circulation and recirculation. The contour distribution demonstrates the thermal interaction between the cooling airflow and the increased server heat load.

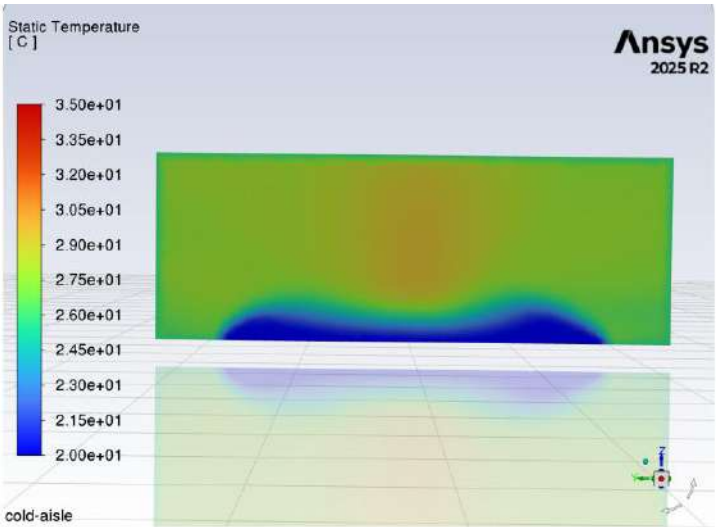

Figure 4. 38 Temperature Contour Cold Aisle Steady-State 70%

Figure 4.38 presents the temperature distribution within the cold aisle region under the 70% server load condition. Lower temperature regions are concentrated near the air supply area at the lower section of the aisle, while the air temperature gradually increases toward the upper region. This distribution indicates that the supplied cooling air enters the cold aisle at a lower temperature before interacting with the surrounding server rows and mixing with the room airflow.

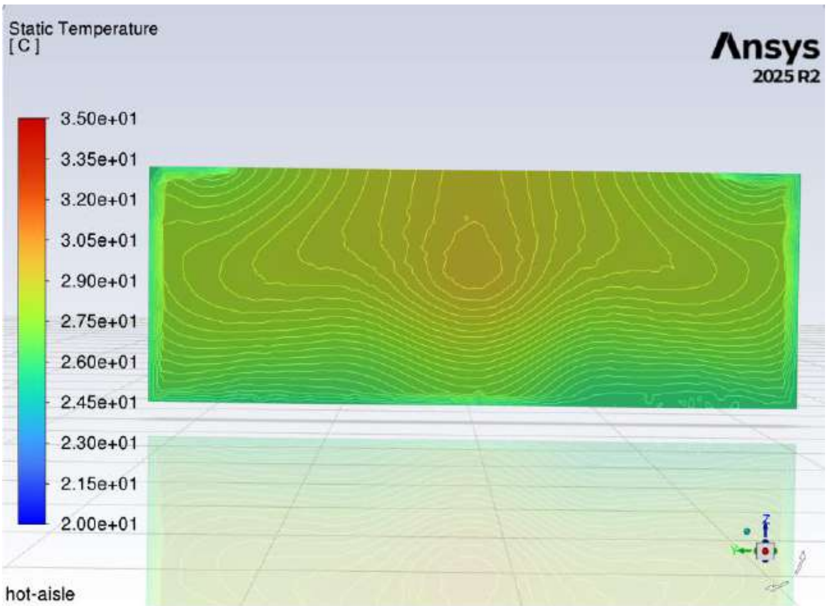

Figure 4. 39 Temperature Contour Hot aisle Steady-State 70%

Figure 4.39 shows the temperature distribution within the hot aisle region under the 70% server load condition. Higher temperature regions are observed within the upper and central sections of the aisle as heat released from the server rows is transferred to the surrounding airflow. The temperature gradient from the lower to upper region indicates the accumulation and upward movement of heated air within the hot aisle.

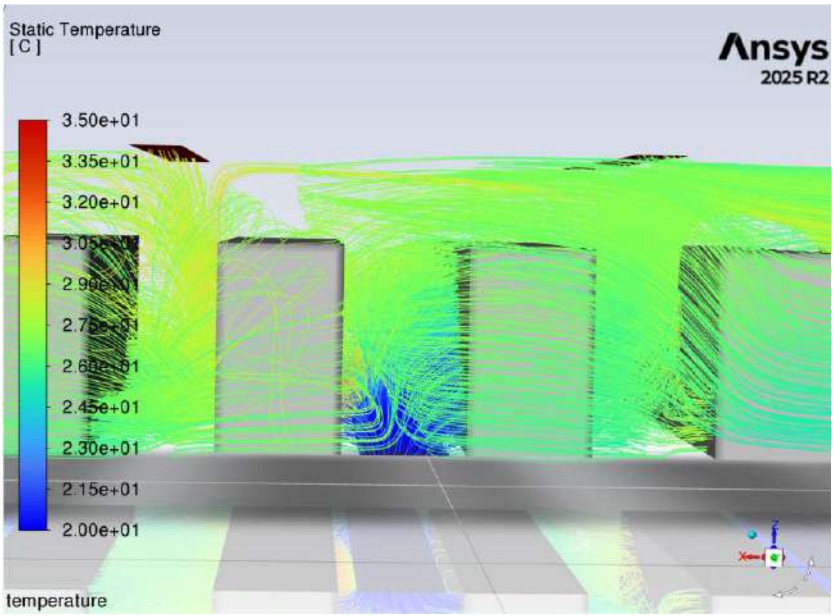

Figure 4. 40 Temperature Pathline Steady-State 70%

Figure 4.40 illustrates the airflow pathlines colored by static temperature under the 70% server load condition. The pathlines show that the supplied cooling air initially remains at a lower temperature near the air supply region before passing through and around the server rows. As the airflow interacts with the server racks, its temperature increases and the warmer air subsequently circulates toward the upper region of the computational domain. The visualization demonstrates the relationship between the previously observed airflow circulation pattern and the resulting thermal distribution within the server room.

Table 4. 31 Case 2 Temperature

Temperature	
Parameter	**Temperature (°C)**
Inlet Average Temperature	20
Outlet Average Temperature	27,51
Left Server Rows Average Temperature	27,19
Right Server Rows Average Temperature	27,24
Cold Aisle Average Temperature	27,17
Hot Aisle Average Temperature	27,79
Minimum Server Row Temperature	20,06
Maximum Server Row Temperature	31,79

Table 4.31 summarizes the temperature characteristics obtained under the 70% server load condition. The inlet average temperature remains at 20°C, while the outlet average temperature increases to 27,51°C. The left and right server row average temperatures are 27,19°C and 27,24°C, respectively, indicating a relatively uniform thermal distribution between the two server row groups. The cold aisle average temperature is 27,17°C, whereas the hot aisle average temperature reaches 27,79°C, showing the expected temperature increase after the cooling air interacts with the server heat load. The minimum and maximum server row temperatures are 20,06°C and 31,79°C, respectively.

The temperature analysis under the 70% server load condition indicates that the cooling airflow maintains the server row temperatures within the evaluated thermal range despite the increased heat load. The relatively similar average temperatures between the left and right server rows demonstrate a balanced thermal distribution across the rack arrangement. A temperature difference between the cold and hot aisle regions is also observed, reflecting the heat transfer from the server racks to the circulating airflow. The maximum server row temperature of 31,79°C indicates the development of localized higher-temperature regions. Similar to the 50% load condition, a slightly higher localized temperature was again observed at Left Rack 3 and Right Rack 3 due to the same localized recirculation pattern at this row position, with this effect becoming marginally more pronounced under the higher heat load while remaining within the acceptable operating range. However, the overall temperature distribution remains controlled under the simulated operating condition.

4.6.3 Relative Humidity Distribution

The relative humidity distribution under the 70% server load condition was evaluated to assess the moisture distribution within the server room as the thermal load increases. The analysis focuses on the relative humidity distribution throughout the computational domain, across the server rows, and within the cold and hot aisle regions. Relative humidity contours and airflow pathlines are presented to identify spatial variations and to examine the interaction between airflow circulation, temperature distribution, and relative humidity within the server room.

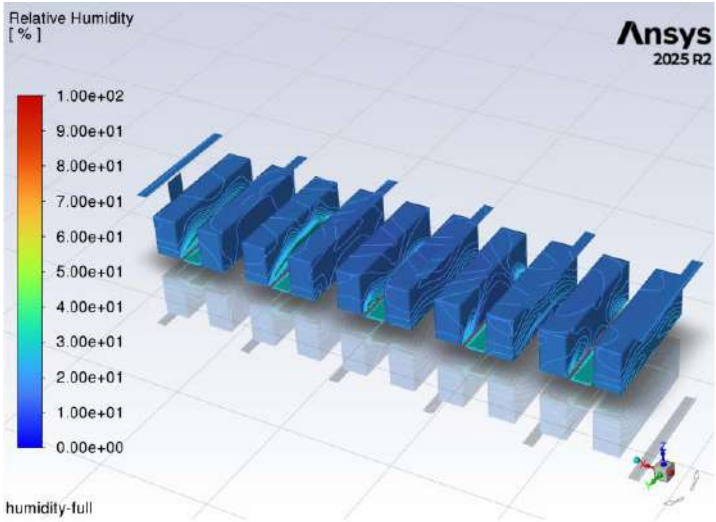

Figure 4. 41 Relative Humidity Contour Room Steady-State 70%

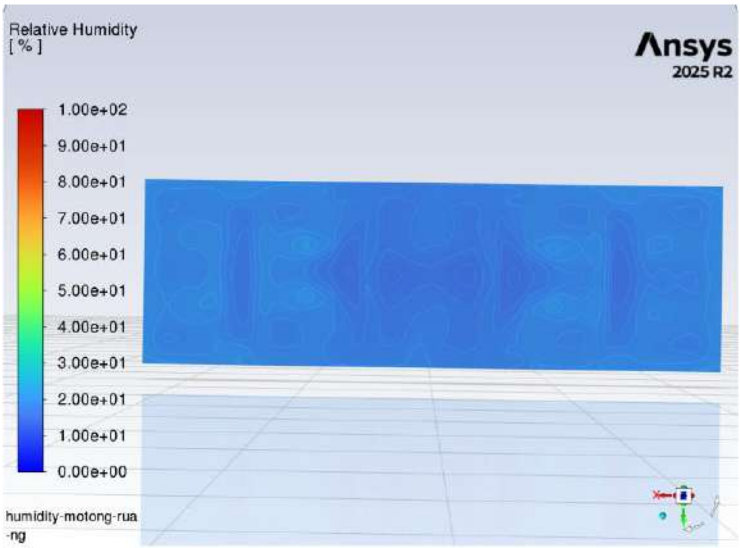

Figure 4. 42 Relative Humidity Contour Plane Steady-State 70%

Figures 4.41 and 4.42 present the relative humidity distribution throughout the server room under the steady-state 70% load condition. The overall contour indicates a relatively uniform humidity distribution across the server rows, although local variations are observed between the rows and within the aisle regions. Most regions exhibit lower relative humidity levels than the inlet condition due to the increase in air temperature as the airflow interacts with the operating server racks. The distribution pattern also indicates a relatively symmetrical humidity condition between the left and right server rows.

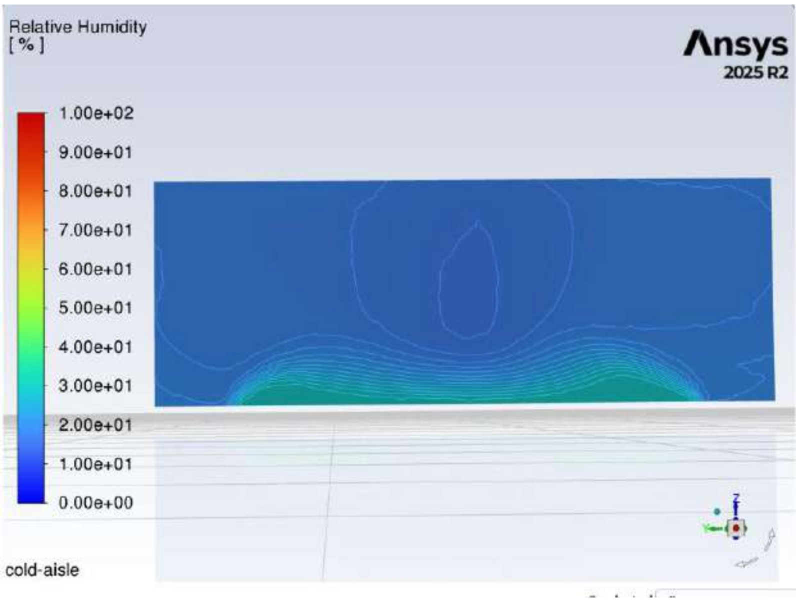

Figure 4. 43 Relative Humidity Contour Cold Aisle Steady-State 70%

Figure 4.43 presents the relative humidity distribution within the cold aisle under the steady-state 70% load condition. Higher relative humidity is observed near the lower section of the aisle, particularly close to the cold-air supply region. The relative humidity gradually decreases toward the upper section as the supplied air interacts with the warmer surrounding airflow. This distribution corresponds to the lower air temperature near the cold-air supply, resulting in higher relative humidity compared with the upper region of the cold aisle.

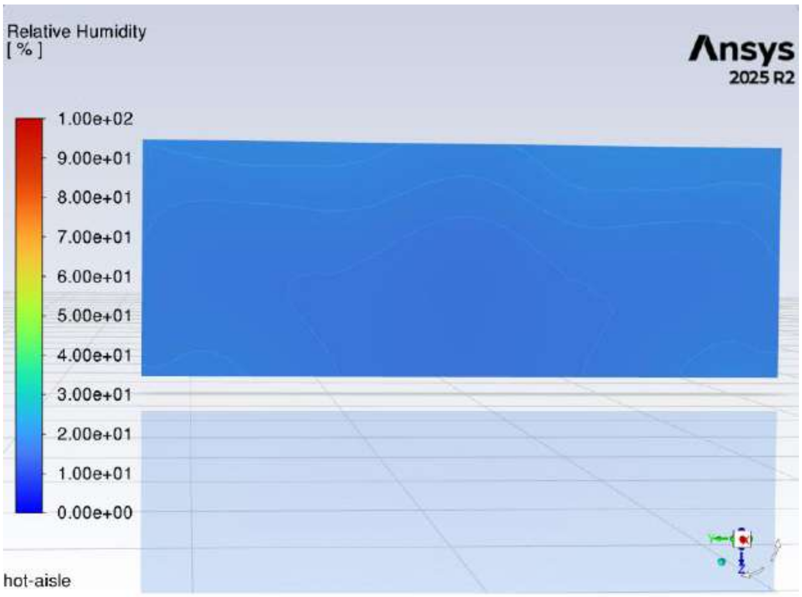

Figure 4. 44 Relative Humidity Contour Hot Aisle Steady-State 70%

Figure 4.44 shows the relative humidity distribution within the hot aisle under the steady-state 70% load condition. The contour indicates a relatively uniform humidity distribution throughout the hot aisle, with generally lower relative humidity compared with the cold aisle. This condition is associated with the increase in air temperature after the airflow passes through the server rows and absorbs the generated heat. Consequently, the relative humidity decreases as the air temperature increases within the hot aisle region.

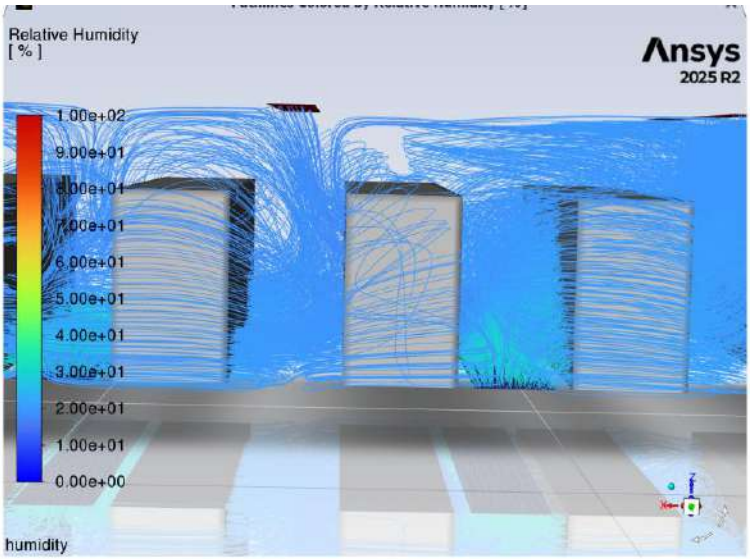

Figure 4. 45 Relative Humidity Pathline Steady-State 70%

Figure 4.45 illustrates the airflow pathlines colored by relative humidity under the steady-state 70% load condition. The pathlines demonstrate the transport of moisture together with the circulating airflow throughout the server room. Higher relative humidity is primarily observed near the cold-air supply region, while lower relative humidity is distributed along the airflow path after passing through the heated server rows. The airflow circulation and recirculation patterns contribute to the redistribution of humidity throughout the computational domain.

Table 4. 32 Case 2 Relative Humidity

Relative Humidity	
Parameter	Relative Humidity (%)
Inlet Average Relative Humidity	30
Outlet Average Relative Humidity	18,95
Left Server Rows Average Relative Humidity	19,45
Right Server Rows Average Relative Humidity	19,39
Cold Aisle Average Relative Humidity	19,52
Hot Aisle Average Relative Humidity	18,65
Minimum Server Row Relative Humidity	14,79
Maximum Server Row Relative Humidity	29,64

Table 4.32 summarizes the relative humidity characteristics under the steady-state 70% load condition. The inlet average relative humidity is 30%, while the outlet average relative humidity decreases to 18,95%. The average relative humidity of the left and right server rows is 19,45% and 19,39%, respectively, indicating a relatively balanced humidity distribution between both server row groups. The cold aisle records an average relative humidity of 19,52%, which is slightly higher than the hot aisle average of 18,65%. The minimum and maximum relative humidity within the server rows are 14,79% and 29,64%, respectively. These results indicate that the relative humidity distribution is influenced by the temperature increase and airflow interaction as the supplied air passes through the server rows.

Overall, the relative humidity analysis under the steady-state 70% load condition indicates that the humidity distribution is closely associated with the temperature and airflow characteristics within the server room. The similar average relative humidity values between the left and right server rows demonstrate a relatively balanced distribution across the server arrangement. The lower relative humidity observed in the hot aisle compared with the cold aisle corresponds to the increase in air temperature after heat absorption from the server rows. Therefore, the results demonstrate that the increased thermal load influences the relative humidity distribution within the server room while maintaining a relatively consistent pattern between both server row groups.

4.7 Case 3: Transient Air Infiltration Simulation with 70% Workload

This section presents the transient simulation results of the proposed cooling system to evaluate the dynamic thermal response of the server room during a temporary door-opening event. The transient simulation was performed using the converged steady-state solution at the 70% server load condition as the initial condition. A temporary disturbance was introduced by opening the server room door for the first 15 s, allowing external air to enter the computational domain. The door was then assumed to be fully closed for the remaining simulation period to evaluate the recovery characteristics of the airflow, temperature, and relative humidity distributions within the server room.

4.7.1 Boundary Conditions

The transient simulation employed the same computational domain, mesh, physical models, and primary boundary conditions used in the steady-state simulation at the 70% server load condition. The converged steady-state solution was used as the initial condition for the transient analysis. To simulate a temporary operational disturbance, the server room door was modeled as a time-dependent velocity inlet. The door remained fully open for the first 15 s, allowing external air at 32°C and 85% relative humidity to enter the computational domain with a velocity of 3 m/s. After 15 s, the inlet velocity was reduced to 0 m/s, representing a fully closed door for the remainder of the simulation period.

Table 4. 33 Case 3 Extra Boundary Conditions

Extra Boundary Conditions		
Parameter	Value	Unit
Initial Condition	Steady-State 70% Load	
External Air Temperature	32	°C
External Relative Humidity	85	%
Door Inlet Velocity (0–15 s)	3	m/s
Door Inlet Velocity (15–60 s)	0	m/s
Door Opening Duration	15	s
Total Simulation Time	60	s
Time Step Size	0,1	-
Number of Time Steps	600	-

Table 4.33 summarizes the boundary conditions applied in the transient simulation. The transient analysis was initialized using the converged steady-state solution at the 70% server load condition. A temporary disturbance was introduced by modeling the server room door as a time-dependent velocity inlet. During the first 15 s of the simulation, the door remained fully open, allowing external air at 32°C and 85% relative humidity to enter the

computational domain with a velocity of 3 m/s. After the door-closing event at 15 s, the inlet velocity was reduced to 0 m/s for the remaining simulation period, while the primary cooling boundary conditions of the server room remained unchanged. The simulation was conducted for a total duration of 60 s using the transient parameters listed in Table 4.33.

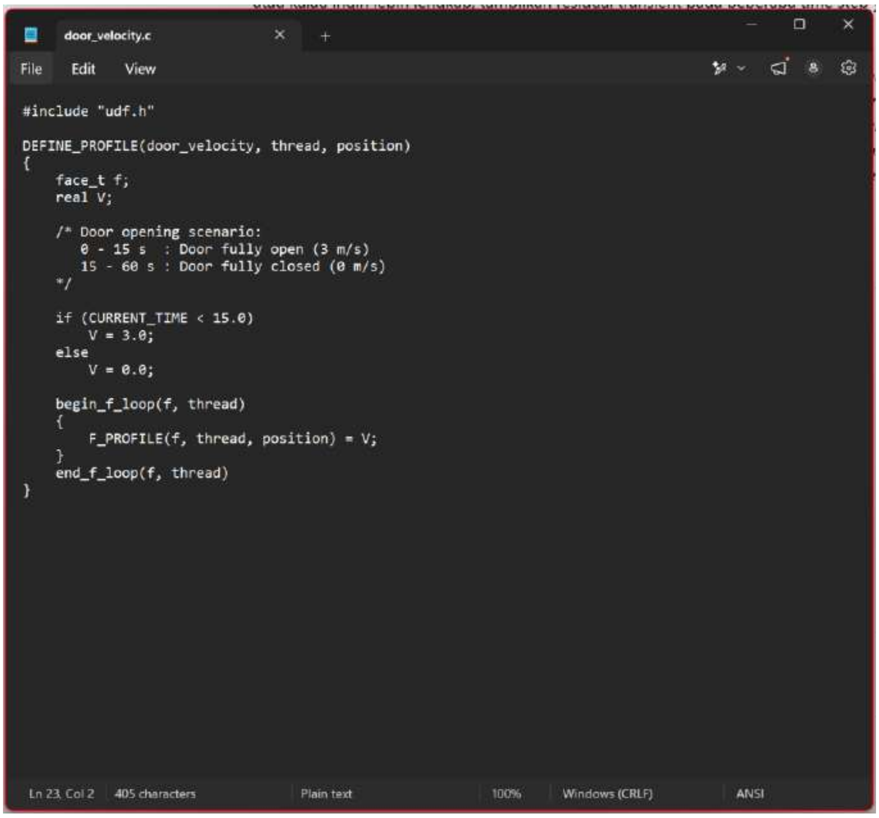

```
#include "udf.h"

DEFINE_PROFILE(door_velocity, thread, position)
{
    face_t f;
    real V;

    /* Door opening scenario:
       0 - 15 s  : Door fully open (3 m/s)
       15 - 60 s : Door fully closed (0 m/s)
    */

    if (CURRENT_TIME < 15.0)
        V = 3.0;
    else
        V = 0.0;

    begin_f_loop(f, thread)
    {
        F_PROFILE(f, thread, position) = V;
    }
    end_f_loop(f, thread)
}
```

Figure 4. 46 udf File for Velocity Inlet

To implement the door-opening scenario during the transient simulation, a User-Defined Function (UDF) was developed in ANSYS Fluent to control the inlet velocity at the access door as a function of simulation time. As shown in Figure 4.41, the UDF specifies a constant inlet velocity of 3 m/s during the first 15 s, representing the period when the access door is fully open. After 15 s, the inlet velocity is automatically reduced to 0 m/s, simulating the complete closure of the door for the remainder of the 60 s simulation. This time-dependent boundary condition enables the transient model to capture the effects of temporary outdoor air infiltration while maintaining all other boundary conditions unchanged.

4.7.2 Simulation Convergence

To ensure the numerical stability and accuracy of the transient simulation, the convergence behavior of the governing equations was monitored using the residual histories throughout the computation. Prior to the transient analysis, a converged steady-state solution was used as the initial condition. During the transient simulation, each time step was solved using a maximum of 30 iterations before advancing to the next time step. This approach minimizes numerical errors while allowing the solution to accurately capture the transient response caused by the temporary opening of the access door.

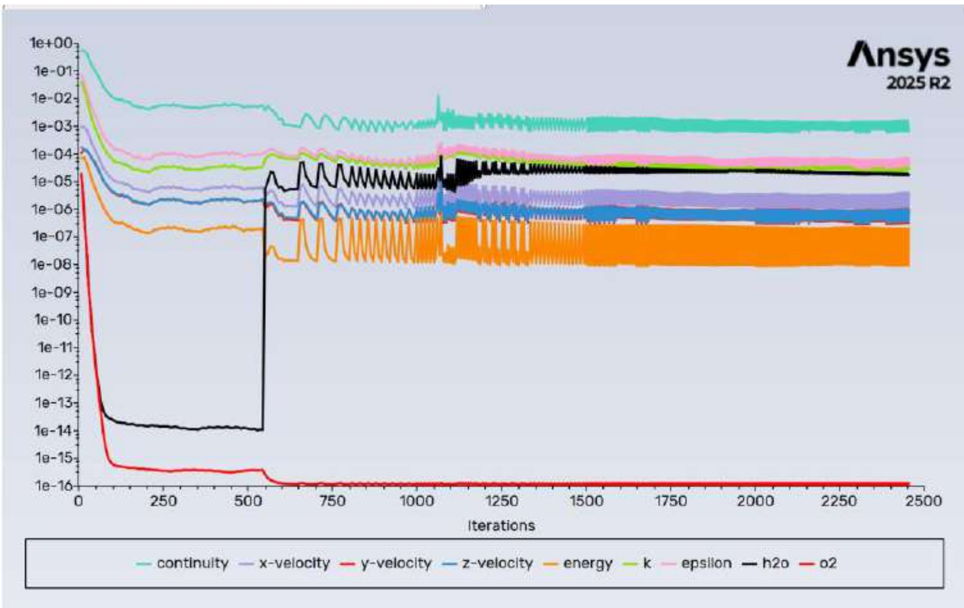

Figure 4. 47 Residual Plot for Transient Simulation

As shown in Figure 4.47, the residuals of continuity, momentum, energy, turbulence quantities (k and ε), and species transport (H_2O and O_2) exhibit a rapid decrease during the initial iterations before reaching relatively stable values throughout the remaining simulation. Minor fluctuations are observed in several residual curves due to the transient nature of the simulation, where the governing equations are repeatedly updated at every time step. These fluctuations are expected in transient CFD simulations and do not indicate numerical instability.

The momentum residuals remained on the order of 10^{-6}, while the energy residual converged to approximately 10^{-7}–10^{-8} throughout the simulation. The turbulence residuals were maintained at approximately 10^{-5}–10^{-4}, whereas the species residuals for water vapor (H_2O) and oxygen (O2) also remained stable after the initial transient response. Although the continuity residual stabilized at approximately 10^{-3}, this level is considered acceptable for transient simulations involving buoyancy, turbulence, and species transport, particularly under time-dependent boundary conditions.

Overall, the residual histories indicate that the numerical solution remained stable during the entire 60 s simulation period without any sign of divergence. Therefore, the transient simulation is considered to have achieved satisfactory numerical convergence, and the obtained airflow, temperature, and relative humidity distributions can be used for further analysis of the server room response to the temporary door-opening event.

4.7.3 Transient Airflow Response

To evaluate the influence of temporary outdoor air infiltration on the airflow characteristics inside the server room, the airflow distribution was analyzed during the transient simulation. The airflow field was evaluated at 14 s, representing the end of the door opening period, and at 60 s, representing the recovery condition after the door had been closed. The analysis includes velocity contours, airflow pathlines, and the average airflow velocity at each server rack to assess the impact of the disturbance on the internal airflow distribution.

Figures 4.48 and 4.49 present the velocity contours at 14 s using both the mid-plane section and the overall three-dimensional view. These contours illustrate the airflow distribution within the server room while the entrance door remained open and outdoor air infiltration was still occurring.

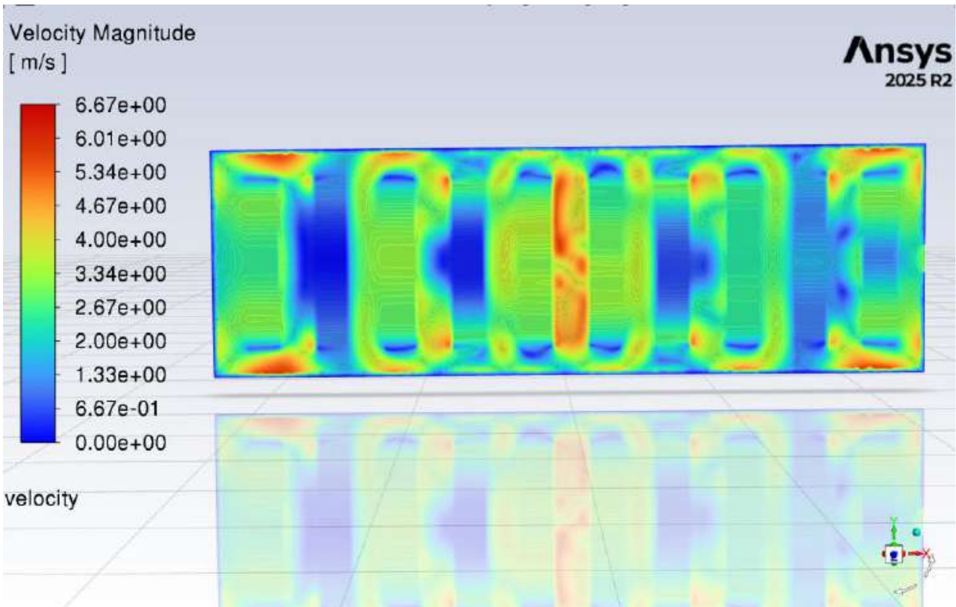

Figure 4. 48 Velocity Contour Plane after 14 seconds

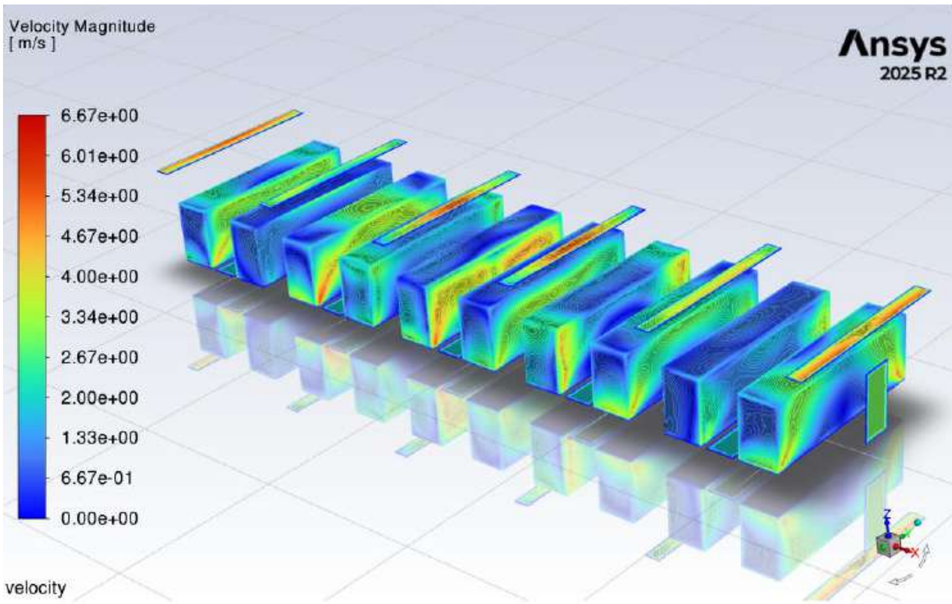

Figure 4. 49 Velocity Contour after 14 seconds

The airflow supplied from the HVAC units remained dominant within the cold aisles, producing relatively uniform airflow through the server racks. Higher airflow velocities were observed near the supply openings and within the cold aisle regions, whereas lower velocities occurred inside the hot aisles due to the reduction in airflow momentum after passing through the porous server racks. Although outdoor air entered through the open door, the overall airflow pattern inside the room remained largely governed by the mechanical ventilation system.

To further examine the airflow movement inside the server room, Figures 4.50 and 4.51 present the velocity pathlines at 14 s. While Figure 4.45 illustrates the overall airflow circulation within the server room, Figure 4.46 specifically tracks the airflow entering from the open door.

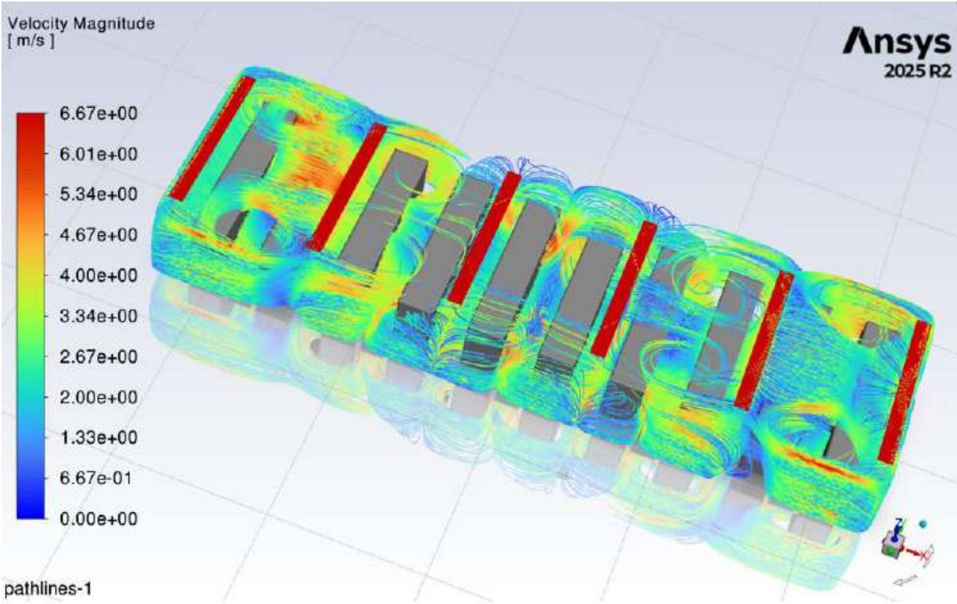

Figure 4. 50 Velocity Pathlines after 14 seconds

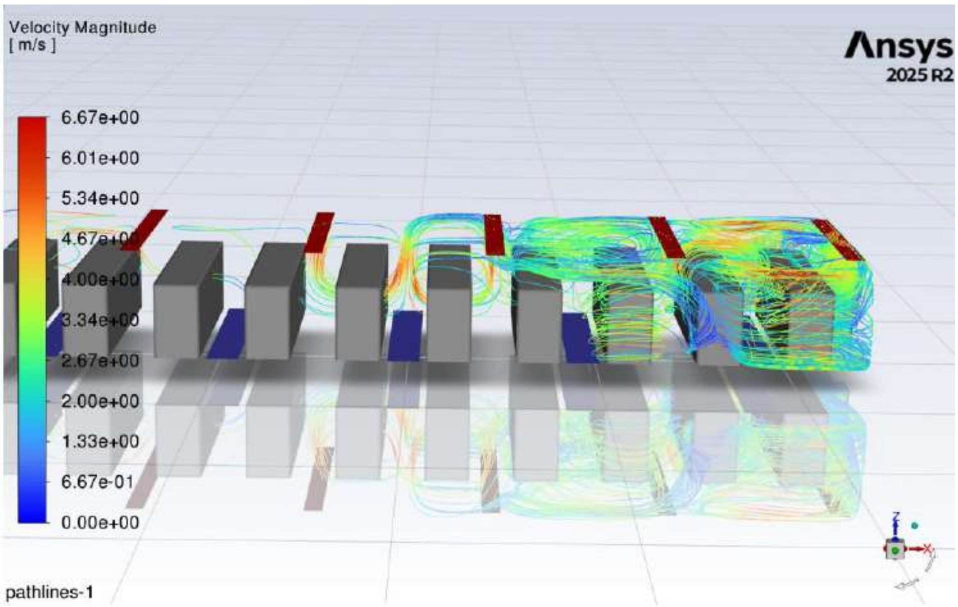

Figure 4. 51 Velocity Pathline from Door after 14 seconds

The overall airflow pathlines indicate that the supply air discharged from the HVAC units continued to circulate through the cold aisles before returning to the ceiling exhaust. The airflow introduced through the entrance door was observed to move primarily toward the upper region of the room, following the dominant circulation generated by the mechanical cooling system. Only a limited portion of the infiltrated air penetrated into the server rack region because the porous server racks imposed a higher flow resistance than the relatively unobstructed airflow path toward the ceiling return. Consequently, the temporary door opening produced only localized airflow disturbances without significantly altering the primary airflow distribution inside the server room.

After the entrance door was closed, the airflow field gradually returned toward its steady operating condition. Figures 4.52 and 4.53 present the velocity contours at 60 s, representing the airflow distribution after the recovery period.

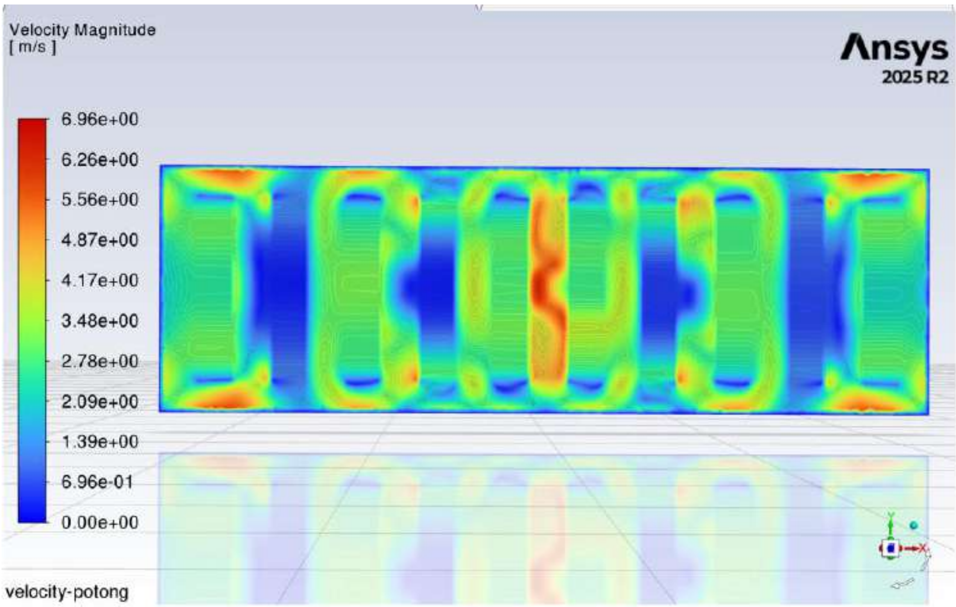

Figure 4. 52 Velocity Contour Plane after 60 seconds

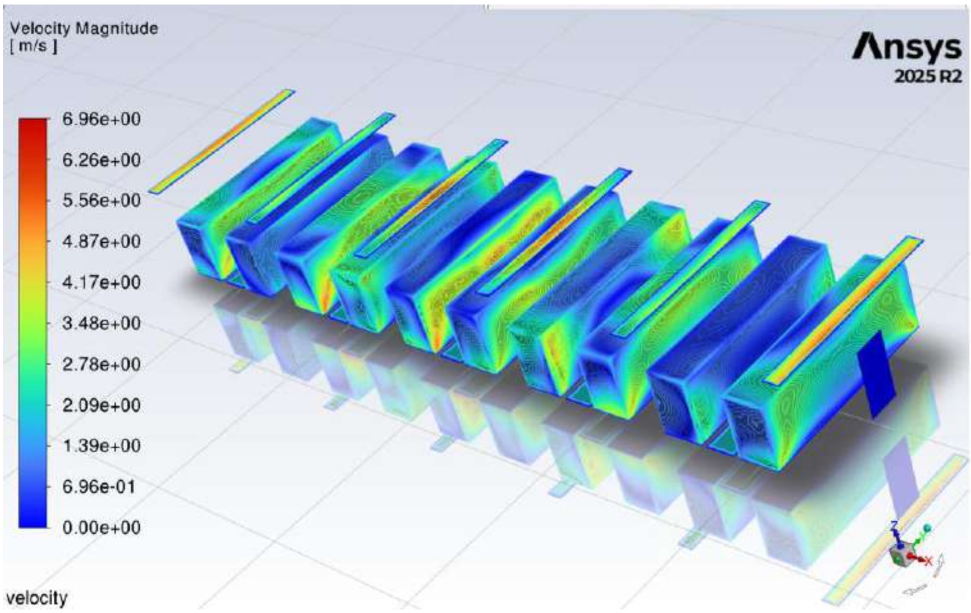

Figure 4. 53 Velocity Contour after 60 seconds

Compared with the airflow distribution at 14 s, the velocity contours at 60 s exhibit a more uniform airflow pattern throughout the cold aisles and server rack region. The localized disturbance observed during the door opening period had substantially diminished, indicating that the HVAC system successfully re-established the intended airflow circulation. The airflow remained concentrated within the cold aisles, while lower velocities persisted inside the hot aisles due to the pressure losses associated with airflow passing through the server racks. The recovery of the airflow circulation is further illustrated by the airflow pathlines shown in Figure 4.54.

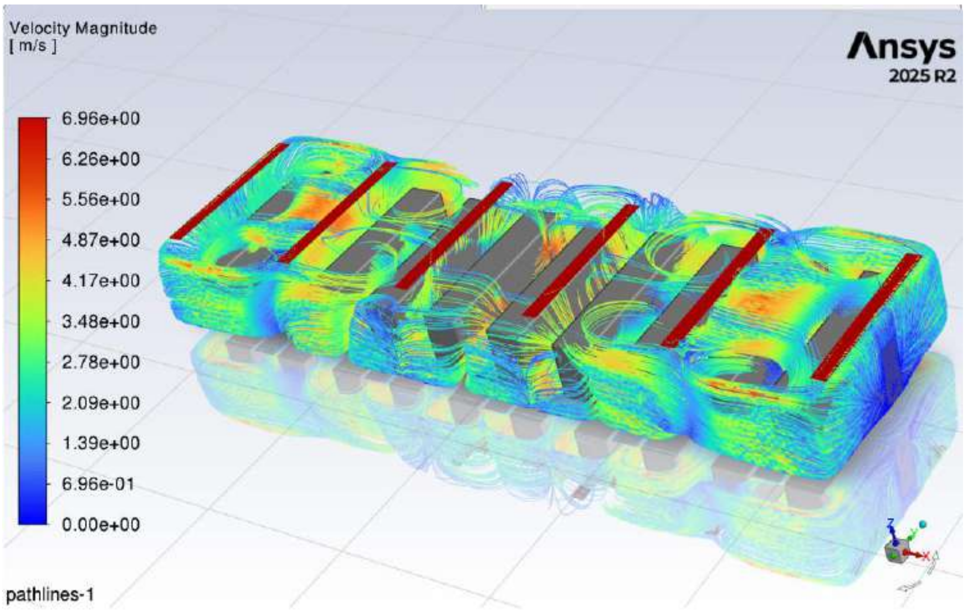

Figure 4. 54 Velocity Pathline After 60 seconds

The airflow trajectories demonstrate that the temporary disturbance generated during the door opening period no longer influenced the overall circulation pattern. The supply airflow again followed its intended path through the cold aisles and server racks before returning toward the ceiling outlet, indicating that the ventilation system rapidly restored the designed airflow distribution once the external airflow source had been removed.

To quantitatively evaluate the influence of the temporary disturbance, the average airflow velocity at each server rack was extracted at six observation times, namely before infiltration (baseline), 1 s, 7 s, 14 s, 30 s, and 60 s, as summarized in Table 4.34.

Table 4. 34 Case 3 Average Velocity on each racks

Average Velocity (m/s)										
Time	Further to Closer to the Door									
	Left Rack 1	Right Rack 1	Left Rack 2	Right Rack 2	Left Rack 3	Right Rack 3	Left Rack 4	Right Rack 4	Left Rack 5	Right Rack 5
Before Infiltration	1,838	0,622	1,836	1,303	1,983	2,003	1,287	1,819	0,793	1,803
1 second	1,854	0,603	1,870	1,292	2,018	1,959	1,319	1,742	0,880	1,682
7 seconds	1,832	0,611	1,881	1,284	2,025	1,955	1,343	1,665	0,946	1,709
14 seconds	1,831	0,725	1,874	1,242	2,001	1,909	1,322	1,649	0,986	1,691
30 seconds	1,883	0,928	1,830	1,302	1,964	1,994	1,285	1,799	1,276	1,782
60 seconds	1,838	0,769	1,841	1,319	1,963	2,023	1,271	1,826	0,727	1,782

The average airflow velocity at each rack exhibits only minor fluctuations throughout the transient simulation. Racks located closer to the entrance experienced slightly greater variations immediately after the door opening, while racks located farther from the entrance remained relatively stable. Nevertheless, the magnitude of these variations was relatively small, indicating that the infiltrated outdoor air had a limited influence on the airflow supplied to the server racks. By 60 s, the airflow velocities at all rack locations had returned to values very close to the baseline condition, confirming the rapid recovery capability of the HVAC ventilation system following the temporary disturbance.

4.7.4 Transient Temperature Response

To investigate the thermal response of the server room during the temporary door opening event, the transient temperature distribution was evaluated at several observation times. The temperature field was analyzed at 1 s, 7 s, 14 s, 30 s, and 60 s to capture the initial response, the maximum disturbance during the door opening period, and the subsequent recovery after the door was closed. Both temperature contours and quantitative average temperatures at each server rack were used to evaluate the thermal resilience of the cooling system. Figures 4.55 and 4.56 present the mid-plane temperature contours at 1 s and 7 s after the transient simulation began. These figures represent the early stage of outdoor air infiltration while the entrance door remained open.

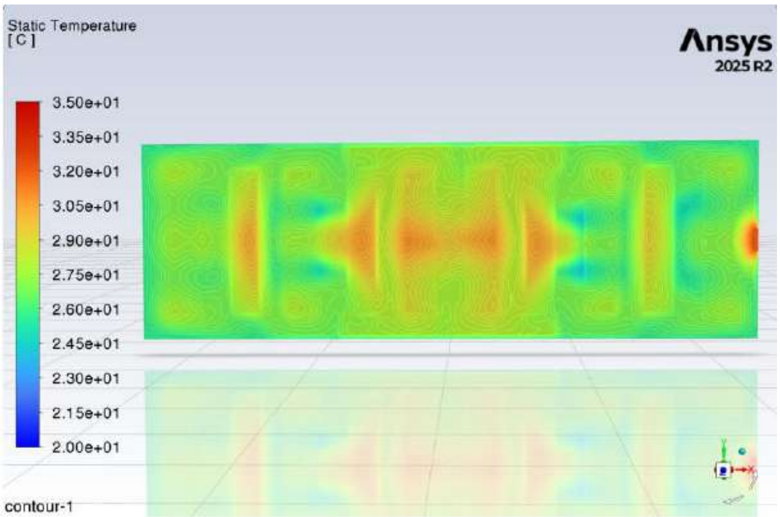

Figure 4. 55 Temperature Contour Plane after 1 second

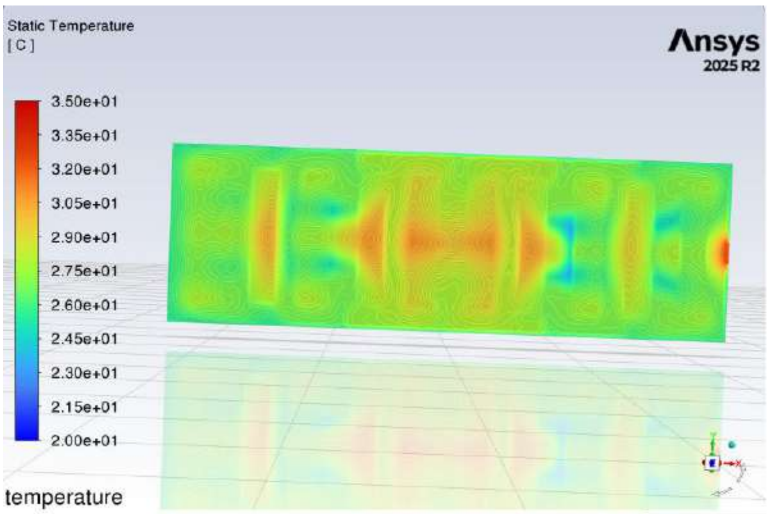

Figure 4. 56 Temperature Contour Plane after 7 seconds

At the beginning of the transient simulation, the temperature distribution remained similar to the steady-state condition because the duration of outdoor air infiltration was still relatively short. The cold aisles maintained lower temperatures due to the continuous supply of conditioned air from the HVAC units, whereas higher temperatures were observed within the hot aisles after the cooling air absorbed heat from the server racks. Although warm outdoor air had entered the server room, its influence on the thermal field remained limited during the first several seconds because the supplied cooling airflow continued to dominate the indoor air circulation. The temperature distribution at the end of the door opening period is illustrated in Figures 4.57 and 4.58 using the overall three-dimensional view and the mid-plane contour, respectively.

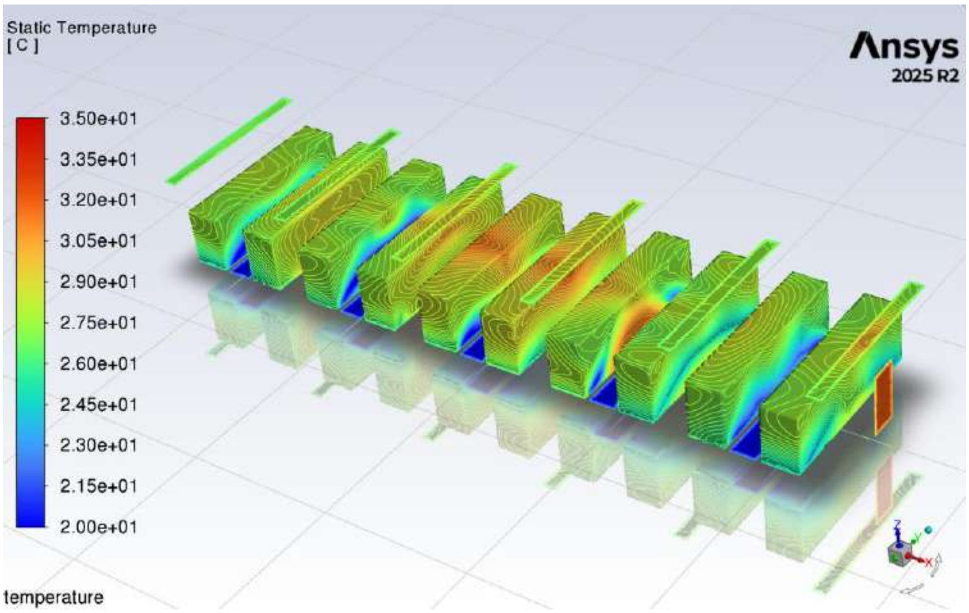

Figure 4. 57 Temperature Contour after 14 seconds

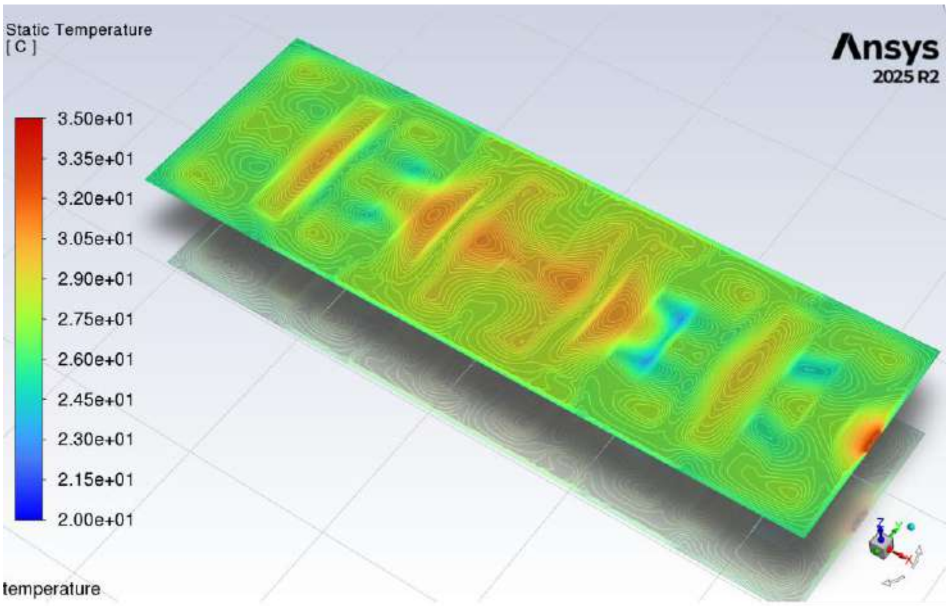

Figure 4. 58 Temperature Contour Plane after 14 seconds

After 14 s of continuous door opening, a localized increase in temperature became more apparent near the airflow path influenced by the outdoor air infiltration. Nevertheless, the cooling system maintained a relatively uniform temperature distribution throughout the server room. Higher temperatures remained concentrated within the hot aisles where the exhaust air from the servers accumulated, while the cold aisles continued to receive conditioned air at lower temperatures. This result indicates that the temporary infiltration produced only localized thermal disturbances without significantly affecting the thermal environment surrounding the server racks. To better illustrate the transport of warm outdoor air inside the server room, Figure 4.59 presents the temperature pathlines originating from the entrance door at 14 s.

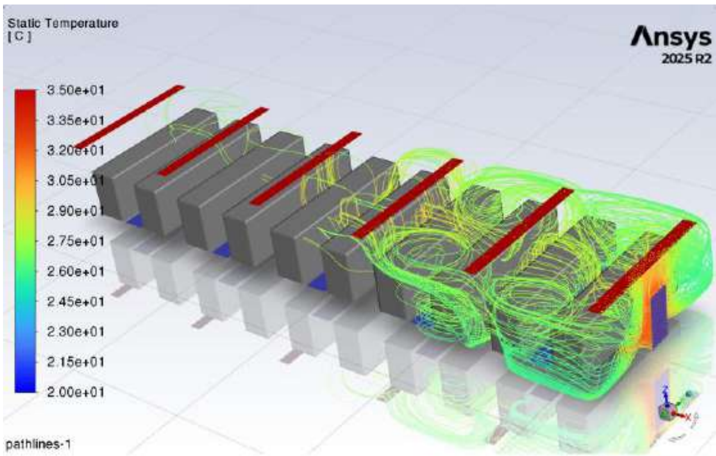

Figure 4. 59 Temperature Pathlines from Door after 14 seconds

The temperature pathlines show that the infiltrated warm air primarily followed the dominant airflow generated by the HVAC system toward the upper region of the room instead of directly entering the server rack inlets. This behavior is consistent with the airflow pathlines discussed in the previous section, where the porous resistance of the server racks limited the penetration of outdoor air into the cold aisles. Consequently, the elevated temperature associated with the infiltrated air remained localized and did not substantially alter the cooling airflow supplied to the IT equipment. After the entrance door was closed, the indoor thermal field gradually returned toward the normal operating condition. Figure 4.60 presents the mid-plane temperature contour at 30 s.

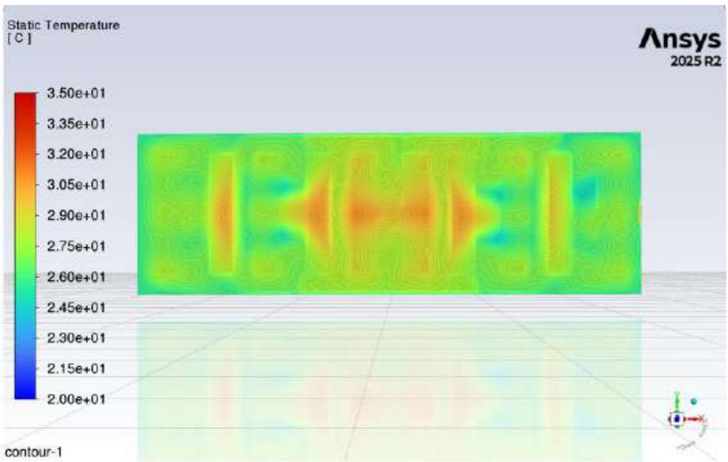

Figure 4. 60 Temperature Contour Plane after 30 seconds

Compared with the condition at 14 s, the localized warm region became less pronounced as the conditioned airflow continuously removed the residual heat introduced during the infiltration period. The temperature distribution throughout the server room became progressively more uniform, indicating the beginning of the thermal recovery process. The temperature contours after 60 s are presented in Figures 4.61 and 4.62 to evaluate the recovery of the server room following the temporary disturbance.

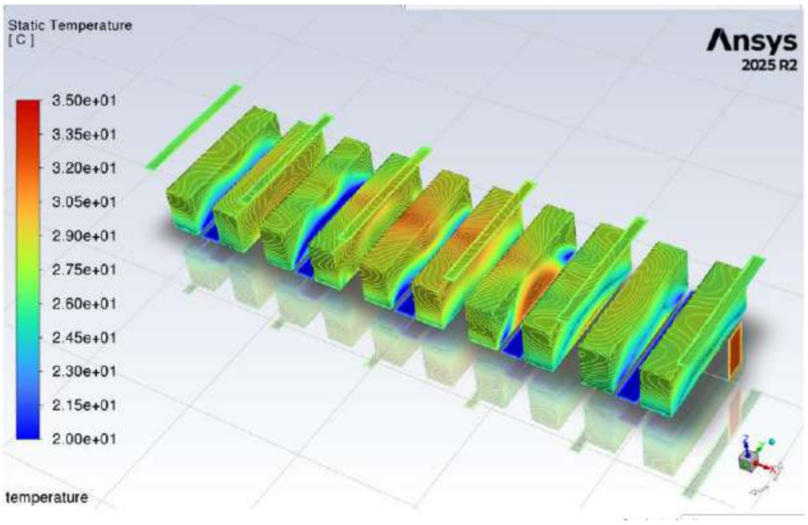

Figure 4. 61 Temperature Contour after 60 seconds

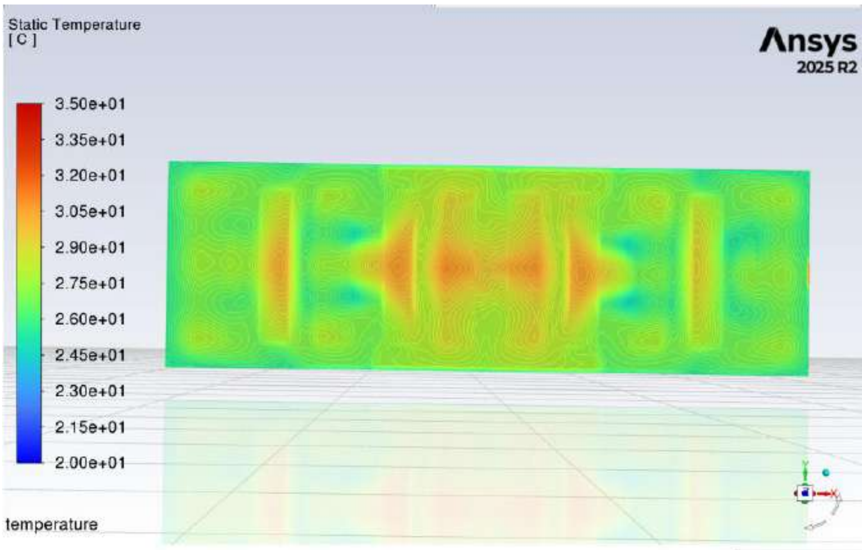

Figure 4. 62 Temperature Contour Plane after 60 seconds

At 60 s, the temperature distribution had nearly returned to the baseline operating condition prior to the door opening. The cold aisles maintained their intended cooling performance, while the hot aisles remained confined to the exhaust regions behind the server racks. No significant residual warm zones were observed, demonstrating that the HVAC system was capable of restoring the thermal environment shortly after the external disturbance had ceased. To quantitatively evaluate the thermal response of each server rack, the average rack temperature was extracted before infiltration and at five observation times throughout the transient simulation. The results are summarized in Table 4.35.

Table 4. 35 Average Temperature Case 3

Average Temperature (°C)										
Time	Further to Closer to the Door									
	Left Rack 1	Right Rack 1	Left Rack 2	Right Rack 2	Left Rack 3	Right Rack 3	Left Rack 4	Right Rack 4	Left Rack 5	Right Rack 5
Before Infiltration	25,81	28,01	26,49	28,28	27,39	27,40	28,33	26,47	27,54	25,73
1 second	25,81	28,01	26,49	28,28	27,39	27,40	28,33	26,47	27,53	25,73
7 seconds	25,81	28,01	26,49	28,28	27,39	27,40	28,33	26,44	27,52	25,76
14 seconds	25,81	28,01	26,49	28,28	27,38	27,39	28,33	26,43	27,51	25,79
30 seconds	25,81	28,01	26,49	28,28	27,39	27,41	28,34	26,46	27,51	25,77
60 seconds	25,81	28,01	27,38	27,41	27,38	27,41	28,33	26,47	27,52	25,75

Only minor temperature variations were observed throughout the transient simulation. Server racks located closer to the entrance experienced slightly larger temperature fluctuations immediately after the door opening, whereas racks farther from the entrance remained comparatively stable. However, the maximum temperature increases at each rack remained relatively small, indicating that the temporary infiltration did not significantly influence the cooling performance delivered to the IT equipment. By the end of the simulation, the average temperatures at all racks had returned to values very close to their baseline condition. The overall thermal response of the server room was further evaluated using the room-average temperature, as presented in Table 4.36.

Table 4. 36 Case 3 Room Average Temperature

Room Average Temperature	
Time (s)	**Average Temperature (°C)**
Before Infiltration	26,85
1	26,90
7	26,98
14	26,99
30	26,87
60	26,85

The room-average temperature increased only slightly from 26,85°C before infiltration to a maximum value of 26,99°C at 14 s, corresponding to an increase of approximately 0,14°C. After the entrance door was closed, the average room temperature gradually decreased to 26,85°C at 60 s, matching the initial steady-state condition. These results demonstrate that the temporary door opening produced only a negligible impact on the overall thermal condition of the server room and that the cooling system rapidly restored the indoor temperature after the disturbance was removed.

4.7.5 Transient Relative Humidity Response

To evaluate the influence of temporary outdoor air infiltration on the moisture condition inside the server room, the transient relative humidity distribution was analyzed at several observation times throughout the simulation. The humidity field was evaluated at 1 s, 7 s, 14 s, 30 s, and 60 s, representing the initial response, the maximum disturbance during the door opening period, and the recovery process after the door was closed. Both contour visualizations and quantitative average relative humidity values were used to assess the moisture response of the server room.

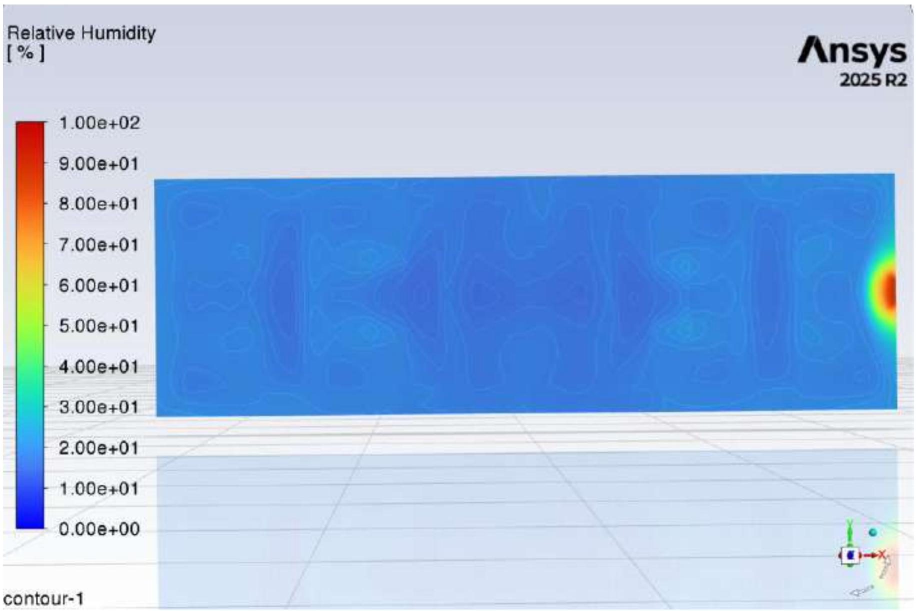

Figure 4. 63 Relative Humidity Contour Plane after 1 second

Figures 4.63 and 4.64 present the mid-plane relative humidity contours at 1 s and 7 s after the beginning of the transient simulation. These figures illustrate the initial moisture response while outdoor air continuously entered the server room through the open entrance door.

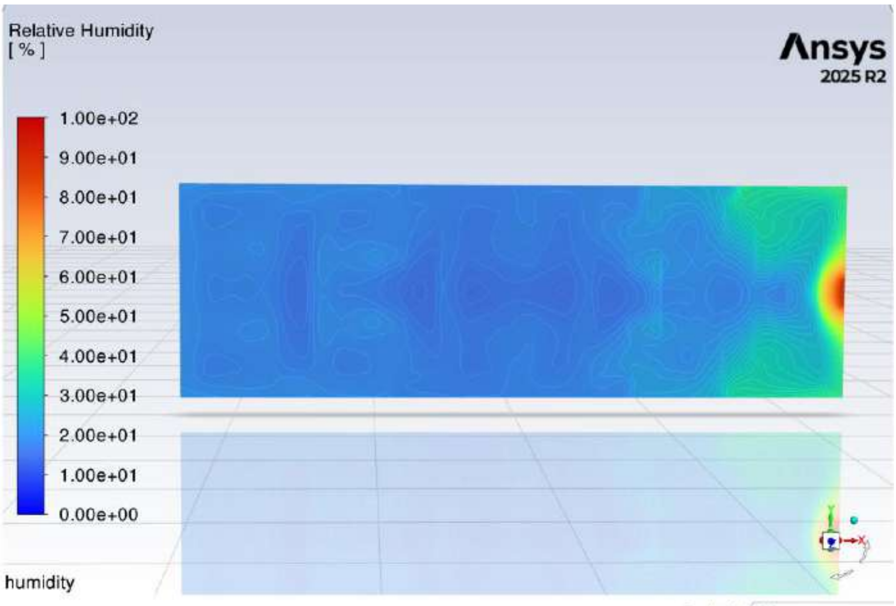

Figure 4. 64 Relative Humidity Contour Plane after 7 seconds

During the first several seconds of infiltration, the overall humidity distribution remained relatively uniform throughout most of the server room. However, a localized increase in relative humidity began to develop near the entrance due to the inflow of warm and humid outdoor air. The conditioned air supplied by the HVAC units continued to dominate the indoor airflow, thereby limiting the spread of moisture toward the cold aisle region. Consequently, the increase in relative humidity during the early stage of the disturbance remained confined to the vicinity of the entrance. The relative humidity distribution at the end of the door opening period is presented in Figures 4.65 and 4.66 using both the overall three-dimensional view and the mid-plane contour.

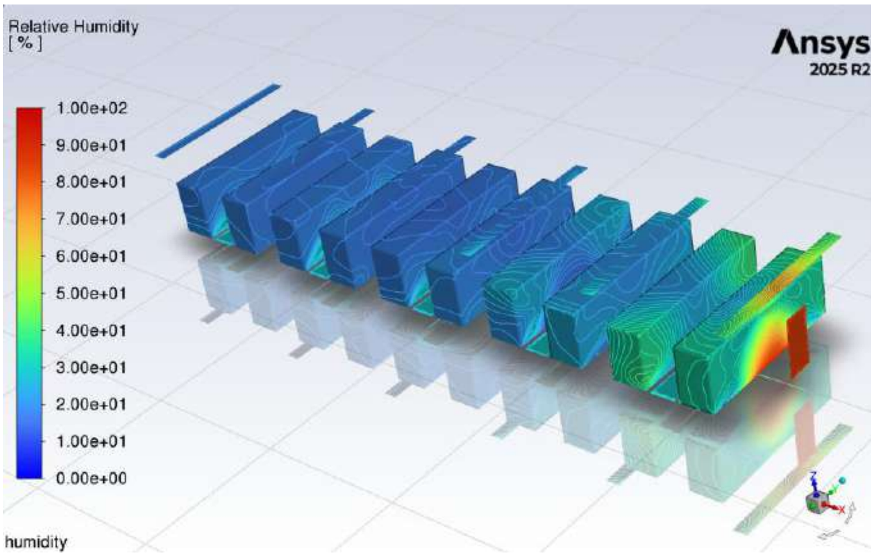

Figure 4. 65 Relative Humidity Contour after 14 seconds

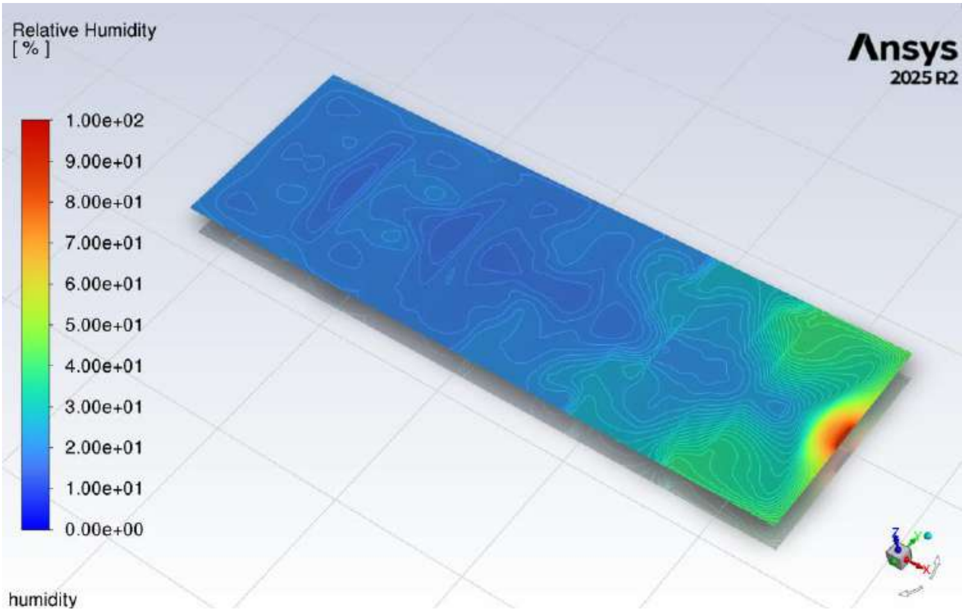

Figure 4. 66 Relative Humidity Contour Plane after 14 seconds

After 14 s of continuous infiltration, the humid outdoor air had spread further into the server room compared with the earlier observation times. Nevertheless, the increase in relative humidity remained localized near the airflow path originating from the entrance. Most of the server rack region continued to maintain relatively low humidity because the conditioned supply air effectively diluted the incoming moisture. This indicates that the temporary infiltration affected only a limited portion of the room without causing a significant increase in humidity throughout the server space. To further illustrate the movement of humid outdoor air, Figure 4.67 presents the relative humidity pathlines originating from the entrance door at 14 s.

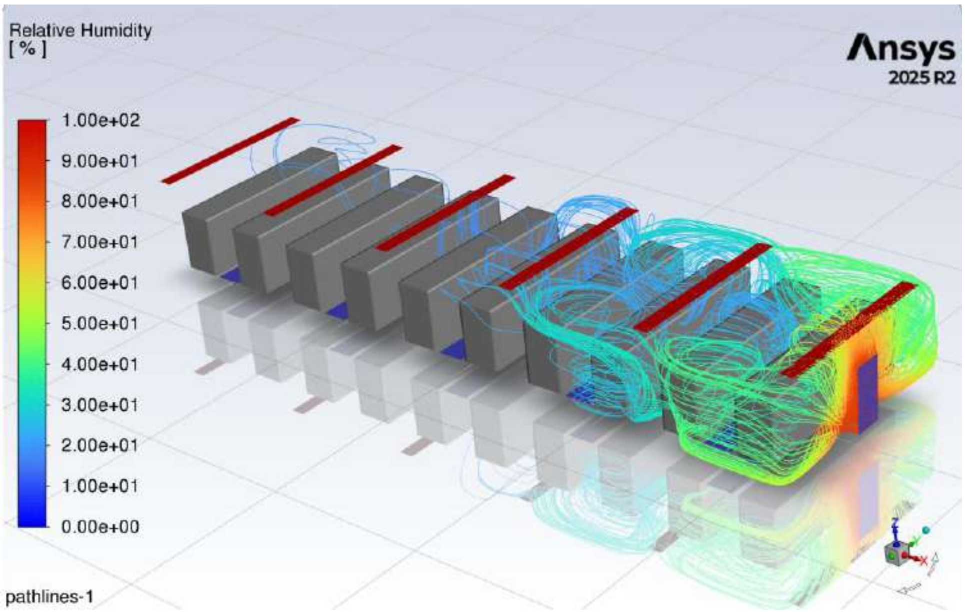

Figure 4. 67 Relative Humidity Pathlines from Door after 14 seconds

The humidity pathlines demonstrate that the incoming moist air primarily followed the dominant airflow generated by the HVAC system toward the ceiling return rather than directly entering the server rack inlets. Similar to the airflow and temperature responses discussed previously, the porous resistance of the server racks reduced the penetration of infiltrated air into the cold aisles. As a result, the increase in humidity remained concentrated near the entrance region and did not significantly affect the airflow supplied to the IT equipment.

Following the closure of the entrance door, the humidity field gradually returned toward its normal operating condition. Figure 4.68 presents the mid-plane relative humidity contour at 30 s.

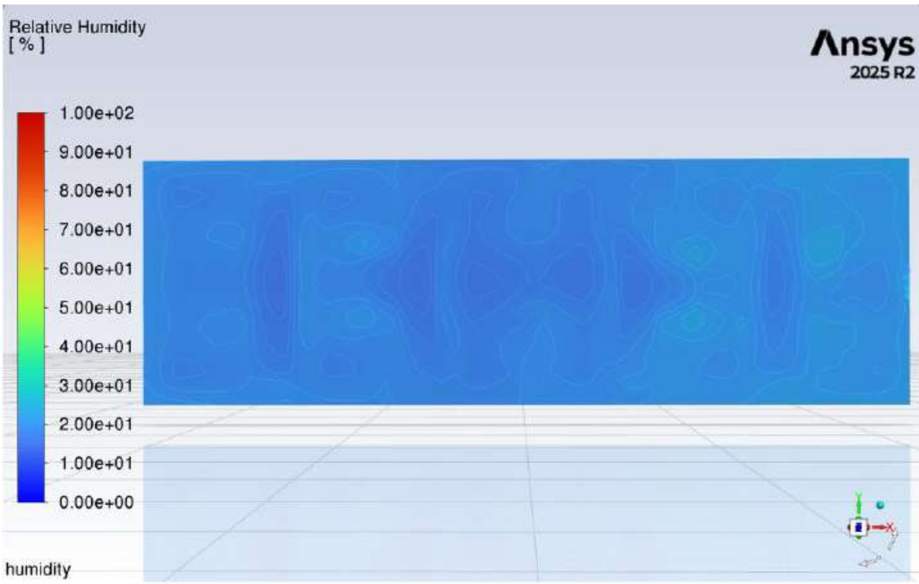

Figure 4. 68 Relative Humidity Contour Plane after 30 seconds

Compared with the condition observed at 14 s, the region with elevated relative humidity had noticeably diminished. Continuous circulation of conditioned air gradually removed the excess moisture introduced during the infiltration period, resulting in a more uniform humidity distribution throughout the server room. The recovery of the indoor humidity condition after the temporary disturbance is illustrated in Figures 4.69 and 4.70 at 60 s.

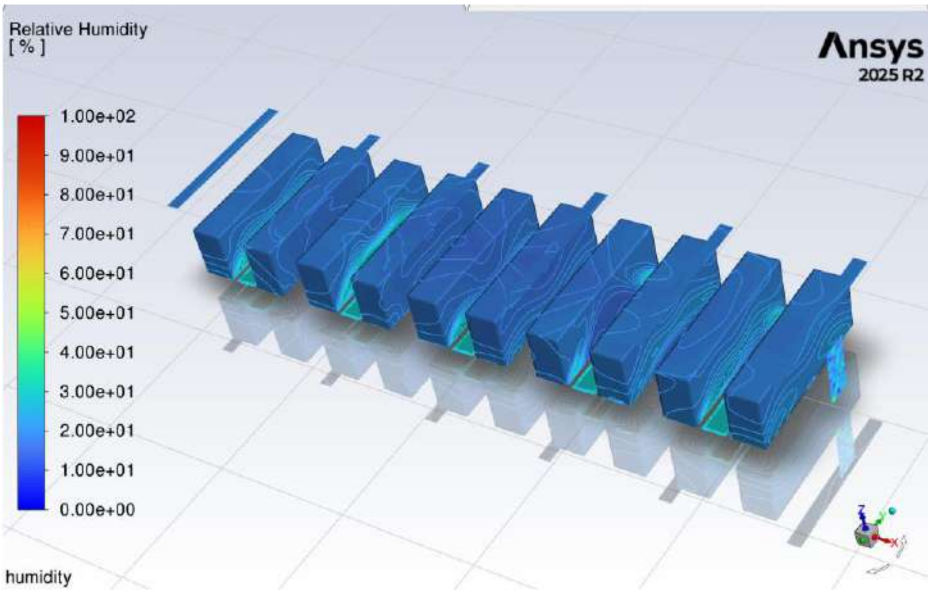

Figure 4. 69 Relative Humidity Contour after 60 seconds

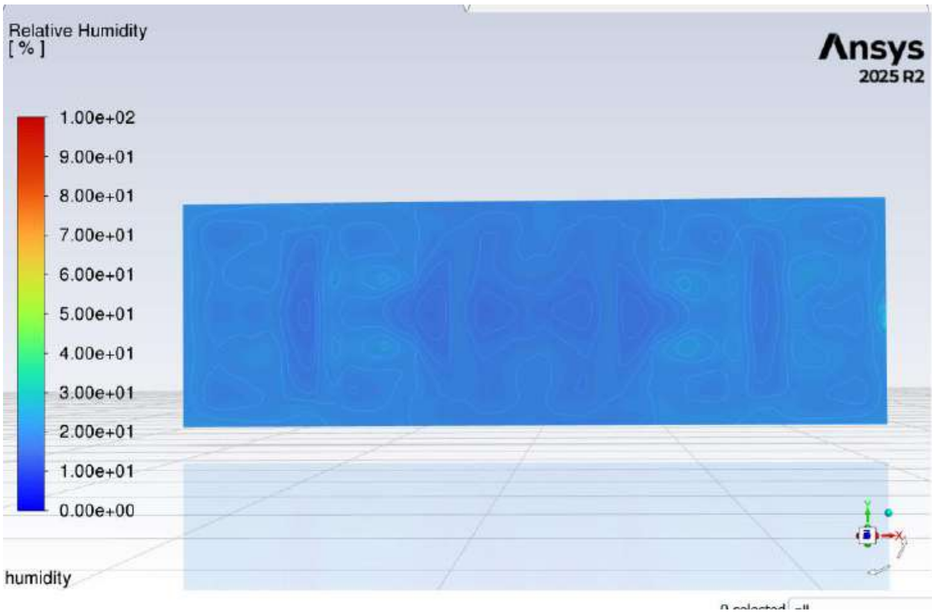

Figure 4. 70 Relative Humidity Contour Plane after 60 seconds

At 60 s, the humidity distribution had nearly returned to the baseline operating condition before the door opening. The localized high-humidity region observed near the entrance was no longer present, indicating that the HVAC system effectively restored the indoor moisture condition after the temporary infiltration ceased. The relative humidity throughout the server room remained within the recommended operating range for IT equipment.

To quantitatively evaluate the moisture response at each server rack, the average relative humidity was extracted before infiltration and at five observation times during the transient simulation. The results are summarized in Table 4.37.

Table 4. 37 Case 3 Average Relative Humidity on each Racks

Average Relative Humidity (%)										
Time	Further to Closer to the Door									
	Left Rack 1	Right Rack 1	Left Rack 2	Right Rack 2	Left Rack 3	Right Rack 3	Left Rack 4	Right Rack 4	Left Rack 5	Right Rack 5
Before Infiltration	21,11	18,48	20,29	18,19	19,30	19,27	18,15	20,32	19,00	21,19
1 second	21,11	18,48	20,29	18,19	19,30	19,27	18,15	20,32	19,01	24,73
7 seconds	21,12	18,48	20,29	18,19	19,35	19,53	19.14	21,56	24,96	33,65
14 seconds	21,14	18,49	20,34	18,44	19,94	20,84	21,22	23,89	27,96	36,55
30 seconds	21,24	18,61	20,47	18,63	19,99	20,46	19,64	21,65	20,52	22,58
60 seconds	21,15	18,52	20,34	18,24	19,41	19,39	18,29	20,44	19,19	21,33

The average relative humidity of the server racks exhibited only moderate variations during the transient simulation. Racks located closer to the entrance experienced larger humidity increases during the door opening period than racks located farther away. Nevertheless, the overall increase remained limited, and the humidity values gradually returned toward their baseline condition after the door was closed. These results indicate that the temporary infiltration had only a localized influence on the moisture condition surrounding the server racks. The overall humidity response of the server room was further evaluated using the room-average relative humidity, as summarized in Table 4.38.

Table 4. 38 Case 3 Room Average Relative Humidity

Room Average Relative Humidity	
Time (s)	**Average Relative Humidity (%)**
Before Infiltration	19,80
1	20,62
7	23,08
14	24,56
30	20,77
60	19,94

The room-average relative humidity increased from 19.80% before infiltration to 20.62% after 1 s, continued to rise to 23.08% at 7 s, and reached a maximum value of 24.56% at 14 s, corresponding to the end of the door opening period. After the entrance door was closed, the conditioned airflow progressively removed the infiltrated moisture, reducing the room-average relative humidity to 20.77% at 30 s and 19.94% at 60 s. The final value differed from the baseline by only 0.14 percentage points, demonstrating that the cooling system effectively restored the indoor moisture condition following the temporary infiltration event.

4.7.6 Transient Simulation Summary

To provide a clearer overview of the transient simulation results, the average temperature and relative humidity responses at both the rack level and the room level are summarized in Figures 4.71–4.74. These graphs present the temporal evolution of the monitored parameters from the baseline condition prior to door opening until the recovery stage after the door was closed. Figure 4.71 presents the average temperature of each server rack throughout the transient simulation.

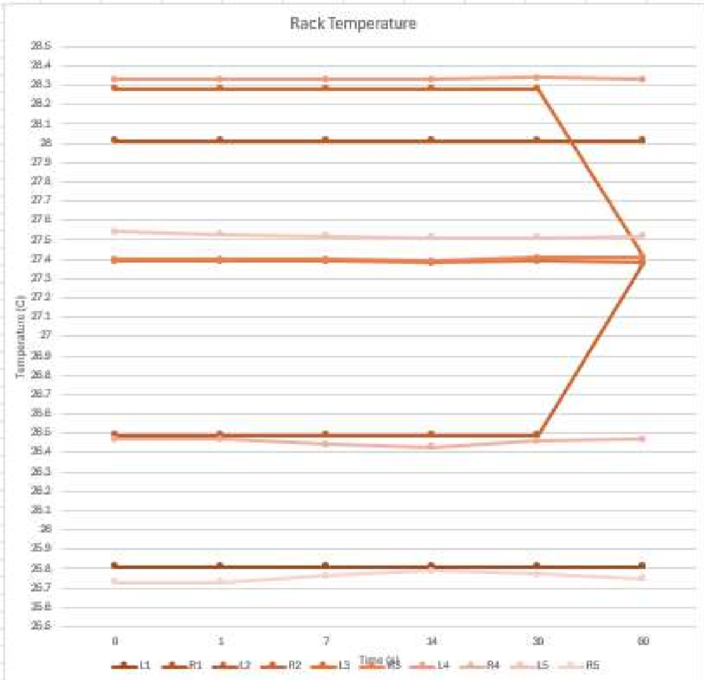

Figure 4. 71 Curve of Server Racks Temperature

Overall, the temperature profiles of the server racks remained relatively stable throughout the transient event. Most racks exhibited only minor temperature variations during the door opening period, indicating that the temporary outdoor air infiltration had a limited influence on the thermal conditions surrounding the IT equipment. Slightly larger fluctuations were observed at several racks located closer to the entrance; however, these variations remained small and gradually returned toward their initial values after the door was closed. This behavior confirms that the HVAC system maintained a stable cooling performance despite the temporary disturbance. The variation in average relative humidity at each server rack is summarized in Figure 4.72.

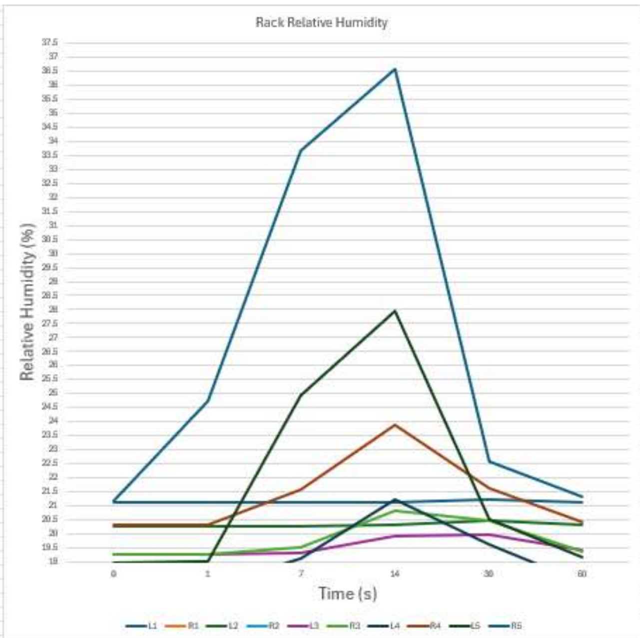

Figure 4. 72 Curve of Server Racks Relative Humidity

Compared with temperature, relative humidity exhibited a more noticeable transient response during the door opening period. Racks located closer to the entrance experienced a larger increase in relative humidity due to the infiltration of warm and humid outdoor air, whereas racks farther from the entrance showed only minor changes. Following the closure of the entrance door, the relative humidity of all racks gradually decreased toward their baseline values, demonstrating the effectiveness of the cooling and ventilation system in removing the infiltrated moisture. Figure 4.73 summarizes the variation in the room-average temperature throughout the transient simulation.

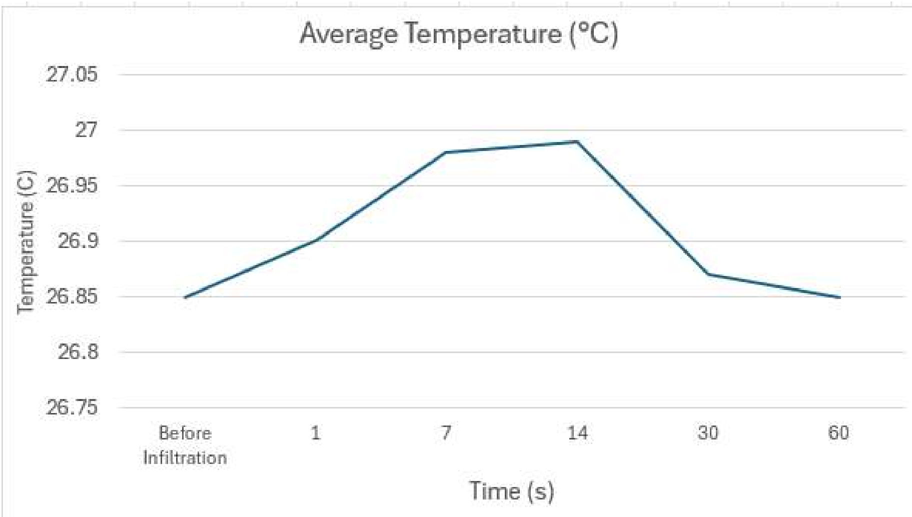

Figure 4. 73 Curve of Room Average Temperature

The room-average temperature increased gradually after the beginning of outdoor air infiltration, reaching a maximum value of 26,99°C at 14 s. Following the closure of the entrance door, the average temperature decreased steadily and returned to 26,85°C at 60 s, matching the baseline condition before infiltration. The maximum increase in room-average temperature was approximately 0,14°C, indicating that the thermal impact of the temporary door opening was negligible. The overall room-average relative humidity response is presented in Figure 4.74.

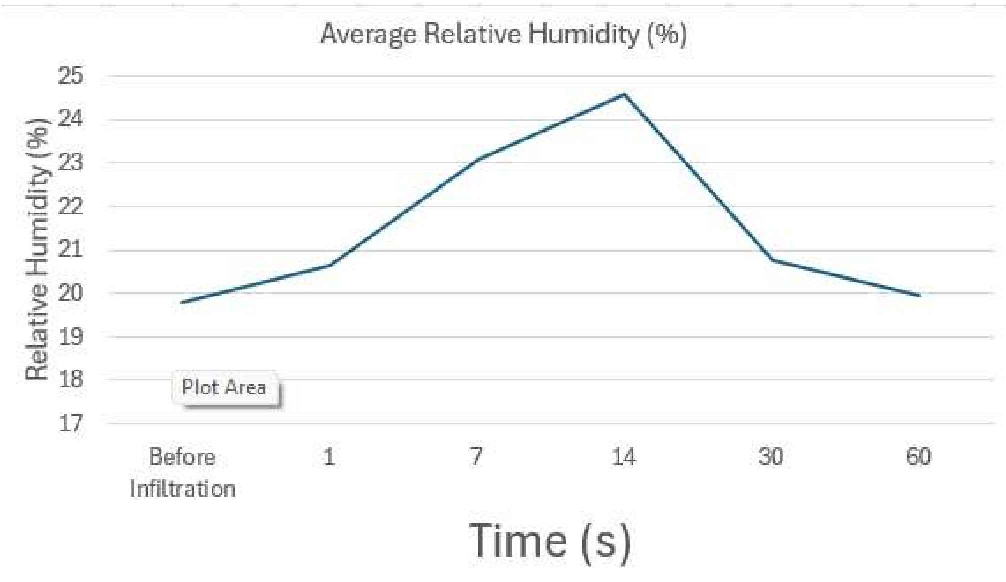

Figure 4. 74 Curve of Room Average Relative Humidity

Unlike temperature, the room-average relative humidity exhibited a more pronounced response to the temporary infiltration. The average relative humidity increased from 19,80% before infiltration to a peak value of 24,56% at 14 s, reflecting the influence of the humid outdoor air entering through the open door. After the door was closed, the conditioned airflow gradually removed the excess moisture, reducing the average relative humidity to 19,94% at 60s. The final value differed from the baseline by only 0,14 percentage points, indicating that the server room rapidly recovered to its normal operating condition.

Overall, the transient simulation demonstrates that the temporary opening of the entrance door produced only a localized and short-term disturbance to the indoor environmental conditions. Although outdoor air infiltration caused a temporary increase in both temperature and relative humidity, the airflow generated by the HVAC system remained dominant throughout the server room, limiting the penetration of warm and humid air into the server rack region. Consequently, the room-average temperature increased by only 0,14°C, while the room-average relative humidity returned to within 0,14 percentage points of its baseline value after 60 s. These findings indicate that the proposed cooling system possesses sufficient resilience to maintain stable thermal and moisture conditions during short-duration door opening events, thereby supporting reliable operation of the IT equipment.

4.8 Compliance Assessment with ASHRAE Guidelines and SNI 8799-1: 2023

To evaluate the suitability of the proposed cooling system for data center applications, the simulation results obtained from the steady-state and transient CFD analyses were assessed against the environmental operating limits recommended by ASHRAE TC 9.9 and SNI 8799-1: 2023 (Standar Nasional Indonesia). This assessment aims to determine whether the proposed room condition is capable of maintaining acceptable environmental conditions for IT equipment under both normal operating conditions and temporary outdoor air infiltration.

4.8.1 ASHRAE Guidelines

Figure 4.75 presents the environmental envelope for IT equipment based on the ASHRAE TC 9.9 Thermal Guidelines for Data Processing Environments (2016). The guideline defines both the Recommended Operating Range, which represents the environmental conditions targeted for normal data center operation, and the Allowable Operating Range for Class A2 equipment, which specifies the acceptable operating limits that ensure reliable server operation under temporary environmental variations. The recommended operating range for temperature is from 18C to 27C. For A2 Allowable operating range have more further range. For temperature, the range is from 10C to 35C. For humidity, the range is from 8% to 80%. Therefore, the simulation results presented in this study are evaluated against both the Recommended Operating Range and the Allowable Operating Range for Class A2 to verify the thermal and humidity performance of the proposed cooling system.(ASHRAE Technical Committee 9.9, 2021)

Equipment Environment Specifications for Air Cooling							
	Product Operation[b,c]					Product Power Off[c,d]	
Class[a]	Dry-Bulb Temp.[e,g], °C	Humidity Range, Noncond.[h, i, k, l, n]	Max. Dew Point[k], °C	Max. Elev.[e,j,m], m	Max. Rate of Change[f], °C/h	Dry-Bulb Temp., °C	RH[k], %
Recommended (suitable for Classes A1 to A4; explore data center metrics in this book for conditions outside this range.)							
A1 to A4	18 to 27	–9°C DP to 15°C DP and 70% rh[n] or 50% rh[n]					
Allowable							
A1	15 to 32	–12°C DP and 8% rh to 17°C DP and 80% rh[k]	17	3050	5/20	5 to 45	8 to 80[k]
A2	10 to 35	–12°C DP and 8% rh to 21°C DP and 80% rh[k]	21	3050	5/20	5 to 45	8 to 80[k]
A3	5 to 40	–12°C DP and 8% rh to 24°C DP and 85% rh[k]	24	3050	5/20	5 to 45	8 to 80[k]
A4	5 to 45	–12°C DP and 8% rh to 24°C DP and 90% rh[k]	24	3050	5/20	5 to 45	8 to 80[k]
B	5 to 35	8% to 28°C DP and 80% rh	28	3050	N/A	5 to 45	8 to 80
C	5 to 40	8% to 28°C DP and 80% rh	28	3050	N/A	5 to 45	8 to 80

* For potentially greater energy savings, refer to Appendix C for the process needed to account for multiple server metrics that impact overall TCO.

Figure 4. 75 Ashrae 2021 Thermal Guidelines(ASHRAE Technical Committee 9.9, 2021)

As shown in Figure 4.75, the ASHRAE TC 9.9 Thermal Guidelines classify the environmental operating conditions for IT equipment into the Recommended Operating Range and the Allowable Operating Range according to the equipment class. The Recommended Operating Range specifies the target environmental conditions for normal data center operation, including a recommended dry-bulb temperature of 18–27°C. Meanwhile, the Allowable Operating Range defines the wider operating limits within which IT equipment can continue to operate safely. For Class A2 equipment, the allowable limits include a dry-bulb temperature of 10–35°C and a relative humidity range of 8–80%. Therefore, the compliance assessment presented in this study focuses on comparing the simulated temperature and relative humidity with the ASHRAE TC 9.9 Recommended Operating Range and the Allowable Operating Range for Class A2 to evaluate the environmental performance of the proposed cooling system.

Table 4. 39 Compliance of Temperature with ASHRAE Recommendation

Recommended Operating Range for Temperature (C)					
Parameter	ASHRAE (C)	Average	Maximum	Minimum	Compliance
50% Workload	18 - 27	25,30	28,84	19,89	Average Temperature comply but the maximum is 1,84 C higher than recommended
70% Workload		26,95	31,86	19,86	Average Temperature comply but the maximum is 4,86 C higher than recommended
With Infiltration (14s)		27,04	32,06	19,78	Average Temperature is 0,04 C higher than recommended and maximum is 5,06 C Higher then recommended

Table 4.39 presents the compliance assessment of the simulated temperature distribution with the ASHRAE TC 9.9 Recommended Operating Range of 18–27°C. Under the 50% IT workload, the average temperature was 25,30°C, which remained within the recommended operating range. The minimum temperature was 19,89°C, while the maximum temperature reached 28,84°C, exceeding the recommended upper limit by 1,84°C. At the 70% IT workload, the average temperature increased to 26,95°C but still satisfied the recommended range. The minimum temperature remained within the recommended limit at 19,86°C, whereas the maximum temperature increased to 31,86°C, exceeding the upper limit by 4,86°C. During the transient simulation with door infiltration at 14 s, the average temperature reached 27,04°C, which was only 0,04°C higher than the recommended upper limit. The minimum temperature was 19,78°C, while the maximum temperature reached 32,06°C, exceeding the recommended upper limit by 5,06°C.

Table 4. 40 Compliance of Temperature with ASHRAE Allowable A2 Class

Allowable A2 Class Range for Temperature (C)					
Parameter	ASHRAE (C)	Average	Maximum	Minimum	Compliance
50% Workload	10 - 35	25,30	28,84	19,89	Comply
70% Workload		26,95	31,86	19,86	Comply
With Infiltration (14s)		27,04	32,06	19,78	Comply

Table 4.40 presents the compliance assessment of the simulated temperature distribution with the ASHRAE TC 9.9 Allowable Operating Range for Class A2, which specifies an acceptable temperature range of 10–35°C. Under the 50% IT workload, the average, maximum, and minimum temperatures were 25,30°C, 28,84°C, and 19,89°C, respectively, all of which remained within the allowable temperature range. At the 70% IT workload, the average temperature increased to 26,95°C, while the maximum and minimum temperatures were 31,86°C and 19,86°C, respectively. During the transient simulation with door infiltration at 14 s, the average temperature reached 27,04°C, with a maximum temperature of 32,06°C and a minimum temperature of 19,78°C. All recorded temperatures remained within the allowable Class A2 operating range, indicating that the proposed cooling system maintained acceptable thermal conditions under both steady-state and transient operating conditions.

Table 4. 41 Compliance of Relative Humidity with Allowable A2 Class Range

Allowable A2 Class Range for Relative Humidity (%)					
Parameter	ASHRAE (%)	Average	Maximum	Minimum	Compliance
50% Workload	8 - 80	21,65	29,95	17,52	Comply
70% Workload		19,70	30,01	14,73	Comply
With Infiltration (14s)		24,07	77,89	14,93	Comply

Table 4.41 presents the compliance assessment of the simulated relative humidity with the ASHRAE TC 9.9 Allowable Operating Range for Class A2, which specifies an acceptable relative humidity range of 8–80%. Under the 50% IT workload, the average relative humidity was 21,65%, with maximum and minimum values of 29,95% and 17,52%, respectively. At the 70% IT workload, the average relative humidity decreased to 19,70%, while the maximum and minimum values were 30,01% and 14,73%, respectively. During the transient simulation with door infiltration at 14 s, the average relative humidity increased to 24,07%, with a maximum value of 77,89% and a minimum value of 14,93%. Despite the temporary increase in humidity caused by outdoor air infiltration, all simulated relative humidity values remained within the allowable Class A2 operating range of 8–80%, demonstrating that the proposed cooling system was capable of maintaining acceptable moisture conditions throughout the simulation.

4.8.2 SNI 8799-1: 2023 (Standar Nasional Indonesia)

The environmental performance of the proposed floating data center server room was also evaluated based on SNI 8799-1. The standard specifies the recommended operating conditions for server rooms, including room temperature, relative humidity, dew point, maximum allowable temperature variation, and maximum allowable relative humidity variation. As presented in Figure 4.76, the recommended environmental limits are identical for Strata 1 to Strata 4 data centers, while the differences between strata mainly relate to redundancy and infrastructure availability rather than indoor environmental condition Based on the designed cooling system adopted in this study, the proposed floating data center generally follows the characteristics of a Strata 2 data center, where the primary infrastructure incorporates backup components but does not implement full N+1 redundancy throughout the entire cooling system The environmental operating limits specified in SNI 8799-1:2023 are identical for all strata, including the recommended room temperature, relative humidity, dew point, and the maximum allowable rates of temperature and humidity variation. Therefore, the CFD simulation results were compared with these environmental requirements to evaluate the thermal performance of the designed server room.(SNI, 2023)

No.	Spesifikasi Teknis	Strata 1	Strata 2	Strata 3	Strata 4
1.	Temperatur ruangan	18 °C – 27 °C	18 °C – 27 °C	18 °C – 27 °C	18 °C – 27 °C
2.	Tingkat perubahan temperatur ruangan per jam maksimum	5 °C	5 °C	5 °C	5 °C
3.	Kelembaban ruangan (*Relative Humidity—RH*)	≤ 60 %	≤ 60 %	≤ 60 %	≤ 60 %
4.	Titik embun	5,5 °C – 15 °C	5,5 °C – 15 °C	5,5 °C – 15 °C	5,5 °C – 15 °C
5.	Tingkat perubahan kelembaban ruangan maksimum per jam	5 % RH	5 % RH	5 % RH	5 % RH

Figure 4. 76 SNI 8799-1: 2023 Room Condition Standard(SNI, 2023)

The average room temperatures obtained from the CFD simulations under different operating conditions were compared with the recommended temperature range of 18–27 °C specified in SNI 8799-1:2023. The comparison is presented in Table 4.42.

Table 4. 42 Compliance with SNI Range of Temperature

SNI Recommended Range for Room Average Temperature (C)			
Parameter	SNI (C)	Average	Compliance
50% Workload	18 - 27	25,30	Comply
70% Workload		26,95	Comply

With Infiltration (14s)		27,04	Slightly higher by 0,4 C

As shown in Table 4.42, the average room temperatures at 50% workload and 70% workload were 25.30 °C and 26.95 °C, respectively, both of which are within the recommended operating range. During the infiltration case, the average room temperature increased to 27.04 °C, exceeding the upper limit by only 0.04 °C. This slight increase is considered negligible and indicates that the proposed cooling system is capable of maintaining acceptable thermal conditions even under transient infiltration events.

The simulated average relative humidity was also evaluated against the SNI maximum recommended value of 60% RH, as summarized in Table 4.43.

Table 4. 43 Compliance with SNI Range of Relative Humidity

SNI Recommended Range for Room Relative Humidity (%)			
Parameter	SNI (%)	Average	Compliance
50% Workload	≤ 60	21,65	Comply
70% Workload		19,70	Comply
With Infiltration (14s)		24,07	Comply

The predicted average relative humidity ranged from 19.70% to 24.07% for all operating scenarios. These values remain significantly below the maximum allowable limit of 60% RH, demonstrating that the proposed HVAC system is capable of maintaining a sufficiently dry environment for reliable server operation.

Besides evaluating the average room condition, the transient temperature response during the infiltration event was compared with the maximum allowable temperature variation specified in SNI 8799-1:2023, which limits the room temperature change to 5 °C per hour.

Table 4. 44 Compliance with SNI maximum rise of Temperature

SNI Maximum Temperature Rise (C)				
Time	SNI (C)	Room Temperature	Temperature Rise	Compliance
Before Infiltration	5 C	26,85	0,14 C	Comply
1 s		26,90		
7 s		26,98		
14 s		26,99		
30 s		26,87		
60 s		26,85		

The room temperature increased from 26.85 °C to a maximum of 26.99 °C, corresponding to a temperature rise of only 0.14 °C throughout the infiltration period. This value is substantially lower than the allowable limit, confirming that the thermal stability of the proposed server room satisfies the SNI requirement.

The variation of room relative humidity during the infiltration event was also assessed using the SNI criterion, which limits the maximum relative humidity variation to 5% RH per hour.

Table 4. 45 Compliance with SNI maximum rise of Relative Humidity

<table>
<tr><th colspan="5">SNI Maximum Relative Humidity Rise (C)</th></tr>
<tr><th>Time</th><th>SNI (%)</th><th>Room RH%</th><th>RH% Rise</th><th>Compliance</th></tr>
<tr><td>Before Infiltration</td><td rowspan="6">5 %</td><td>19,80</td><td rowspan="6">4,74 %</td><td rowspan="6">Comply</td></tr>
<tr><td>1 s</td><td>20,62</td></tr>
<tr><td>7 s</td><td>23,08</td></tr>
<tr><td>14 s</td><td>24,56</td></tr>
<tr><td>30 s</td><td>20,77</td></tr>
<tr><td>60 s</td><td>19,94</td></tr>
</table>

The relative humidity increased from 19.80% to a peak value of 24.56%, corresponding to a humidity increase of 4.74% RH. Since this value remains below the maximum allowable variation of 5% RH, the proposed cooling system satisfies the SNI requirement for humidity stability during transient infiltration conditions.

This page is intentionally left blank

CHAPTER V

CONCLUSION

5.1 Conclusion

This research was conducted to evaluate the environmental performance of a representative server room in a 1 MW Floating Data Center (FDC), where maintaining appropriate airflow, temperature, and relative humidity is essential to ensure reliable operation of high-density IT equipment. As server power density continues to increase, ineffective airflow management may result in hot air recirculation, thermal hotspots, and unstable environmental conditions that reduce equipment reliability and operational efficiency. Therefore, this study focused on investigating the airflow characteristics, thermal behavior, and humidity distribution inside a modular server room employing a hot aisle–cold aisle configuration as one of the most widely adopted airflow management strategies in modern data centers.

To achieve this objective, a Computational Fluid Dynamics (CFD) approach was employed using ANSYS Fluent. The server room geometry was developed as a representative module of a 1 MW Floating Data Center equipped with a raised-floor air distribution system, where conditioned air was supplied through perforated floor tiles and returned through ceiling-mounted HVAC units. The server racks were simplified using a porous-media approach with anisotropic viscous resistance, directional momentum sources, and volumetric heat generation to represent internal airflow and heat dissipation while maintaining computational efficiency. The analysis consisted of a preliminary wall heat transfer simulation, a single-rack validation study, two steady-state simulations under 50% and 70% IT workloads, and a transient air infiltration simulation representing temporary door opening. The predicted airflow, temperature, and relative humidity distributions were then evaluated against the environmental requirements specified in ASHRAE TC 9.9 and SNI 8799-1:2023 to assess the suitability of the proposed server room configuration under the investigated operating conditions. From this research, the conclusion obtained are:

1. The CFD simulation demonstrated that the hot aisle–cold aisle configuration effectively controlled the airflow distribution within the 1 MW floating data center server room. The supply air delivered through the raised-floor plenum was directed into the cold aisles before entering the server racks, while the heated exhaust air was confined to the hot aisles and returned to the HVAC units. This airflow pattern minimized the mixing of hot and cold air, resulting in a stable thermal environment throughout the server room. Although localized hot spots were observed near the server exhaust regions and servers in the middle of the room, the average room temperature remained within the recommended operating range under steady-state conditions, indicating that the proposed cooling system effectively removed the generated IT heat load.

2. The airflow configuration also contributed to maintaining acceptable relative humidity within the server room during both steady-state and transient operating conditions. During the transient simulation, temporary outdoor air infiltration caused a short-term increase in temperature and relative humidity; however, the airflow generated by the HVAC units rapidly restored the environmental conditions after the door was closed. The compliance assessment showed that all simulated temperatures remained within the

ASHRAE TC 9.9 Allowable Class A2 temperature range of 10–35°C, while the relative humidity consistently satisfied the allowable range of 8–80%. The simulation also complies with SNI standards. Only the average temperature that is 0,4 C higher than the required. Therefore, the proposed room condition is capable of maintaining a reliable thermal and humidity environment for the operation of Class A2 IT equipment and SNI standards under the investigated operating conditions.

5.2 Suggestion

Suggestions that could be given towards future development of similar research topics are:

1. Future studies are recommended to investigate different IT load conditions and operational scenarios, including higher server utilization, varying outdoor environmental conditions, and longer door-opening durations. In addition to create a more stable condition, containment is advised to be added to the domain to control the hot aisle and cold aisle conditions. Such analyses would provide a more comprehensive understanding of the thermal and humidity performance of the proposed cooling system under a wider range of operating conditions.

2. The present study employed a simplified porous-media representation of the server racks. Future research may utilize detailed server rack geometries with realistic fan characteristics and internal airflow distribution to improve the accuracy of airflow, temperature, and humidity predictions within the server room.

BIBLIOGRAPHY

Andrae, A., & Edler, T. (2015). On Global Electricity Usage of Communication Technology: Trends to 2030. *Challenges*, *6*(1), 117–157. https://doi.org/10.3390/challe6010117

ASHRAE Technical Committee 9.9. (2021). *2021 Equipment Thermal Guidelines for Data Processing Environments: ASHRAE TC 9.9 Reference Card*.

Budiyanto, M. A., Imamudien, O., Lubis, A., Alhamid, M. I., & Shinoda, T. (2023). Air flow distribution and cooling performance on modular cold storage for fishery commodity. *Energy Reports*, *9*, 162–171. https://doi.org/10.1016/j.egyr.2023.05.241

Charara, A. (2023). *CFD Analysis of a Data Center: Thermal and Airflow Optimization*.

Chethana, G. D., & Sadashivegowda, B. (2024). A Comparative Numerical Study of Effectiveness of Cold Aisle Containment in Data Centers by Varying Rack Porosity Using Computational Fluid Dynamics. *CFD Letters* , *16*(9), 94–113. https://doi.org/10.37934/cfdl.16.9.94113

Hassan, N. M. S., Khan, M. M. K., & Rasul, M. G. (2013). Temperature monitoring and CFD analysis of data centre. *Procedia Engineering*, *56*, 551–559. https://doi.org/10.1016/j.proeng.2013.03.159

Herlin, M. (2008). Airflow and Cooling Performance of Data Centers. *ASHRAE Transactions*, *114*(2).

Macedo, D., Godina, R., Gaspar, P. D., da Silva, P. D., & Covas, M. T. (2019). A parametric numerical study of the airflow and thermal performance in a real data center for improving sustainability. *Applied Sciences (Switzerland)*, *9*(18). https://doi.org/10.3390/app9183850

Seong, N.-C., Kim, J.-H., & Kim, J.-H. (2017). CFD Analysis of Temperature and Relative Humidity Distribution as Air Flow Rate Variation in the Underground Utility Pipe Tunnel. *Journal of KIAEBS*, *11*(4), 273–282. https://doi.org/10.12972/jkiaebs.20170001

SNI. (2023). *Teknologi informasi-Pusat data-Bagian 1: Spesifikasi teknis pusat data*. www.bsn.go.id

Versteeg, H. K., & Malalasekera, W. (n.d.). *An Introduction to Computational Fluid Dynamics Second Edition*. Retrieved www.pearsoned.co.uk/versteeg

Zhang, F., & Ryu, Y. (2021). Simulation study on indoor air distribution and indoor humidity distribution of three ventilation patterns using computational fluid dynamics. *Sustainability (Switzerland)*, *13*(7). https://doi.org/10.3390/su13073630

This page is intentionally left blank

ATTACHMENT

Boundary conditions

Parameter	Value	Parameter	Value
Room size	6.79 x 5.49 x 3m	Tile size	0.534 x 0.534 x 0.1m
Number of racks	14	Tile porosity	0.25
Rack size	0.61 x 0.915 x 2 m	Inlet temperature	12.3^{0}C
Rack porosity	0.35 to 0.75 (Step size 0.1)	Inlet velocity	1m/s
Cooling fan size	0.61 x 0.5 x 0.0763m	Mesh size	0.05 m
Fan momentum	25 N/m^3	CFD solver model	k-Epsilon turbulence

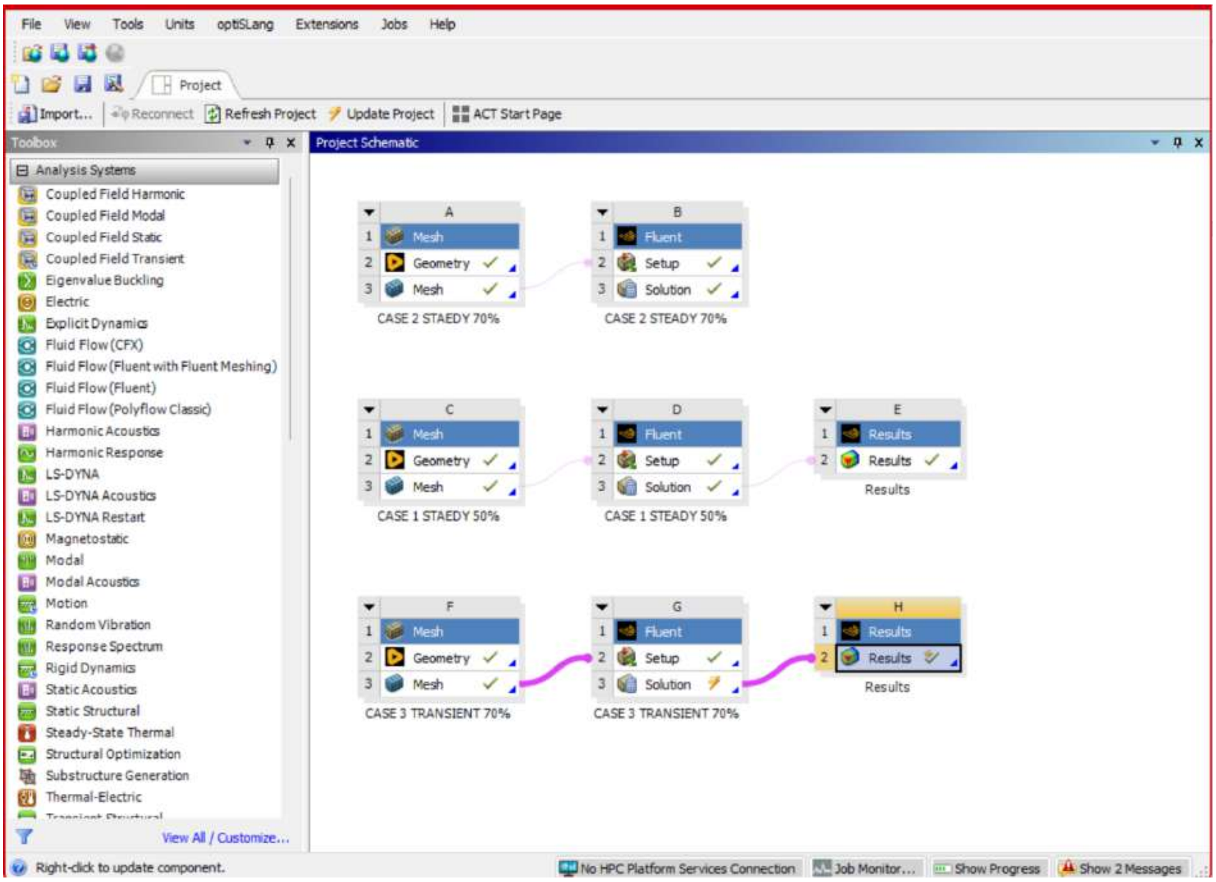

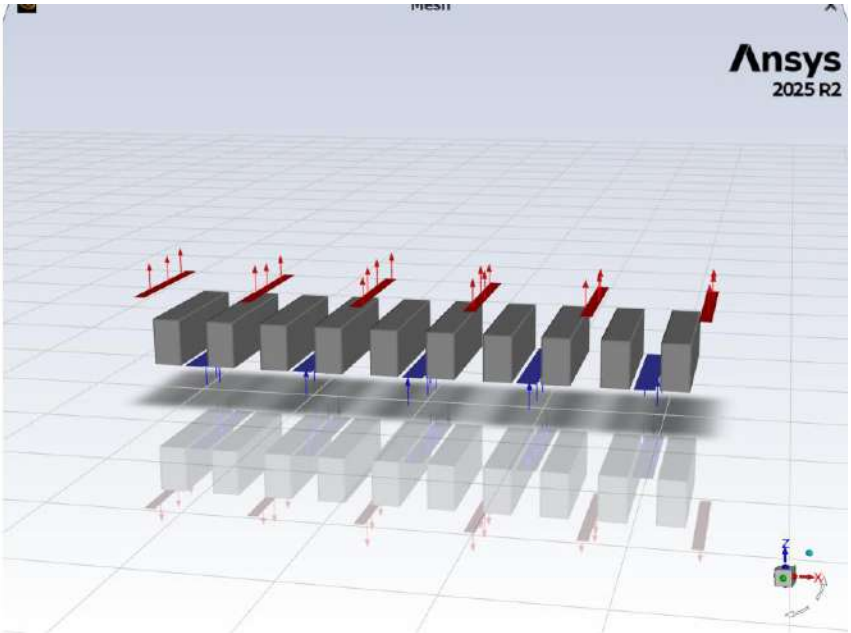
Ansys
2025 R2

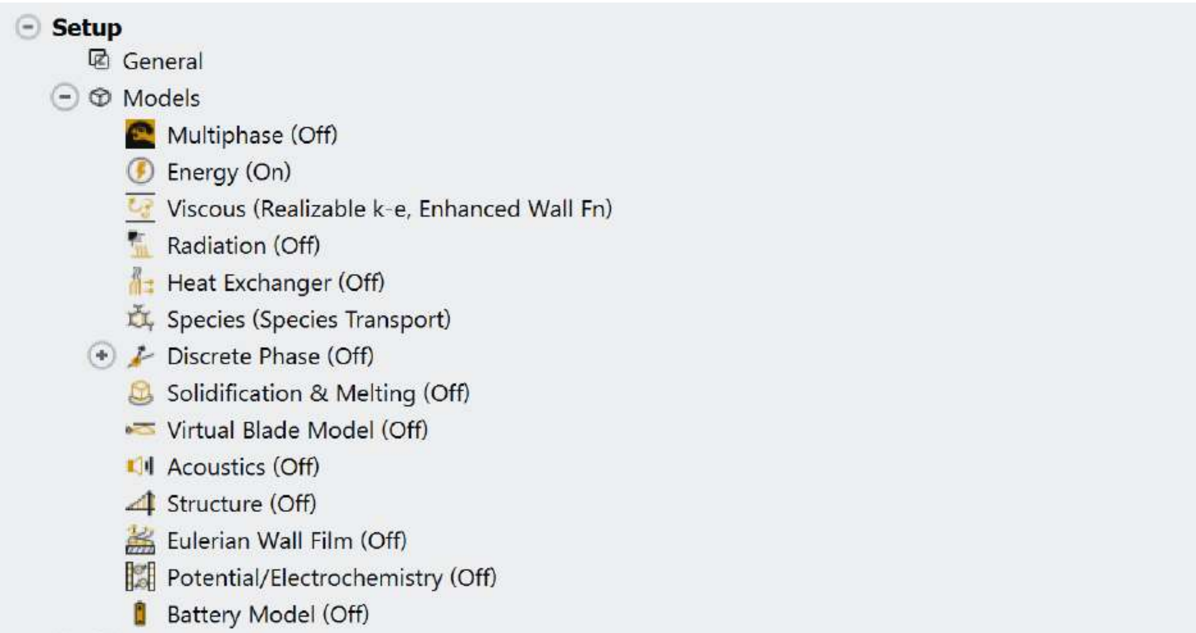
Setup
General
Models
Multiphase (Off)
Energy (On)
Viscous (Realizable k-e, Enhanced Wall Fn)
Radiation (Off)
Heat Exchanger (Off)
Species (Species Transport)
Discrete Phase (Off)
Solidification & Melting (Off)
Virtual Blade Model (Off)
Acoustics (Off)
Structure (Off)
Eulerian Wall Film (Off)
Potential/Electrochemistry (Off)
Battery Model (Off)

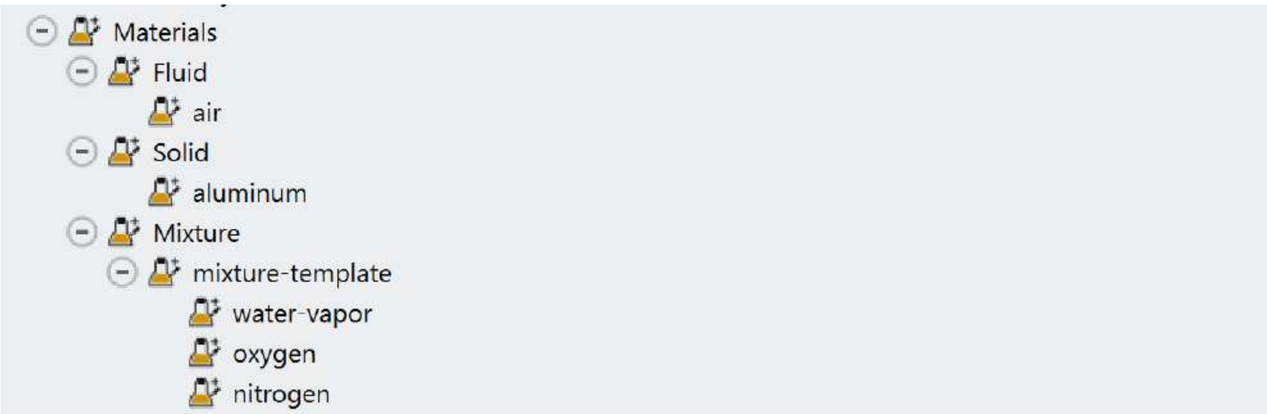
Materials
Fluid
air
Solid
aluminum
Mixture
mixture-template
water-vapor
oxygen
nitrogen

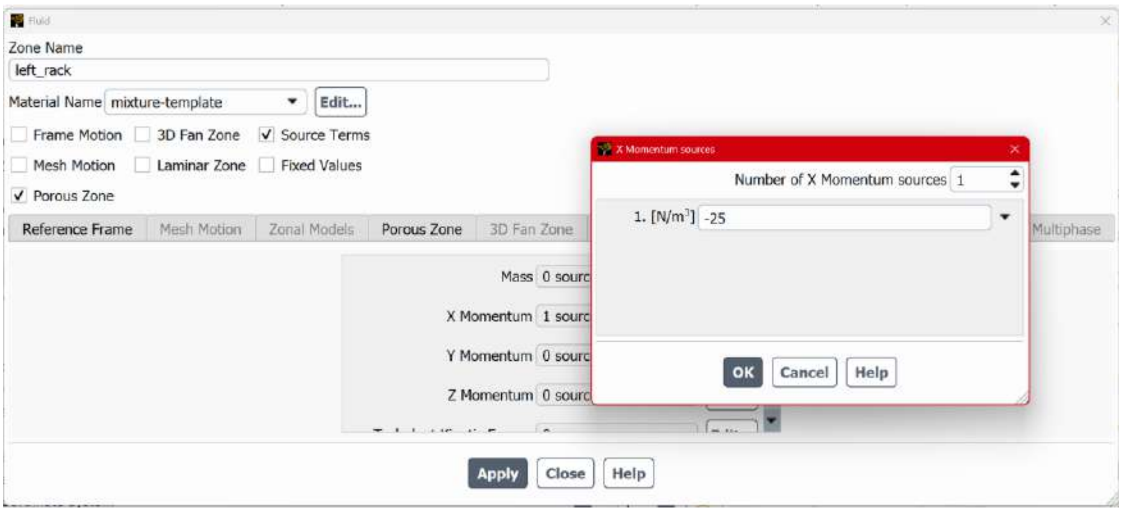
Zone Name
left_rack
Material Name mixture-template
Edit...
Frame Motion
3D Fan Zone
Source Terms
Mesh Motion
Laminar Zone
Fixed Values
Porous Zone
Reference Frame
Mesh Motion
Zonal Models
Porous Zone
3D Fan Zone
Multiphase
Mass 0 sourc
X Momentum 1 sourc
Y Momentum 0 sourc
Z Momentum 0 sourc
X Momentum sources
Number of X Momentum sources 1
1. [N/m3] -25
OK
Cancel
Help
Apply
Close
Help
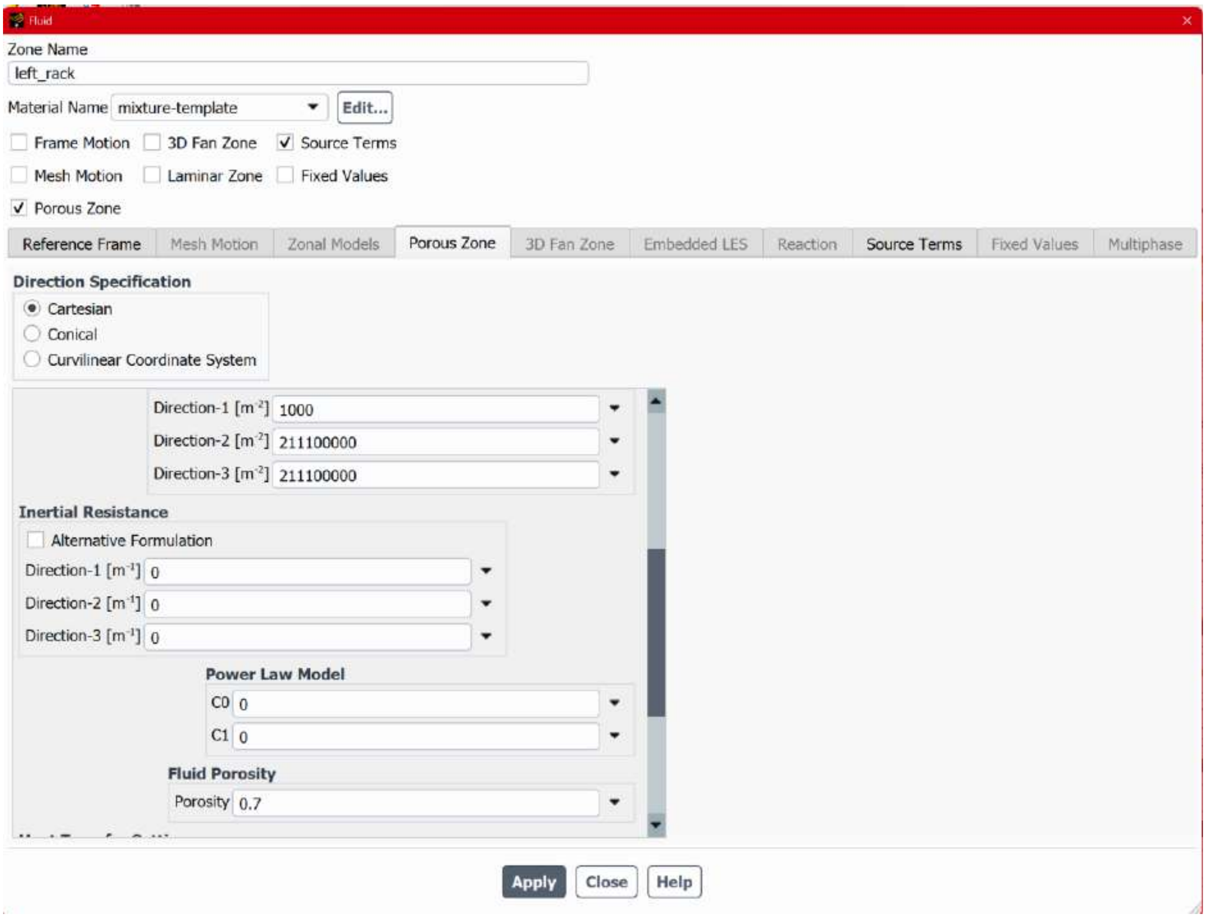
Fluid
Zone Name
left_rack
Material Name mixture-template
Edit...
Frame Motion
3D Fan Zone
Source Terms
Mesh Motion
Laminar Zone
Fixed Values
Porous Zone
Reference Frame
Mesh Motion
Zonal Models
Porous Zone
3D Fan Zone
Embedded LES
Reaction
Source Terms
Fixed Values
Multiphase
Direction Specification
Cartesian
Conical
Curvilinear Coordinate System
Direction-1 [m-2] 1000
Direction-2 [m-2] 211100000
Direction-3 [m-2] 211100000
Inertial Resistance
Alternative Formulation
Direction-1 [m-1] 0
Direction-2 [m-1] 0
Direction-3 [m-1] 0
Power Law Model
C0 0
C1 0
Fluid Porosity
Porosity 0.7
Apply
Close
Help

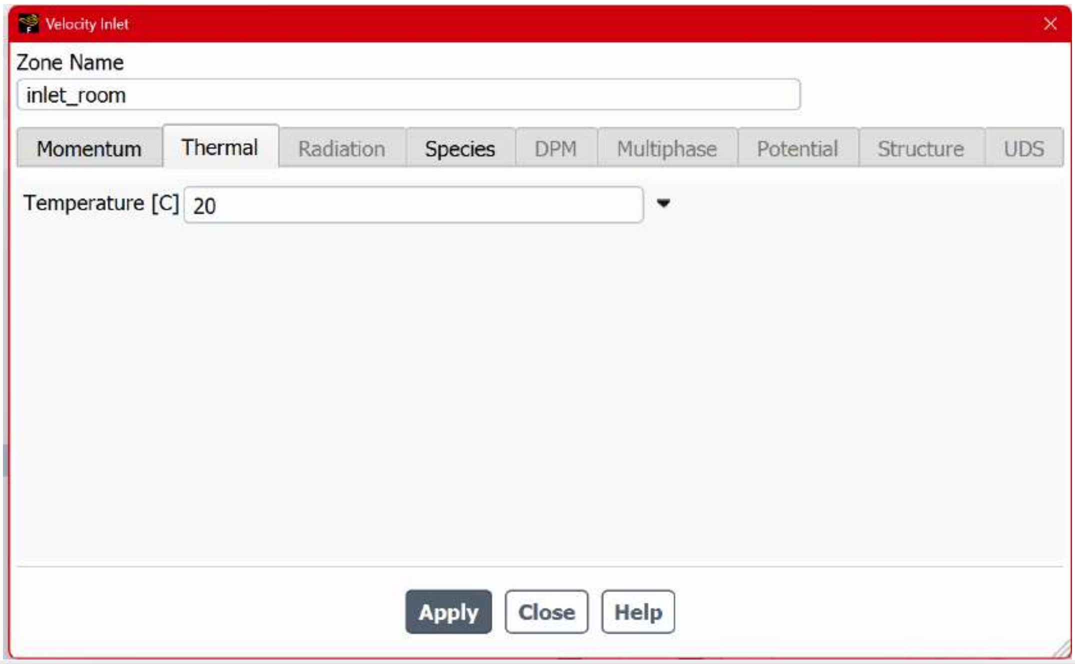
Velocity Inlet
Zone Name
inlet_room
Momentum
Thermal
Radiation
Species
DPM
Multiphase
Potential
Structure
UDS
Temperature [C]
20
Apply
Close
Help

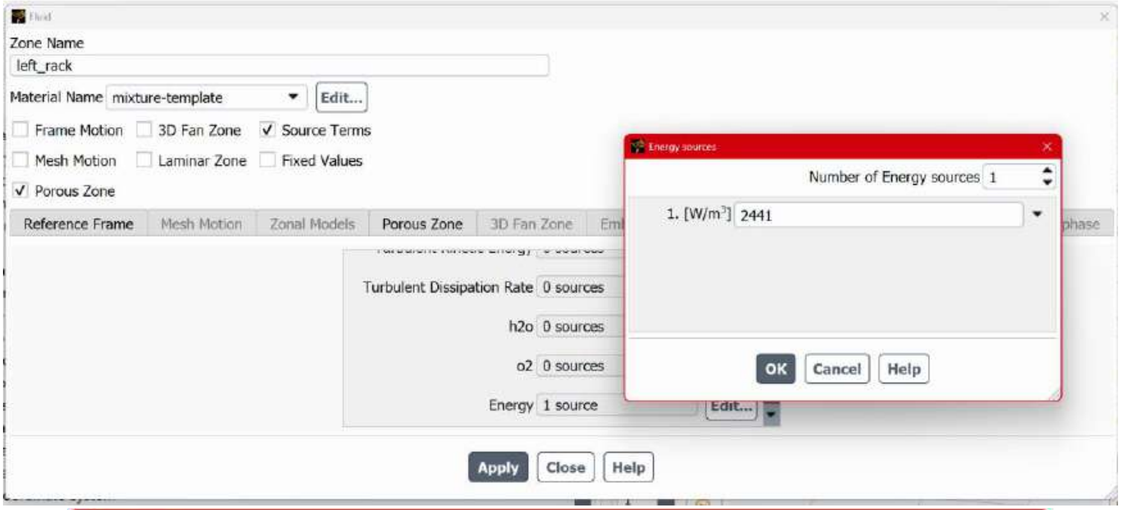
Zone Name
left_rack
Material Name
mixture-template
Edit...
Frame Motion
3D Fan Zone
Source Terms
Mesh Motion
Laminar Zone
Fixed Values
Porous Zone
Reference Frame
Mesh Motion
Zonal Models
Porous Zone
3D Fan Zone
Turbulent Dissipation Rate
0 sources
h2o
0 sources
o2
0 sources
Energy
1 source
Edit...
Energy sources
Number of Energy sources
1
1. [W/m3]
2441
OK
Cancel
Help
Apply
Close
Help

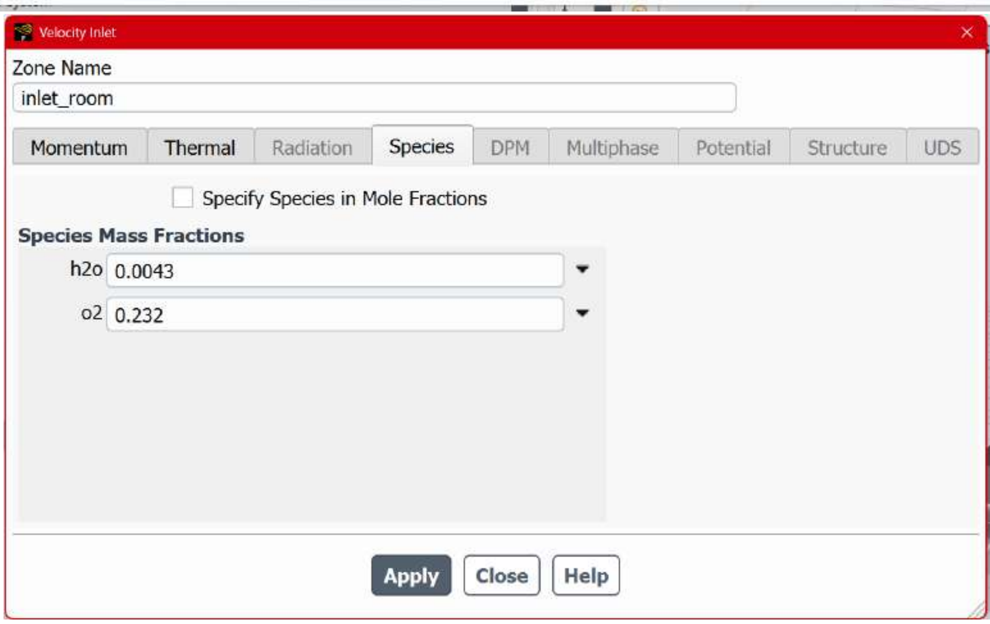
Velocity Inlet
Zone Name
inlet_room
Momentum
Thermal
Radiation
Species
DPM
Multiphase
Potential
Structure
UDS
Specify Species in Mole Fractions
Species Mass Fractions
h2o
0.0043
o2
0.232
Apply
Close
Help

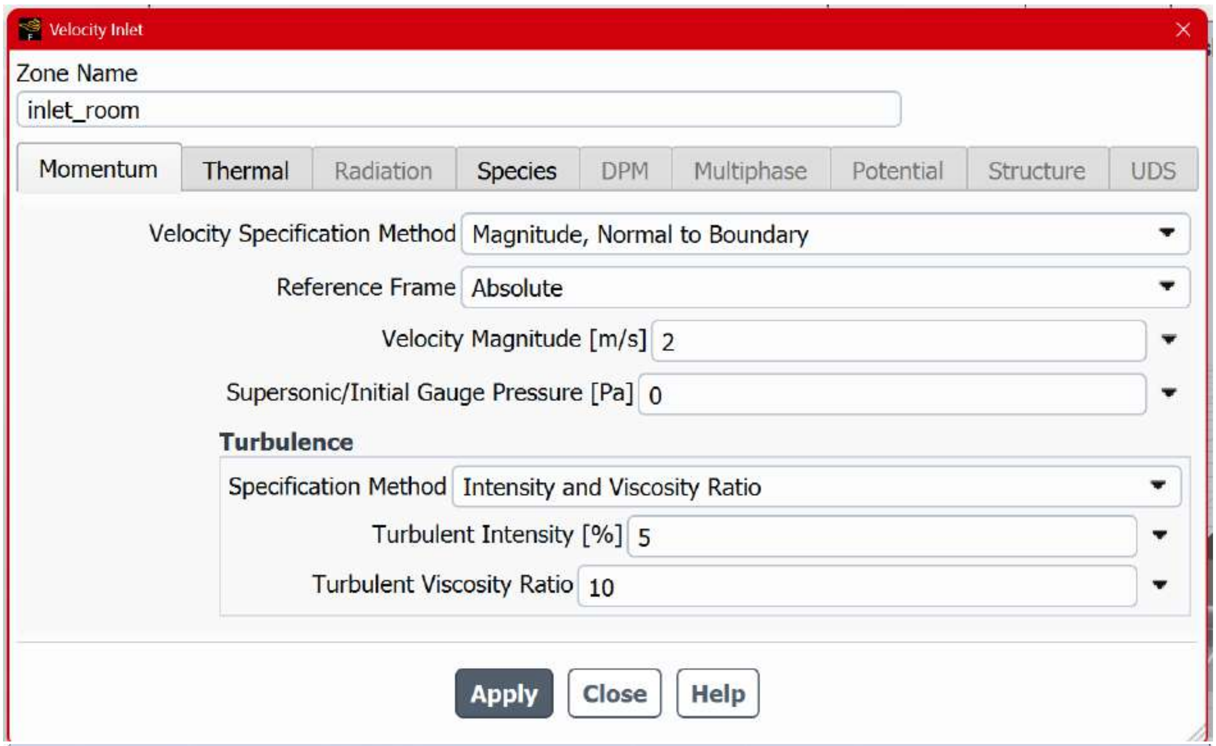
Velocity Inlet
Zone Name
inlet_room
Momentum
Thermal
Radiation
Species
DPM
Multiphase
Potential
Structure
UDS
Velocity Specification Method
Magnitude, Normal to Boundary
Reference Frame
Absolute
Velocity Magnitude [m/s]
2
Supersonic/Initial Gauge Pressure [Pa]
0
Turbulence
Specification Method
Intensity and Viscosity Ratio
Turbulent Intensity [%]
5
Turbulent Viscosity Ratio
10
Apply
Close
Help

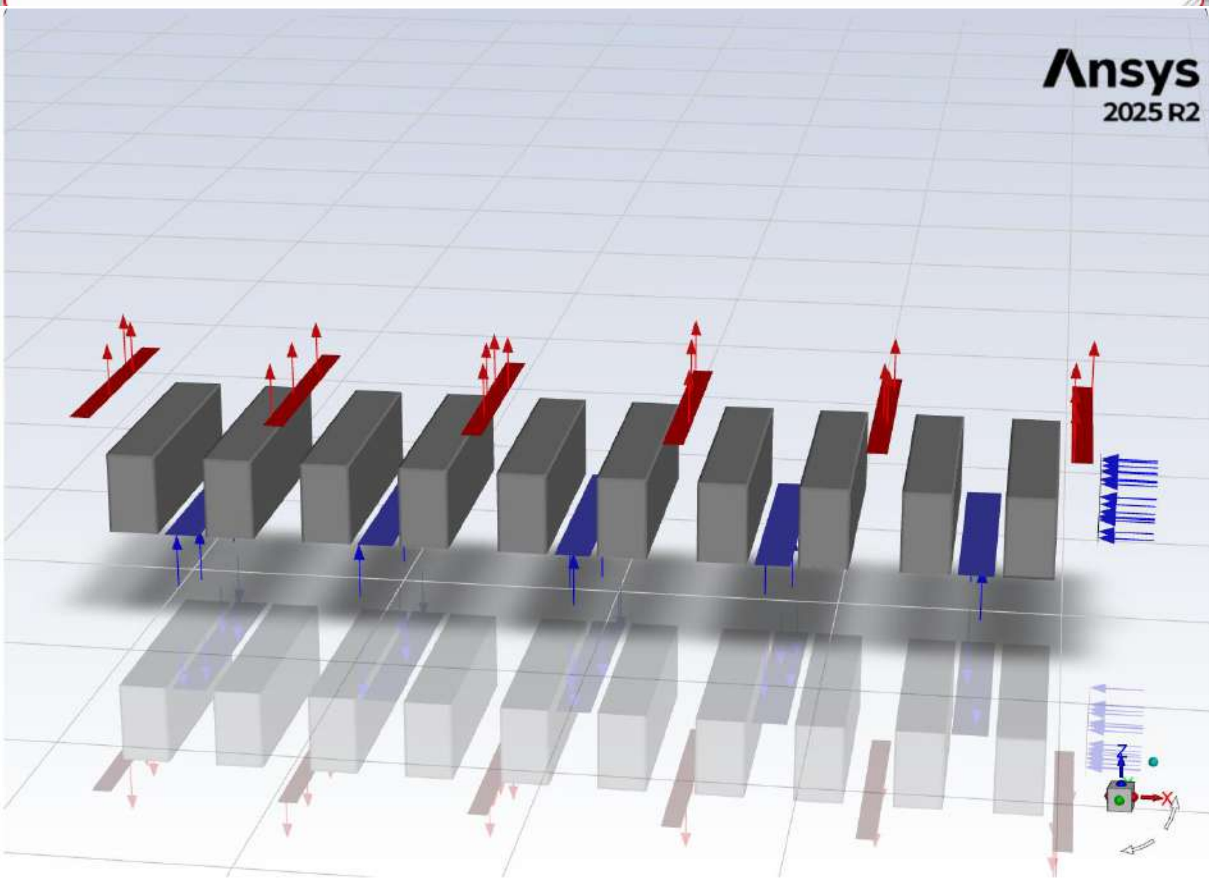
Ansys
2025 R2

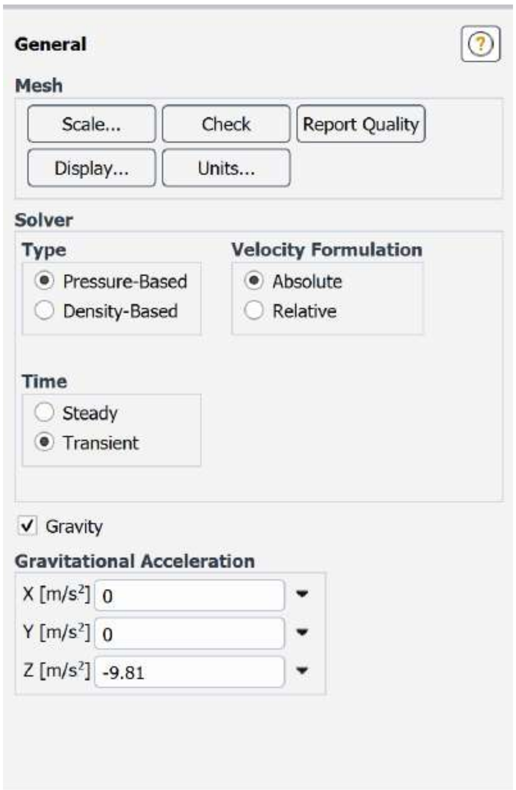
General
Mesh
Scale...
Check
Report Quality
Display...
Units...
Solver
Type
Pressure-Based
Density-Based
Velocity Formulation
Absolute
Relative
Time
Steady
Transient
Gravity
Gravitational Acceleration
X [m/s²] 0
Y [m/s²] 0
Z [m/s²] -9.81

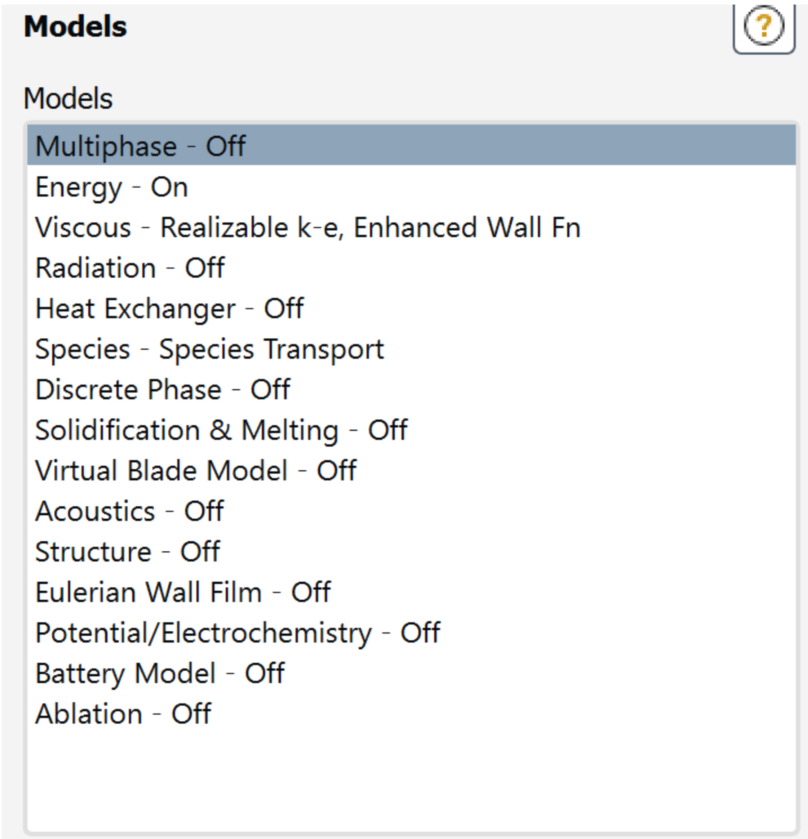
Models
Models
Multiphase - Off
Energy - On
Viscous - Realizable k-e, Enhanced Wall Fn
Radiation - Off
Heat Exchanger - Off
Species - Species Transport
Discrete Phase - Off
Solidification & Melting - Off
Virtual Blade Model - Off
Acoustics - Off
Structure - Off
Eulerian Wall Film - Off
Potential/Electrochemistry - Off
Battery Model - Off
Ablation - Off

6.4.2.6 Doors

Doors shall be a minimum of 1 m (3 ft) wide and 2.13 m (7 ft) high, with 2.44 m (8 ft) or higher recommended, or larger as required by AHJ, and should be sized to accommodate the largest expected equipment. The door shall have no doorsills and be hinged to open outward (code permitting), slide side-to-side, or be removable. Doors shall be fitted with locks and have either no center posts or removable center posts to facilitate access for large equipment. Exit requirements for the room shall meet the requirements of the AHJ.

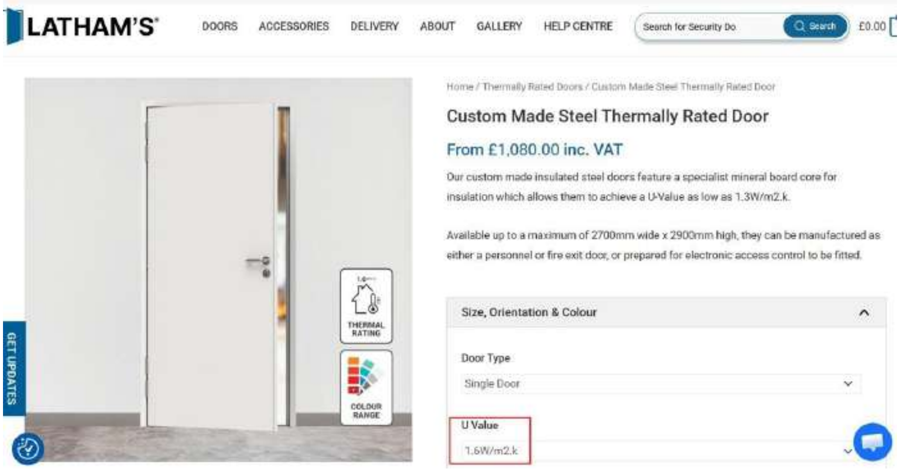

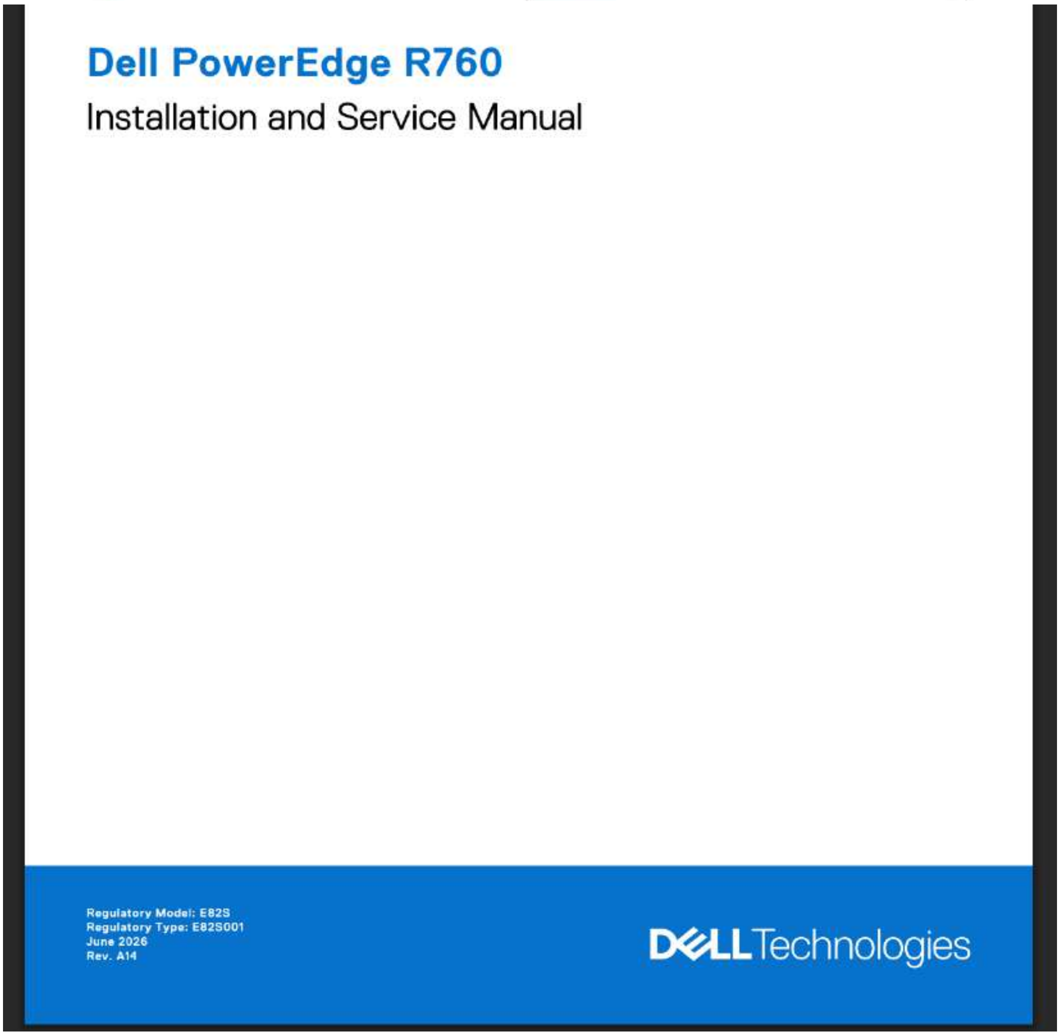

Dell PowerEdge R760

Installation and Service Manual

Regulatory Model: E82S
Regulatory Type: E82S001
June 2026
Rev. A14

DELL Technologies

Environmental specifications

ⓘ **NOTE:** For additional information about environmental certifications, refer to the *Product Environmental Datasheet* located with the *Documentation* on Dell Support.

Table 27. Continuous Operation Specifications for ASHRAE A2

Temperature	**Specifications**
Allowable continuous operations	
Temperature range for altitudes <= 900 m (<= 2953 ft)	10–35°C (50–95°F) with no direct sunlight on the equipment
Humidity percent range (non-condensing at all times)	8% RH with -12°C (10.4°F) minimum dew point to 80% RH with 21°C (69.8°F) maximum dew point
Operational altitude de-rating	Maximum temperature is reduced by 1°C/300 m (1.8°F/984 Ft) above 900 m (2953 Ft)

Table 28. Continuous Operation Specifications for ASHRAE A3

Temperature	**Specifications**		
Allowable continuous operations			
Temperature range for altitudes <= 900 m (<= 2953 ft)	5–40°C (41–104°F) with no direct sunlight on the equipment		
	Excursion Limited Operation	5-35°C (41-95°F) Continuous Operation	
		35-40°C (95-104°F) 10% Annual Runtime	

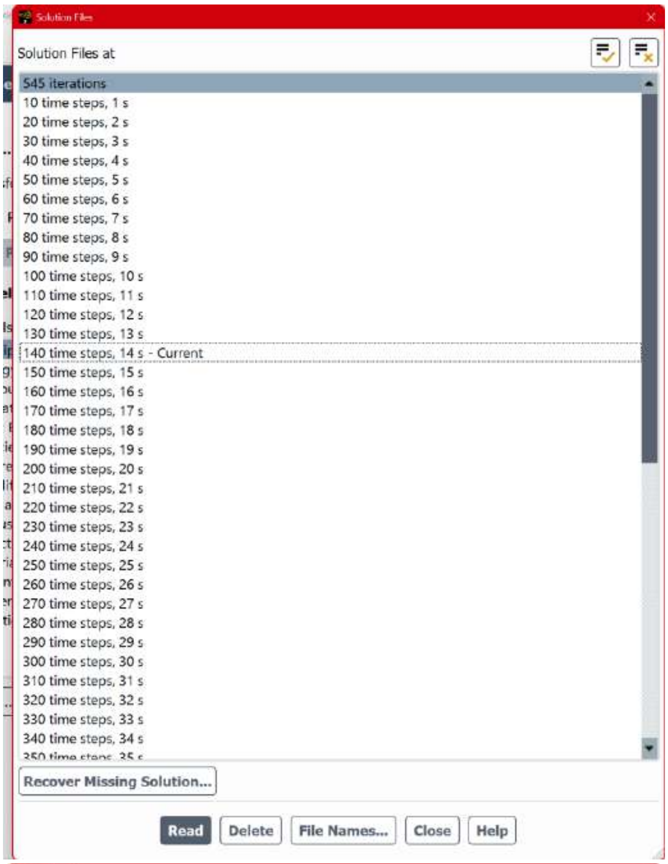
Solution Files
Solution Files at
545 iterations
10 time steps, 1 s
20 time steps, 2 s
30 time steps, 3 s
40 time steps, 4 s
50 time steps, 5 s
60 time steps, 6 s
70 time steps, 7 s
80 time steps, 8 s
90 time steps, 9 s
100 time steps, 10 s
110 time steps, 11 s
120 time steps, 12 s
130 time steps, 13 s
140 time steps, 14 s - Current
150 time steps, 15 s
160 time steps, 16 s
170 time steps, 17 s
180 time steps, 18 s
190 time steps, 19 s
200 time steps, 20 s
210 time steps, 21 s
220 time steps, 22 s
230 time steps, 23 s
240 time steps, 24 s
250 time steps, 25 s
260 time steps, 26 s
270 time steps, 27 s
280 time steps, 28 s
290 time steps, 29 s
300 time steps, 30 s
310 time steps, 31 s
320 time steps, 32 s
330 time steps, 33 s
340 time steps, 34 s
Recover Missing Solution...
Read
Delete
File Names...
Close
Help

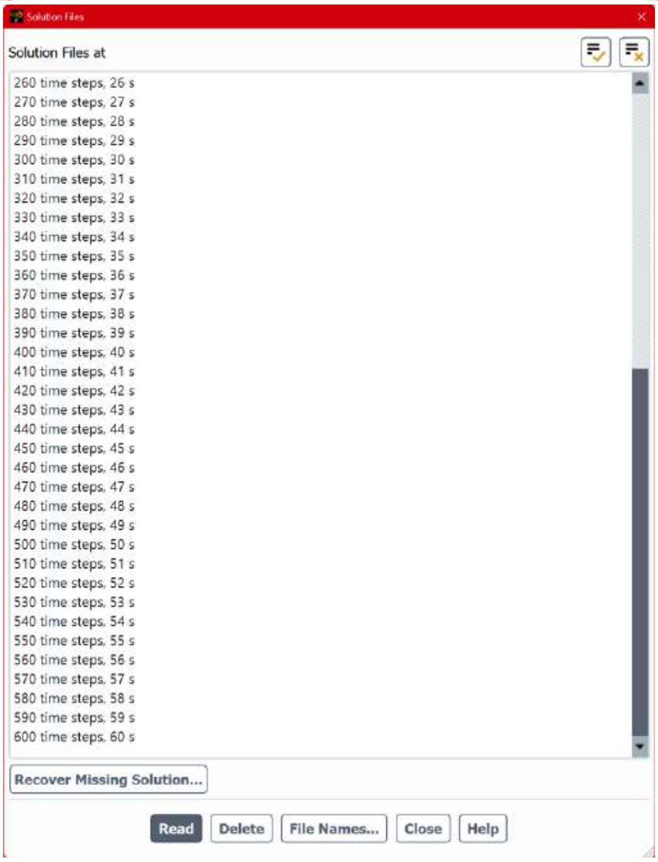
Solution Files
Solution Files at
260 time steps, 26 s
270 time steps, 27 s
280 time steps, 28 s
290 time steps, 29 s
300 time steps, 30 s
310 time steps, 31 s
320 time steps, 32 s
330 time steps, 33 s
340 time steps, 34 s
350 time steps, 35 s
360 time steps, 36 s
370 time steps, 37 s
380 time steps, 38 s
390 time steps, 39 s
400 time steps, 40 s
410 time steps, 41 s
420 time steps, 42 s
430 time steps, 43 s
440 time steps, 44 s
450 time steps, 45 s
460 time steps, 46 s
470 time steps, 47 s
480 time steps, 48 s
490 time steps, 49 s
500 time steps, 50 s
510 time steps, 51 s
520 time steps, 52 s
530 time steps, 53 s
540 time steps, 54 s
550 time steps, 55 s
560 time steps, 56 s
570 time steps, 57 s
580 time steps, 58 s
590 time steps, 59 s
600 time steps, 60 s
Recover Missing Solution...
Read
Delete
File Names...
Close
Help

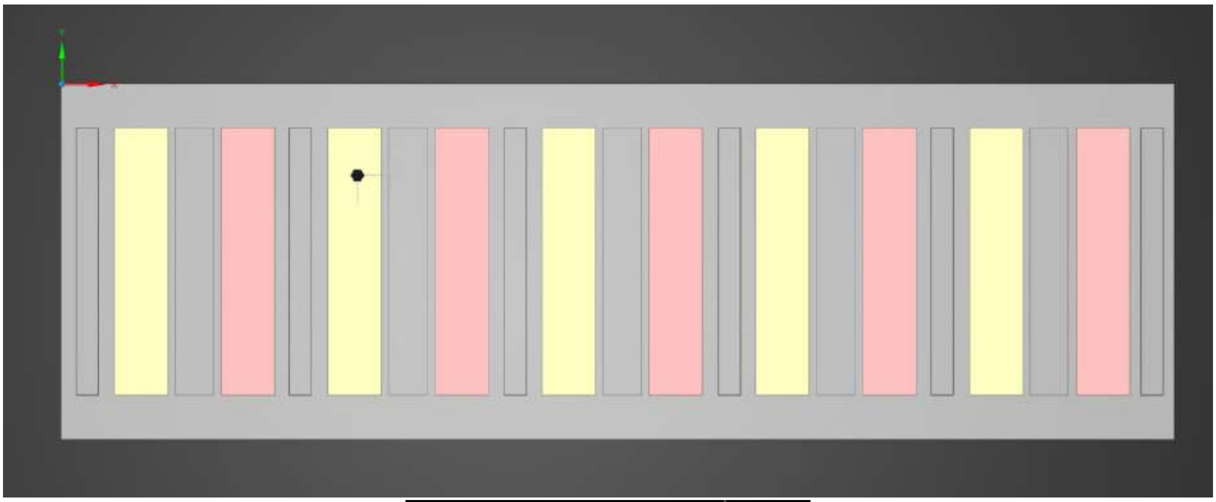

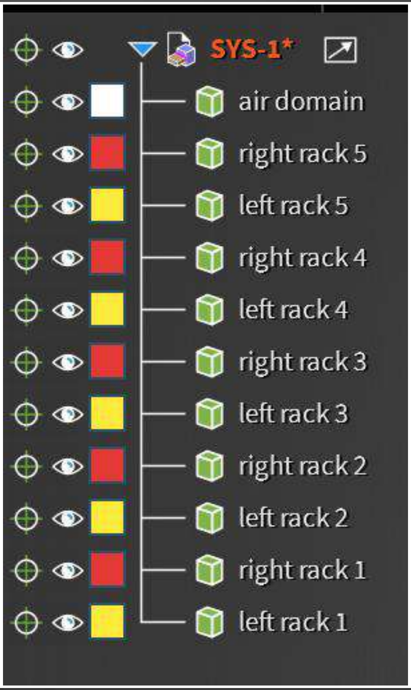
SYS-1*
air domain
right rack 5
left rack 5
right rack 4
left rack 4
right rack 3
left rack 3
right rack 2
left rack 2
right rack 1
left rack 1

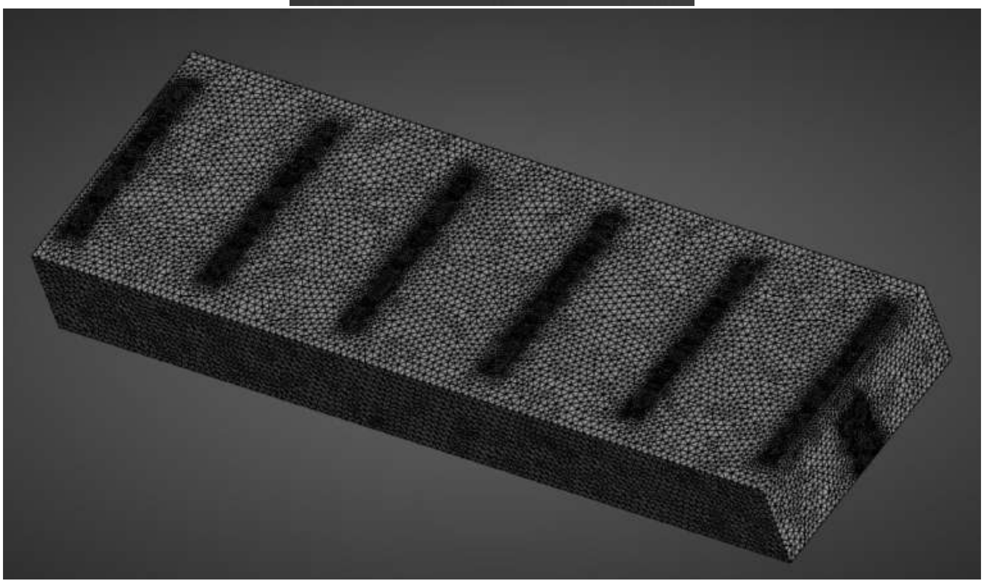

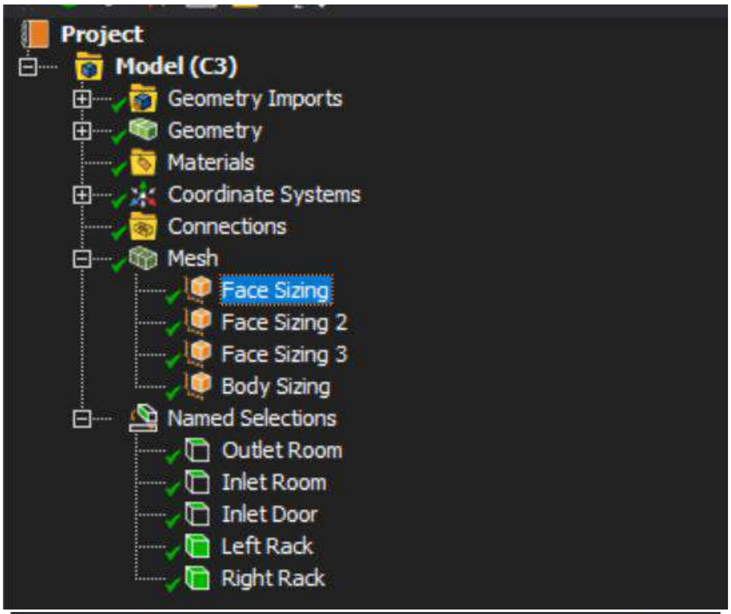
Project
Model (C3)
Geometry Imports
Geometry
Materials
Coordinate Systems
Connections
Mesh
Face Sizing
Face Sizing 2
Face Sizing 3
Body Sizing
Named Selections
Outlet Room
Inlet Room
Inlet Door
Left Rack
Right Rack

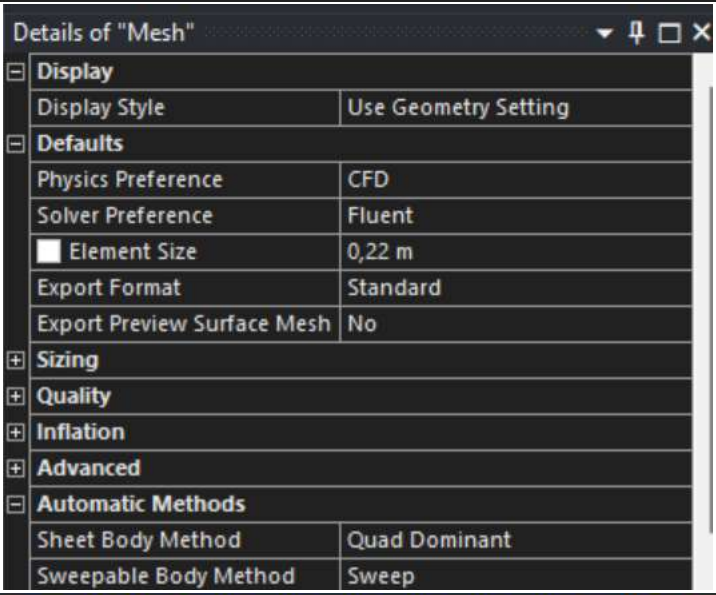
Details of "Mesh"
Display
Display Style
Use Geometry Setting
Defaults
Physics Preference
CFD
Solver Preference
Fluent
Element Size
0,22 m
Export Format
Standard
Export Preview Surface Mesh
No
Sizing
Quality
Inflation
Advanced
Automatic Methods
Sheet Body Method
Quad Dominant
Sweepable Body Method
Sweep

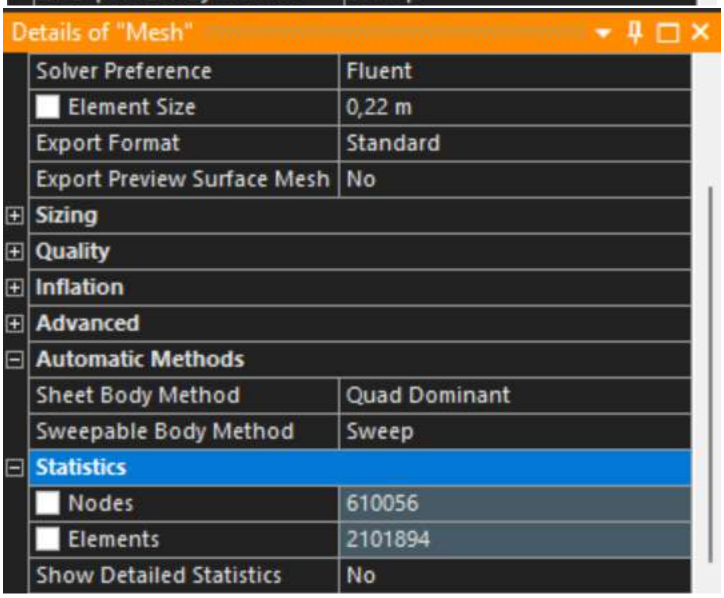
Details of "Mesh"
Solver Preference
Fluent
Element Size
0,22 m
Export Format
Standard
Export Preview Surface Mesh
No
Sizing
Quality
Inflation
Advanced
Automatic Methods
Sheet Body Method
Quad Dominant
Sweepable Body Method
Sweep
Statistics
Nodes
610056
Elements
2101894
Show Detailed Statistics
No

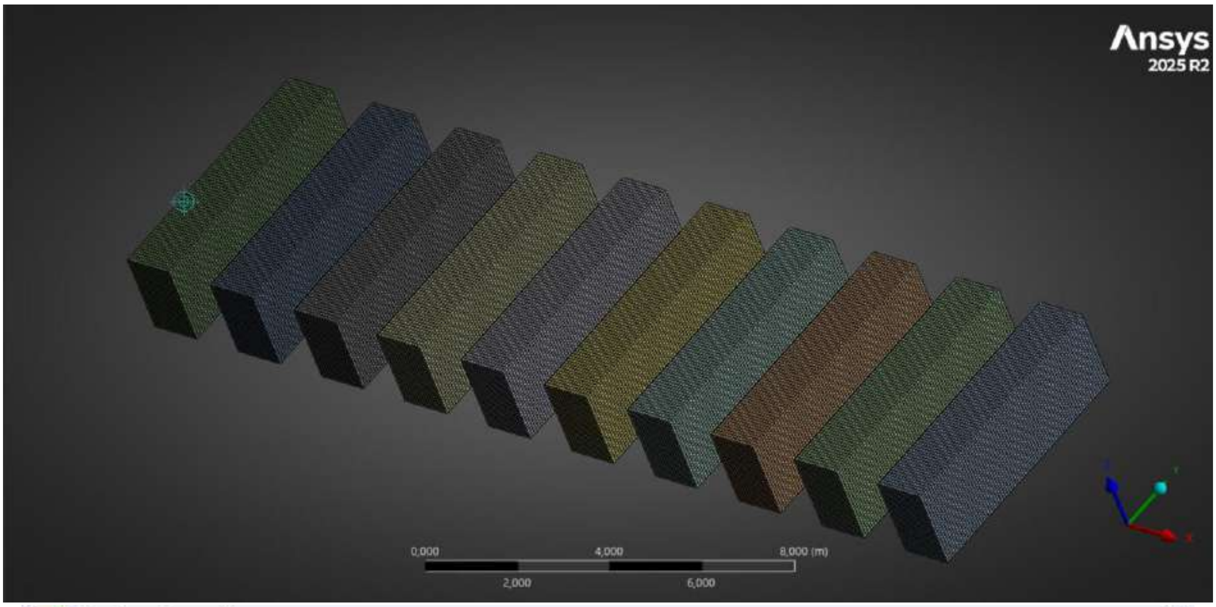

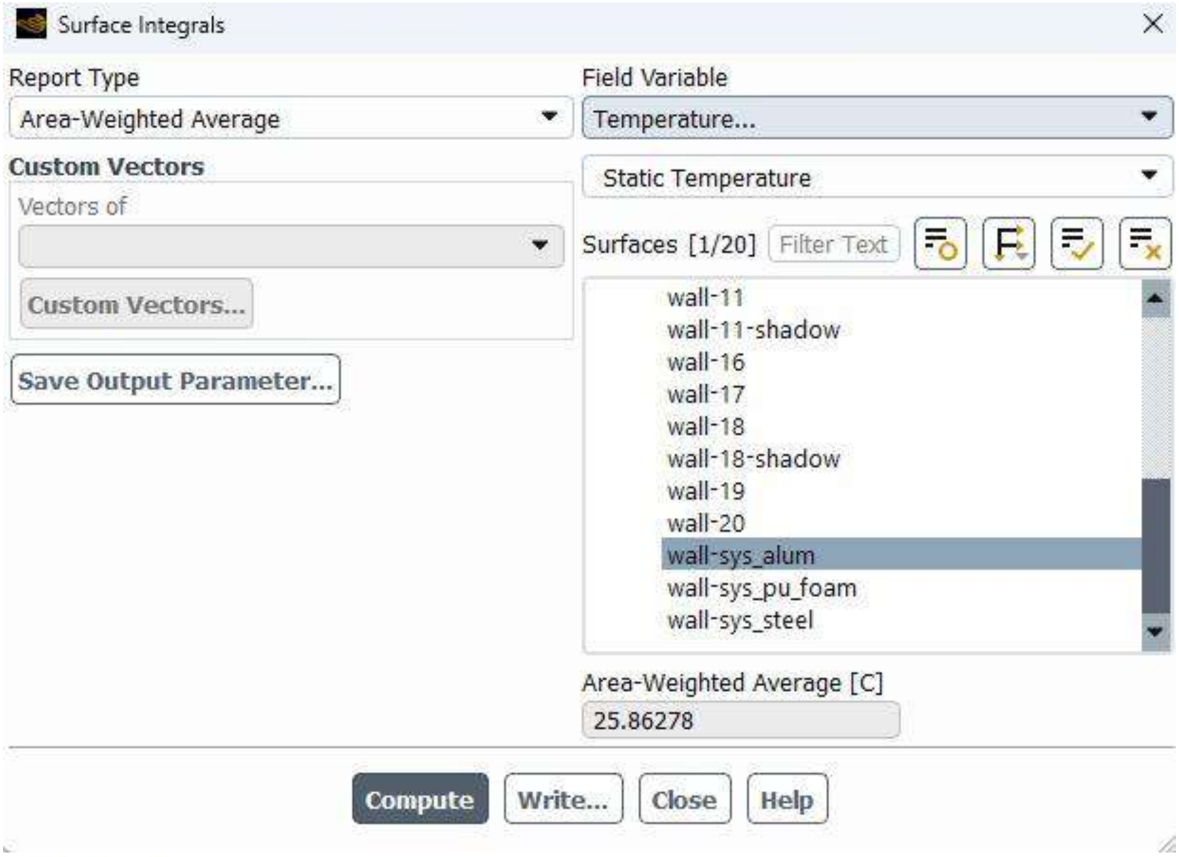

4.1.2 Kondisi perencanaan udara luar ruang

Untuk keseragaman perhitungan beban pendinginan, kondisi perencanaan udara luar ruang ditetapkan 33 °C DB dan 27 °C WB, kecuali terdapat pertimbangan lain. Kondisi perencanaan udara luar ruang untuk perhitungan beban pendinginan yang lebih teliti untuk beberapa kota di Indonesia dapat menggunakan informasi dalam Tabel 1 dengan nilai frekuensi kejadian kumulatif tahunan sebesar 0,4%, 1%, atau 2%.

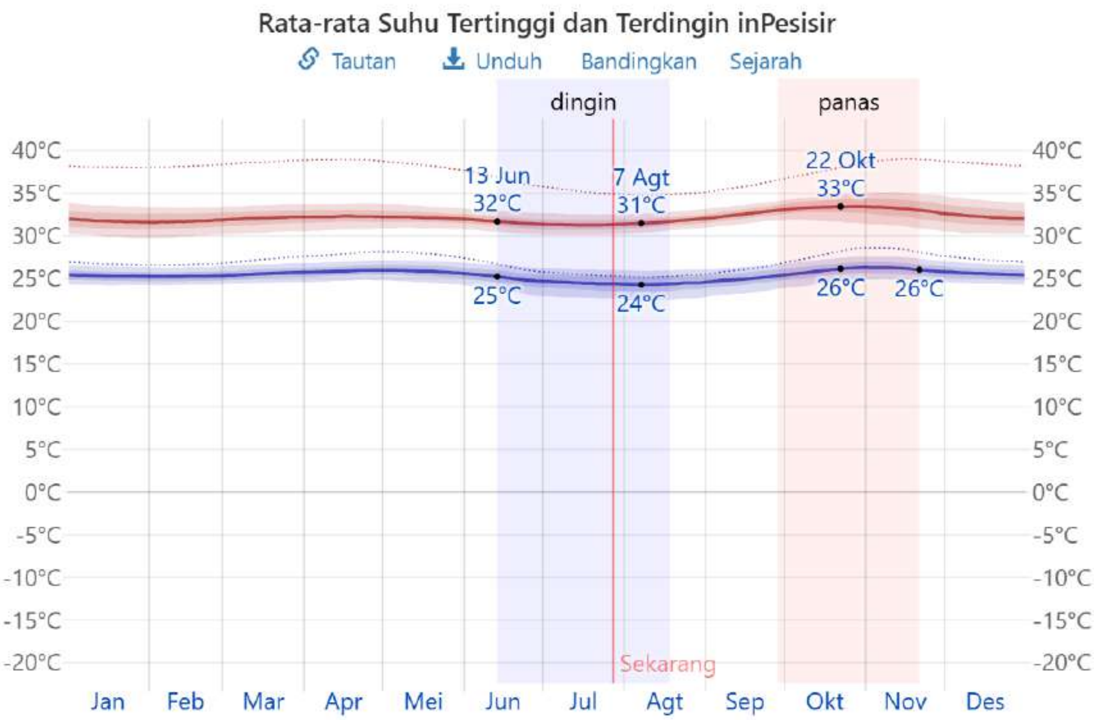

Suhu rata-rata harian tertinggi (garis merah) dan terdingin (garis biru), dengan pita persentil ke-25 hingga ke-75 dan ke-10 hingga ke-90. Garis putus-putus tipis adalah suhu rata-rata yang dirasakan.

Pesisir Suhu Rata-rata Per Bulan

Rata-rata	Jan	Feb	Mar	Apr	Mei	Jun	Jul	Agt	Sep	Okt	Nov	Des
Tinggi	32°C	32°C	32°C	32°C	32°C	32°C	31°C	32°C	33°C	33°C	33°C	32°C
Suhu	28°C	28°C	28°C	29°C	29°C	28°C	28°C	28°C	29°C	29°C	29°C	28°C
Rendah	25°C	25°C	26°C	26°C	26°C	25°C	24°C	24°C	25°C	26°C	26°C	26°C

Tingkat Kenyamanan Kelembaban di Pesisir

Tautan Unduh Bandingkan Sejarah

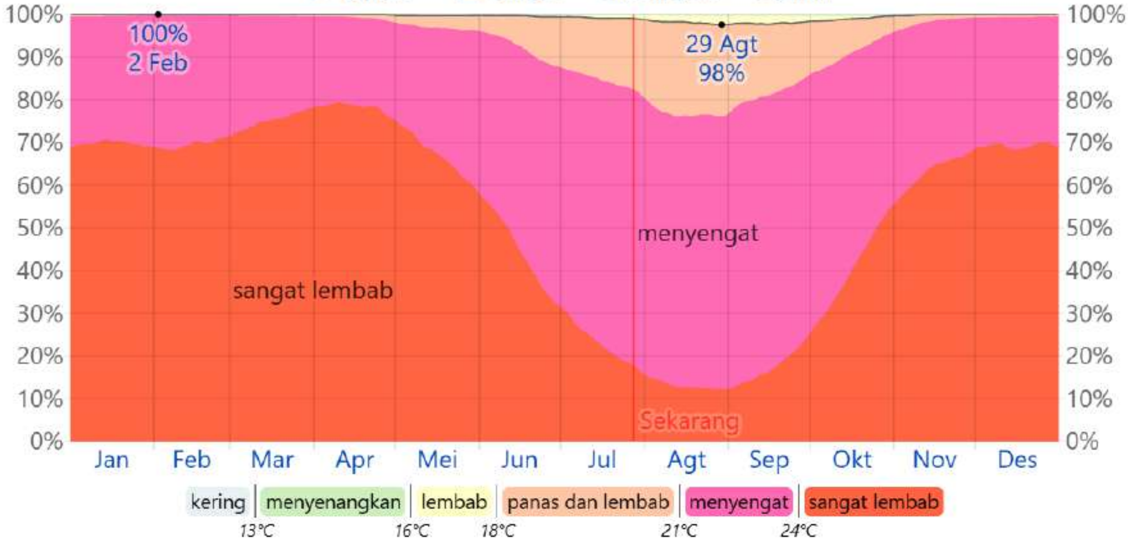

Persentase waktu yang dihabiskan pada berbagai tingkat kenyamanan kelembaban, yang dikategorikan menurut titik embun.

	Jan	Feb	Mar	Apr	Mei	Jun	Jul	Agt	Sep	Okt	Nov	Des
Hari Lembab dan Panas	31,0hr	28,0hr	31,0hr	30,0hr	30,9hr	29,9hr	30,7hr	30,4hr	29,4hr	30,7hr	30,0hr	31,0hr

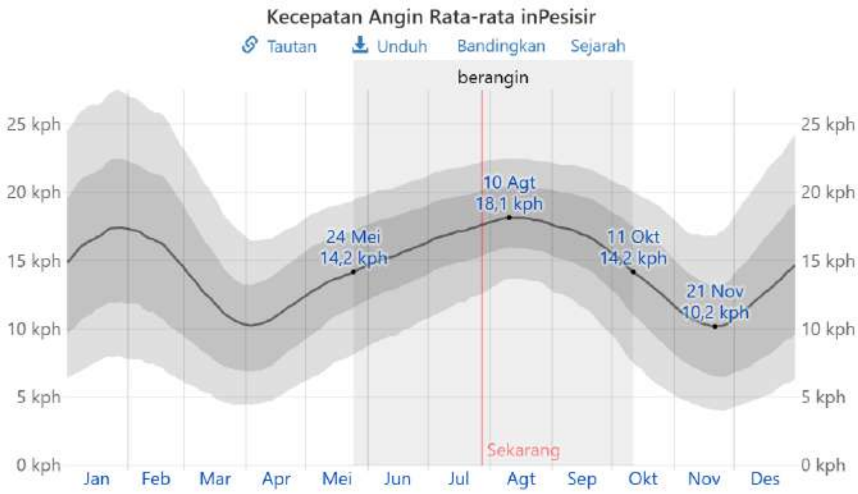

Rata-rata kecepatan angin per jam rata-rata (garis abu-abu tua), dengan pita persentil ke-25 hingga ke-75 dan ke-10 hingga ke-90.

	Jan	Feb	Mar	Apr	Mei	Jun	Jul	Agt	Sep	Okt	Nov	Des
Kecepatan angin (kph)	16.6	16.2	11.9	11.1	13.7	15.5	17.2	18.0	16.7	13.5	10.6	12.8

Tabel 1 – Kondisi perencanaan udara luar ruang untuk sistem tata udara

Lokasi			*Cooling* DB/MCWB (°C)						*Evaporation* WB/MCDB (°C)						*Dehumidification* DP/MCDB dan HR (°C dan $g_{cairan}/kg_{udara\ kering}$)								
			0.4%		1%		2%		0.4%		1%		2%		0.4%			1%			2%		
Kabupaten/ Kota	Koordinat	Stasiun Cuaca	DB	MC WB	DB	MC WB	DB	MC WB	WB	MC DB	WB	MC DB	WB	MC DB	DP	HR	MC DB	DP	HR	MC DB	DP	HR	MC DB
Aceh Besar	5.524N, 95.420E	Sultan Iskandar Muda Intl	34,4	24,4	33,8	24,6	33,2	24,8	27,0	31,3	26,6	30,9	26,2	30,5	25,9	21,3	29,2	25,5	20,7	28,7	25,1	20,3	28,3
Aceh Utara	5.227N, 96.950E	Malikus Saleh	32,7	26,0	32,2	26,0	31,7	25,9	27,1	31,0	26,8	30,7	26,6	30,4	26,0	21,4	29,5	25,7	21,0	29,2	25,5	20,7	28,9
Ambon	3.710S, 128.089E	Pattimura	32,6	25,6	32,0	25,8	31,5	25,8	27,0	30,5	26,7	30,2	26,5	30,1	26,0	21,4	29,5	25,7	20,9	29,2	25,4	20,6	28,9
Badung	8.748S, 115.167E	Bali Ngurah Rai Intl	32,5	26,6	32,1	26,5	31,7	26,4	27,7	30,7	27,2	30,4	27,1	30,2	26,9	22,6	29,9	26,2	21,7	29,2	26,1	21,6	29,2
Balikpapan	1.268S, 116.894E	Aji Muhammad Sulaiman Intl	32,9	27,4	32,2	27,0	31,8	26,9	28,2	31,4	27,8	30,9	27,5	30,6	21,7	23,0	30,2	27,0	22,7	30,1	26,6	22,2	29,7
Bandar Lampung	5.242S, 105.179E	Radin Inten II	34,1	24,2	33,3	24,6	32,7	24,8	26,6	30,7	26,3	30,4	26,2	30,2	25,6	21,1	28,1	25,2	20,6	28,0	25,1	20,4	27,9
Banggai	1.039S, 122.772E	Luwuk Bubung	32,2	26,2	31,9	26,3	31,5	26,2	27,2	30,8	27,0	30,8	26,7	30,5	26,1	21,5	30,0	25,7	21,1	29,8	25,6	20,8	29,7
Banjarbaru	3.442S, 114.763E	Syamsudin Noor	34,8	24,5	34,1	25,0	33,4	25,1	27,1	31,3	26,7	30,9	26,6	30,6	26,1	21,5	28,6	25,8	21,1	28,3	25,5	20,8	28,1
Banyuwangi	8.217S, 114.383E	Banyuwang	32,9	26,1	32,4	26,1	32,0	26,0	27,2	31,2	26,9	30,9	26,6	30,6	26,0	21,4	29,6	25,7	21,0	29,2	25,5	20,7	29,1

Tabel 1 – Kondisi perencanaan udara luar ruang untuk sistem tata udara (2 dari 7)

Lokasi			*Cooling* DB/MCWB (°C)						*Evaporation* WB/MCDB (°C)						*Dehumidification* DP/MCDB dan HR (°C dan $g_{cairan}/kg_{udara\ kering}$)								
			0.4%		1%		2%		0.4%		1%		2%		0.4%			1%			2%		
Kabupaten/ Kota	Koordinat	Stasiun Cuaca	DB	MC WB	DB	MC WB	DB	MC WB	WB	MC DB	WB	MC DB	WB	MC DB	DP	HR	MC DB	DP	HR	MC DB	DP	HR	MC DB
Batam	1.117N, 104.117E	Hang Nadim	32,7	25,8	32,1	25,9	31,8	25,9	27,2	30,4	26,9	30,1	26,7	29,8	26,2	21,7	28,5	26,1	21,6	28,4	25,9	21,3	28,2
Belitung	2.746S, 107.755E	HAS Hanandjoeddin	33,2	24,3	32,6	24,6	32,1	25,0	26,8	29,9	26,6	29,7	26,3	29,4	26,0	21,5	28,2	25,7	21,1	27,9	25,5	20,8	27,7
Bengkulu	3.864, 102.339E	Fatmawati Soekarno	32,3	25,8	32,0	25,8	31,6	25,7	27,0	30,8	26,7	30,5	26,5	30,2	25,9	21,3	29,1	25,6	20,9	28,8	25,4	20,6	28,6
Biak Numfor	1.190S, 136.108E	Frans Kaisiepo	31,5	26,7	31,2	26,6	30,9	26,6	27,7	30,3	27,4	30,1	27,1	29,9	27,0	22,7	29,9	26,6	22,2	29,5	26,2	21,7	29,1
Bima	8.540S, 118.687E	Muhammad Salahuddin	35,1	25,1	34,4	25,1	33,7	25,2	27,2	31,7	26,8	31,3	26,6	30,9	26,0	21,5	29,1	25,7	21,0	28,7	25,5	20,7	28,4
Bitung	1.433N, 125.183E	Bitung	33,3	25,7	32,9	25,7	32,5	25,8	27,1	31,4	26,7	31,0	26,6	30,9	25,9	21,2	29,7	25,6	20,8	29,5	25,2	20,4	29,2
Cilacap	7.645S, 109.034E	Tunggul Wulung	32,6	26,3	32,1	26,3	31,7	26,2	27,2	31,1	27,0	30,9	26,7	30,5	26,1	21,6	29,6	25,8	21,1	29,2	25,6	20,9	29,0
Gorontalo	0.637N, 122.850E	Jalaluddin	33,6	24,9	33,0	25,0	32,5	25,1	26,7	31,1	26,5	30,8	26,2	30,4	25,6	21,0	28,6	25,3	20,5	28,3	25,1	20,3	28,1
Indragiri Hulu	0.353S, 102.335E	Japura	33,7	26,0	33,2	25,9	32,8	25,9	27,4	31,3	27,1	31,1	26,8	30,8	26,4	21,9	29,6	26,1	21,5	29,4	25,7	21,0	29,1

Tabel 1 – Kondisi perencanaan udara luar ruang untuk sistem tata udara (3 dari 7)

Lokasi			*Cooling* DB/MCWB (°C)						*Evaporation* WB/MCDB (°C)						*Dehumidification* DP/MCDB dan HR (°C dan $g_{cairan}/kg_{udara\ kering}$)								
			0.4%		1%		2%		0.4%		1%		2%		0.4%			1%			2%		
Kabupaten/ Kota	Koordinat	Stasiun Cuaca	DB	MC WB	DB	MC WB	DB	MC WB	WB	MC DB	WB	MC DB	WB	MC DB	DP	HR	MC DB	DP	HR	MC DB	DP	HR	MC DB
Jakarta Pusat	6.183S, 106.833E	Jakarta Observatory	34,2	25,7	33,7	25,7	33,3	25,7	27,2	32,3	26,9	32,0	26,7	31,6	25,7	21,0	30,2	25,5	20,7	29,9	25,2	20,4	29,6
Jakarta Utara	6.100S, 106.867E	Jakarta Tanjung Priok	33,8	25,8	33,2	25,8	32,9	25,8	27,2	32,0	27,1	31,8	26,8	31,4	26,0	21,3	30,2	25,7	21,0	30,0	25,5	20,7	29,8
Jambi	1.638S, 103.644E	Thaha	33,2	25,6	32,7	25,6	32,4	25,5	27,1	30,8	26,7	30,5	26,5	30,3	26,1	21,5	29,0	25,7	21,0	28,7	25,5	20,7	28,5
Kabupaten Jayapura	2.577S, 140.516E	Sentani	33,6	26,0	33,1	26,0	32,8	25,9	27,5	31,6	27,1	31,4	26,8	31,0	26,2	21,9	30,2	25,9	21,5	29,8	25,6	21,1	29,3
Kepulauan Tanimbar	7.983S, 131.300E	Saumlaki	33,2	26,9	32,7	26,8	32,2	26,6	27,7	31,6	27,4	31,2	27,2	30,8	26,6	22,2	29,9	26,3	21,8	29,4	26,1	21,6	29,2
Kotawaringin Barat	2.705S, 111.673E	Iskandar	33,2	27,4	32,7	27,3	32,2	27,1	28,7	32,0	28,2	31,6	28,0	31,4	27,7	23,8	31,4	27,2	23,1	30,9	27,0	22,8	30,7
Kubu Raya	0.151S, 109.404E	Supadio Intl	34,1	26,3	33,7	26,3	33,2	26,2	27,7	31,8	27,4	31,5	27,1	31,2	26,7	22,2	30,2	26,2	21,6	29,5	26,1	21,4	29,3
Kupang	10.172S, 123.671E	El Tari	34,6	24,9	33,8	25,0	33,1	25,0	28,1	31,2	27,7	30,9	27,2	30,6	27,2	23,2	30,3	26,8	22,7	30,0	26,3	22,0	29,4
Lingga	0.479S, 104.579E	Dabo	32,7	27,0	32,3	26,9	32,0	26,8	28,1	31,5	27,7	31,3	27,4	31,0	27,1	23,0	30,8	26,7	22,4	30,4	26,4	21,9	30,0

Tabel 1 – Kondisi perencanaan udara luar ruang untuk sistem tata udara (4 dari 7)

Lokasi			*Cooling* DB/MCWB (°C)						*Evaporation* WB/MCDB (°C)						*Dehumidification* DP/MCDB dan HR (°C dan $g_{cairan}/kg_{udara\ kering}$)								
			0.4%		1%		2%		0.4%		1%		2%		0.4%			1%			2%		
Kabupaten/ Kota	Koordinat	Stasiun Cuaca	DB	MC WB	DB	MC WB	DB	MC WB	WB	MC DB	WB	MC DB	WB	MC DB	DP	HR	MC DB	DP	HR	MC DB	DP	HR	MC DB
Lombok Tengah	8.750S, 116.267E	Lombok Intl	33,0	25,9	32,4	25,8	32,1	25,8	27,5	31,1	27,0	30,8	26,7	30,4	26,4	22,1	29,8	26,0	21,6	29,4	25,6	21,1	28,9
Luwu Utara	2.550S, 120.367E	Masamba Andi Jemma	33,7	26,2	33,0	26,3	32,5	26,2	27,7	31,8	27,3	31,4	27,0	31,1	26,5	22,2	30,5	26,1	21,6	30,1	25,8	21,2	29,7
Majene	2.500S, 119.000E	Majene	33,0	25,9	32,5	26,0	32,1	26,0	27,2	31,4	27,1	31,2	26,8	30,9	26,1	21,5	30,3	25,7	21,0	29,9	25,6	20,8	29,8
Maluku Tenggara	5.683S, 132.750E	Tual Dumatubun	32,7	27,0	32,2	26,9	31,7	26,8	28,1	31,3	27,7	30,9	27,4	30,5	27,2	22,9	30,2	26,8	22,4	29,8	26,5	22,1	29,5
Manado	1.549N, 124.926E	Sam Raturangi Intl	33,1	24,4	32,6	24,5	32,1	24,7	26,6	30,6	26,2	30,2	26,0	30,0	25,3	20,6	28,5	25,1	20,4	28,3	24,9	20,2	28,1
Maros	5.062S, 119.554E	Hasanuddin Intl	34,3	24,1	33,8	24,3	33,1	24,7	27,7	30,8	27,3	30,6	27,0	30,4	27,1	22,9	28,9	26,6	22,2	28,6	26,2	21,6	28,4
Medan	3.8000N, 98.700E	Medan Belawan	32,8	26,6	32,2	26,6	31,9	26,6	27,8	31,3	27,4	31,0	27,1	30,8	26,7	22,3	30,3	26,2	21,7	29,9	26,0	21,4	29,7
Medan	3.558N, 98.672E	Medan Polonia Intl	34,2	26,0	33,8	26,0	33,1	26,0	27,5	31,8	27,1	31,4	26,8	31,0	26,2	21,7	29,6	26,0	21,5	29,4	25,7	21,1	29,1
Merauke	8.520S, 140.418E	Mopah	32,7	26,1	32,2	26,1	31,8	26,0	27,2	30,9	27,0	30,8	26,7	30,4	26,2	21,6	29,2	25,9	21,3	29,0	25,7	20,9	28,8

Tabel 1 – Kondisi perencanaan udara luar ruang untuk sistem tata udara (5 dari 7)

Lokasi			*Cooling* DB/MCWB (°C)						*Evaporation* WB/MCDB (°C)						*Dehumidification* DP/MCDB dan HR (°C dan $g_{cairan}/kg_{udara\ kering}$)								
			0.4%		1%		2%		0.4%		1%		2%		0.4%			1%			2%		
Kabupaten/ Kota	Koordinat	Stasiun Cuaca	DB	MC WB	DB	MC WB	DB	MC WB	WB	MC DB	WB	MC DB	WB	MC DB	DP	HR	MC DB	DP	HR	MC DB	DP	HR	MC DB
Nagan Raya	4.250N, 96.117E	Meulaboh Cut Nyak	31,8	26,9	31,5	26,8	31,1	26,6	28,1	30,8	27,7	30,5	27,4	30,3	27,2	23,3	30,4	26,9	22,8	30,1	36,6	22,3	29,8
Padang	0.875S, 100.352E	Minangkabau Intl	32,2	25,9	31,9	25,9	31,5	25,8	27,2	30,9	26,8	30,5	26,6	30,3	26,1	21,5	29,5	25,7	21,0	29,2	25,4	20,6	29,0
Palangkaraya	2.225S, 113.943E	Tjilik Riwut	34,0	25,6	33,5	25,6	33,0	25,2	27,2	31,2	26,8	30,9	26,6	30,7	26,2	21,6	28,7	25,8	21,1	28,3	25,6	20,9	28,2
Palembang	2.898S, 104.701E	Mahmud Badaruddin II Intl	34,0	24,8	33,4	25,1	33,0	25,2	27,1	30,7	26,7	30,4	26,6	30,2	26,1	21,6	28,7	25,9	21,2	28,5	25,6	20,8	28,2
Palu	0.919S, 119.910E	Palu Mutiara	34,7	25,0	34,2	25,0	33,6	24,9	26,4	31,7	26,1	31,3	25,9	31,0	25,2	20,5	28,0	24,8	20,1	27,7	24,6	19,8	27,6
Pangkalpinang	2.170S, 106.130E	Depati Amir	32,7	25,4	32,2	25,6	31,9	25,6	27,0	30,8	26,7	30,4	26,6	30,2	26,0	21,4	28,8	25,7	21,0	28,5	25,5	20,8	28,4
Pekanbaru	0.461N, 101.445E	Syarif Kasim II Intl	34,6	26,4	34,1	26,4	33,7	26,3	28,0	32,8	27,6	32,3	27,2	31,9	26,6	22,3	31,2	26,2	21,7	30,7	26,0	21,4	30,4
Samarinda	0.485S, 117.157E	Temindung	33,8	26,1	33,3	26,1	32,8	26,0	27,2	31,5	26,9	31,2	26,7	30,8	26,1	21,5	29,0	25,8	21,1	28,6	25,6	20,9	28,5
Semarang	6.973S, 110,375E	Ahmad Yani Intl	34,6	23,8	33,8	24,2	33,1	24,4	27,0	31,0	26,7	30,7	26,5	30,5	26,0	21,3	29,3	25,6	20,8	29,0	25,2	20,4	28,7

Tabel 1 – Kondisi perencanaan udara luar ruang untuk sistem tata udara (6 dari 7)

Lokasi			*Cooling* DB/MCWB (°C)						*Evaporation* WB/MCDB (°C)						*Dehumidification* DP/MCDB dan HR (°C dan $g_{cairan}/kg_{udara\ kering}$)								
			0.4%		1%		2%		0.4%		1%		2%		0.4%			1%			2%		
Kabupaten/ Kota	Koordinat	Stasiun Cuaca	DB	MC WB	DB	MC WB	DB	MC WB	WB	MC DB	WB	MC DB	WB	MC DB	DP	HR	MC DB	DP	HR	MC DB	DP	HR	MC DB
Serang	6.117S, 106.133E	Serang	33,5	25,0	33,0	25,1	32,5	25,2	26,8	30,7	26,6	30,5	26,4	30,3	25,8	21,2	28,5	25,6	20,9	28,3	25,3	20,5	28,1
Sidoarjo	7.380S, 112.787E	Juanda Intl	34,1	24,4	33,5	24,5	33,0	24,7	27,0	31,0	26,7	30,6	26,5	30,4	26,0	21,4	28,8	25,6	20,9	28,6	25,2	20,4	28,4
Sikka	8.641S, 122.237E	Frans Seda	33,9	25,8	33,3	25,8	32,8	25,8	27,8	31,7	27,3	31,3	27,1	31,0	26,7	22,3	30,6	26,2	21,6	29,9	25,9	21,2	29,5
Sorong	0.926S, 131.121E	Jefman	32,2	26,2	31,9	26,1	31,5	26,1	27,3	30,6	27,1	30,4	26,8	30,2	26,4	21,9	29,3	26,1	21,5	29,0	25,9	21,2	28,7
Sumba Timur	9.669S, 120.302E	Umbu Mehang Kunda	33,4	25,9	33,0	26,0	32,5	25,9	27,9	31,5	27,5	31,3	27,1	31,2	26,9	22,6	30,7	26,3	21,8	30,3	25,9	21,3	29,9
Sumbawa	8.489S, 117.412E	Brangbiji	34,5	24,3	33,7	24,6	33,1	24,8	27,3	31,0	27,0	30,8	26,7	30,4	26,2	21,6	29,6	25,9	21,3	29,2	25,7	20,9	29,0
Sumenep	7.050S, 113.967E	Kalianget Madura Island	33,3	27,7	32,9	27,6	32,4	27,4	29,1	32,3	28,6	31,9	28,2	31,5	28,2	24,4	31,9	27,7	23,6	31,4	27,2	23,0	31,0
Tangerang	6.126S, 106.656E	Soekarno Hatta Intl	34,0	25,5	33,2	25,6	33,0	25,7	27,7	31,3	27,4	31,0	27,0	30,8	26,9	22,6	30,1	26,2	21,7	29,3	26,1	21,5	29,2
Tanjungpinang	0.923N, 104.532E	Raja Haji Fisabilillah	32,5	25,9	32,1	25,9	31,7	25,9	27,2	30,6	26,9	30,3	26,7	30,0	26,2	21,7	28,7	26,0	21,4	28,6	25,7	21,0	28,3

Tabel 1 – Kondisi perencanaan udara luar ruang untuk sistem tata udara (7 dari 7)

Lokasi			*Cooling* DB/MCWB (C)						*Evaporation* WB/MCDB (C)						*Dehumidification* DP/MCDB dan HR (C dan $g_{cairan}/kg_{udara\ kering}$)								
			0.4%		1%		2%		0.4%		1%		2%		0.4%			1%			2%		
Kabupaten/ Kota	Koordinat	Stasiun Cuaca	DB	MC WB	DB	MC WB	DB	MC WB	WB	MC DB	WB	MC DB	WB	MC DB	DP	HR	MC DB	DP	HR	MC DB	DP	HR	MC DB
Tapanuli Tengah	1.556N, 98.889E	Sibolga Pinangsori	33,0	25,9	32,6	25,8	32,1	25,8	27,6	31,1	27,2	30,7	26,9	30,4	26,6	22,2	30,0	26,2	21,7	29,6	25,9	21,3	29,3
Tarakan	3.327N, 117.566E	Juwata Intl	32,2	26,4	31,7	26,4	31,5	26,3	27,5	30,6	27,2	30,4	27,0	30,2	26,5	22,1	29,5	26,2	21,7	29,1	26,1	21,5	28,9
Tegal	6.850S, 109,150E	Tegal	33,1	25,0	32,6	25,2	32,2	25,4	27,2	31,0	26,9	30,8	26,7	30,5	26,1	21,5	29,7	25,7	21,0	29,3	25,6	20,9	29,2
Ternate	0.831N, 127.381E	Babullah	32,1	25,5	31,7	25,5	31,3	25,6	26,9	30,4	26,7	30,1	26,5	29,9	25,9	21,2	29,0	25,6	20,9	28,9	25,4	20,7	28,7

Sumber: *ASHRAE Handbook – Fundamentals 2017 – Chapter 14 Climatic Design Information*

Author Biography

The author, Gemilang Friyan Finn Pakpahan, was born in 23 January 2004, Jakarta, Indonesia. He is the son of Mr. Mangatur Disneyland Wijaya and Mrs. Agatha Kristina. He completed his elementary and junior high school education at Bukit Sion School, Jakarta, before continuing his senior high school education at SMA Negeri 6 Jakarta. In 2022, he was admitted to the Double Degree Undergraduate Program in Marine Engineering between Institut Teknologi Sepuluh Nopember (ITS), Indonesia, and Hochschule Wismar – University of Applied Sciences: Technology, Business and Design, Germany. He is currently enrolled in the Department of Marine Engineering, Faculty of Marine Technology, Institut Teknologi Sepuluh Nopember (ITS), with student identification number 5019221062. During his undergraduate studies, the author actively participated in various technical training programs to enhance his engineering knowledge and practical skills, including AutoCAD, SolidWorks, and CAESAR II training. Besides his academic activities, he has been actively involved in the Marine Fluid Machinery (MMS) Laboratory, serving as both a laboratory member and a student administrator. Through these activities, he gained valuable experience in engineering research, laboratory management, and technical problem-solving. The completion of this bachelor thesis marks an important milestone in his academic journey and reflects his interest in fluid machinery, thermal systems, Computational Fluid Dynamics (CFD), and marine engineering applications. The author welcomes constructive comments, suggestions, and feedbacks from readers for future improvement and development. The author can be contacted via e-mail at: gemilangpakpahan23@gmail.com